GRAPH THEORY ANALYSES ON CONNECTIVITY MAPS OBTAINED BY PARTIAL DIRECTED COHERENCE USING EEG DATA OF DYSLEXIC AND HEALTHY CHILDREN

A THESIS SUBMITTED TO
THE GRADUATE SCHOOL OF NATURAL AND APPLIED SCIENCES
OF
MIDDLE EAST TECHNICAL UNIVERSITY

BY

EKİN CAN ERKUŞ

IN PARTIAL FULFILLMENT OF THE REQUIREMENTS
FOR
THE DEGREE OF MASTER OF SCIENCE
IN
BIOMEDICAL ENGINEERING

AUGUST 2017

Approval of the thesis:

GRAPH THEORY ANALYSES ON CONNECTIVITY MAPS OBTAINED BY PARTIAL DIRECTED COHERENCE USING EEG DATA OF DYSLEXIC AND HEALTHY CHILDREN

submitted by **EKİN CAN ERKUŞ** in partial fulfilment of the requirements for the degree of **Master of Science in Biomedical Engineering, Middle East Technical University** by,

Prof. Dr. Gülbin Dural Ünver _____
Dean, Graduate School of **Natural and Applied Sciences**

Prof. Dr. Hakan I. Tarman _____
Head of Program, **Biomedical Engineering**

Doç. Dr. İlkay Ulusoy _____
Supervisor, **Electrical and Electronics Engineering Dept., METU**

Prof. Dr. Metehan Çiçek _____
Co-Supervisor, **Faculty of Medicine, Ankara University**

Examining Committee Members:

Prof. Dr. Canan Kalaycıoğlu _____
Faculty of Medicine, Ankara University

Doç. Dr. İlkay Ulusoy _____
Electrical and Electronics Engineering, METU

Prof. Dr. Metehan Çiçek _____
Faculty of Medicine, Ankara University

Prof. Dr. Uğur Halıcı _____
Electrical and Electronics Engineering, METU

Prof. Dr. Hakan I. Tarman _____
Mechanical Engineering, METU

Date: 17.08.2017

I hereby declare that all information in this document has been obtained and presented in accordance with academic rules and ethical conduct. I also declare that, as required by these rules and conduct, I have fully cited and referenced all material and results that are not original to this work.

Name, Last name: Ekin Can Erkuş

Signature :

ABSTRACT

GRAPH THEORY ANALYSES ON CONNECTIVITY MAPS OBTAINED BY PARTIAL DIRECTED COHERENCE USING EEG DATA OF DYSLEXIC AND HEALTHY CHILDREN

Erkuş, Ekin Can
M.Sc., Biomedical Engineering

Supervisor: Doç. Dr. İlkay ULUSOY
Co-Supervisor: Prof. Dr. Metehan ÇİÇEK

August 2017, 116 pages

Dyslexia is a common brain disorder which is defined as reading and sometimes learning disability. In this thesis study, EEG data which were collected from 31 dyslexics and 27 non-dyslexic children during reading task were used. First, multivariate autoregressive modelling was made. Then using MVAR models, brain connectivity networks were obtained with partial directed coherence (PDC) algorithms. Using brain connectivity networks, graph theory properties such as "characteristic path length", "clustering coefficient", "global efficiency" and "small-world measure" were calculated. Finally, group analyses were done based on the graph theory properties using statistical analyses. Between groups, for after stimulus condition, there was a significant difference in terms of "small-world measure". Between before stimulus and after stimulus conditions, "global efficiency" was found to have significant difference in control group. Similarly, "characteristic path length" and "clustering coefficient" properties were found to have significant difference in dyslexic group. Also, main hub nodes were discovered for each subject using

connectivity maps. Hub nodes distributions had differences between groups in right frontal and right occipito-parietal regions of brains. All the results were compared with literature and discussed.

Keywords: Dyslexia, brain connectivity, graph theory, EEG, hub nodes analyses

ÖZ

DİSLEKSİK VE SAĞLIKLI ÇOCUKLARDAN TOPLANAN EEG VERİLERİ KULLANILARAK KISMİ YÖNLÜ KOHERANS İLE ELDE EDİLMİŞ BEYİN BAĞLANTISALLIK HARİTALARINDA ÇİZGE TEORİSİ ANALİZLERİ

Erkuş, Ekin Can
Yüksek Lisans, Biyomedikal Mühendisliği

Tez Yöneticisi: Doç. Dr. İlkay ULUSOY
Ortak Tez Yöneticisi: Prof. Dr. Metehan ÇİÇEK

Ağustos 2017, 116 sayfa

Disleksi, okuma ve bazen de öğrenme bozukluğu şeklinde tanımlanan, yaygın bir beyin işlevi bozukluğudur. Bu tez çalışmasında disleksi teşhisi konulmuş 31 çocuk ile disleksi teşhisi konulmamış 27 çocuktan okuma sırasında toplanan elektroensefelografi (EEG) verileri kullanılmıştır. Sırası ile çok değişkenli otoregresif modelleme yapılmış, kısmi yönlü koherans (KYK) ile beyin bağlantısallık haritaları çıkartılmış; bu bağlantısallık haritalarından çizge teorisinin değişkenlerinden "karakteristik bağlantı uzunluğu", "kümelenme katsayısı", "bağlantısal verimlilik" ve "küçük-dünya değeri" hesaplanmış ve bu hesaplanan değerler istatistiksel fark analizleri ile incelenmiştir. Gruplar arasında stimulus sonrası durum için "küçük-dünya değeri" bakımından fark tespit edilmiştir. Stimulus öncesi ve sonrası durumlar karşılaştırıldığında ise kontrol grubunda "bağlantısal verimlilik"; disleksi grubunda ise "karakteristik bağlantı uzunluğu" ve "kümelenme katsayısı" değerleri bakımından farklar görülmüştür. Bağlantısallık haritaları ile aynı zamanda düğüm bölgeleri analizleri de yapılarak gelen ve giden bağlantıların toplandığı düğüm bölgeleri tespit

edilmiştir. Düğüm bölgeleri incelendiğinde ise sağ frontal bölge ile sağ oksipito-parietal bölgede gruplar arasında farklılıklar tespit edilmiştir. Bulunan sonuçlar literatür ile karşılaştırılmış ve tartışılmıştır.

Anahtar kelimeler: Disleksi, beyin bağlantısallığı, çizge teorisi, EEG, düğüm bölgeleri analizi

To my parents and people who supported me during this journey

ACKNOWLEDGEMENTS

The data used in this thesis were collected by members of Ankara University under the project of:

"Gelişimsel Disleksi: Dilbilim Ve Eeg Verilerinin İlişkilendirilmesi"

"Developmental Dyslexia: Defining the relations between linguistics and EEG data"

Project coordinator: Dr.Canan Kalaycıoğlu

The people who contributed to collecting of the data:

Psikolog Korhan Büyüktürkoğlu, Biyolog Simge Aykan: A. Ü. SBE Disiplinlerarası Sinirbilim ABD

Psikolog Başak Alpas, A.Ü. Tıp Fak. Çocuk ve Ergen Ruh Sağ. Hast. ABD

Dr. Cihat Kağan Gürkan

Psikolog Meryem Oğuzhan, Psik. A.Ü.DTCF Klinik Psikoloji

Dr. İlkay Ulusoy Parnas, ODTÜ Elektrik-Elektronik Müh. Böl.

Dr. Hacer İclal Ergenç, Dr. Sıla Ay, İpek Pınar Bekar, A.Ü. Dil, Tarih ve Coğrafya Fakültesi Dilbilim Bölümü

Proje Numarası: 10B3030001

Ankara Üniversitesi Bilimsel Araştırma Projeleri

Ankara–2014

I would like to thank my supervisor Dr. İlkay Ulusoy for her patience, guidance and morale support through this thesis study. Her feedbacks were really helpful for me to correct my mistakes for both this thesis and my academic aspect. I would like to express my gratitude to Dr. Canan Kalaycıoğlu for her support and her research group for letting me use of their data which were collected for their project. I also thank my co-supervisor Dr. Metehan Çiçek and other jury members: Dr. Hakan Tarman and Dr. Uğur Halıcı for their guidance and important feedbacks which were helpful in making the expression of this thesis better and will be helpful for me in the way to pursue my academic career.

I would also like to thank all my friends, especially Özlem Kahraman for supporting me during hard times and being respective to my study times. A bone-full thanks to my companion "Meelo" for sharing some of his unlimited energy.

Most importantly, I am grateful to my parents for their patience and efforts in raising me while showing me the importance of discipline, patience, respect and creativity. I would like to thank my father, Dr. Adnan Erkuş for his guidance to select the statistical analyses to be used in analysing the data.

TABLE OF CONTENTS

LIST OF TABLES

LIST OF FIGURES

CHAPTER 1

INTRODUCTION

1.1. Motivation

Dyslexia is one of the neurobiological disorders that is related with improper reading and sometimes learning inability and would cause several problems in a person's life. The problems can be even more severe on school aged children due to their social environments with other same aged children in their schools. A school aged child with dyslexia may not show persistent development in reading related tasks and lessons. Therefore, may be excluded by his/her social environment. Such social externalizations may cause even worse psychological conditions that effect a person's characteristic development and personality. Early diagnosing of dyslexia would prevent dyslexic children to be exposed to negative social and psychological factors.

Like most brain disorders, dyslexia cause abnormalities in functions or structures in some brain areas. The discovery of abnormally functioning brain areas of dyslexic brains would provide researchers to focus their study on those areas. Narrowing the studies on those brain areas for computationally complex researches would save time and money to achieve results. However, according to Peterson R.L (2015), the core of neurobiological causes of dyslexia are yet to be discovered [1].

In literature, there are mostly fMRI and PET studies for determining the abnormal brain areas of dyslexics. And many of them only focused on some specific regions and connections such as reading circuitry in the brain. However, considering whole brain as field of interest and using as many of the methods as possible would provide better results.

In 1996, Paulesu et al. suggested that the dyslexia is rather a disconnection syndrome [2]. This suggestion implies that dyslexia cause significant changes in brain connections. To test this hypothesis, data from dyslexic and healthy people should be collected to be analysed in terms of brain connectivity methods. The results should be compared with other indicators of dyslexia.

There are three main brain connectivity estimation types: Structural connectivity to investigate physical connections, functional connectivity to show direct correlations at zero time lag and effective connectivity to analyse causal relations between different brain regions [3] [4]. Several methods exist to perform connectivity estimations. For example, some estimators depend on the multivariate autoregressive properties and their calculations can be performed in frequency domain such as Directed Transfer Function (DTF) and Partially Directed Coherence (PDC) or time domain such as Dynamic Bayesian Networks (DBN). PDC and DTF mainly depend on the principles of Granger causality [5] which seeks the causal influence of a channel into another channel of data series. DBN depends on probabilistic modelling. See Chapter 2 "Background Information" for detailed information about those modelling algorithms. Exploring the connections between brain regions would further aid the understanding of how dyslexic brains work.

Diagnosing of dyslexia by using biological signals can be accomplished by discovering the diversities of dyslexic and healthy brains in many aspects. A way is investigating anatomical structures of brain such as white matter and grey matter; magnetic resonance imaging (MRI) and diffusion tensor imaging (DTI) are common methods to perform this [6]. Another method is by comparing the data obtained by functional/physiological responses to stimuli as electroencephalography (EEG), functional magnetic resonance imaging (fMRI) and positron emission tomography (PET) analyses do [7]. Functional connectivity analyses can be performed using time series data such as EEG or fNIRS data to explain how a structure's functioning influences another structure [8]. Similar to functional connectivity, effective connectivity maps can be obtained from time series data like EEG or fNIRS data to identify how a structure's past behaviours effect another structure's future behaviour [9]. A supportive analysis for above methods can be statistically analysing the data which consist of several channels and time series [10]. Researchers tend to use only

one of those methods to obtain results [11] [12] [13]. However, making conclusions about the results from combinations of those methods may yield better knowledge on the way to discovering the abnormalities of dyslexic brains.

For the studies with early diagnosing of dyslexia, the subjects would be pre-school children. Due to measurement duration, fear and motion artefacts that children may cause (or be exposed), MRI based imaging techniques are not proper choice for this problem. Rather, the imaging is better to be performed in short time, without exceptional noise and closed environment that may cause fear in children. Such reasons may put Electroencephalography (EEG) measurement suitable for children studies. EEG is also better choice for functional and effective connectivity analyses thanks to its relatively high temporal resolution that is more capable to represent momentarily neuronal activities and therefore connectivities. However, due to EEG's being a surface measurement imaging modality, it is not possible to distinguish signals from inner brain regions.

Analysing the connectivity networks is another important issue. Cole et al. (2010) [14] and Rubinov - Sporns (2010) [15] proposed importance of detection of hub nodes in brain networks in transmission of information. A dysfunction in hub node would cause slower information transmission or loss in some information. As neuronal disorders might be causing dysfunction in such hub nodes, detection of common hub nodes would be important for both diagnosis and treatment. Graph theory is a common name for several brain connectivity analysing techniques which are based on basic statistical calculations over connectivity strengths and node-node neighbouring. Graph theory measures such as clustering coefficient, global efficiency and characteristic path length values change according to the structure of the connectivity network and therefore can be used to distinguish connectivity networks. In 2013, a study by Hosseini et al. used both graph theory and hub node analyses for structural brain connectivity networks [16]. Such combination can correct the results of both methods.

This study aims to show diversities among groups (healthy and dyslexics) by focusing on connectivity maps of brain regions using partially directed coherence (PDC) algorithms applied on EEG data. Graph theory components were used on the connectivity networks to see if there are differences in terms of clustering and

information transmission efficiency. Statistical difference analyses were used to find the variations between different groups or conditions.

1.2. Problem Definition and Purpose of the Study

The main problem is dyslexia's causing negative factors in a child's social and mental development. Therefore, some actions are required to prevent a dyslexic child's experiencing such negative factors. Early diagnosis is required and to early diagnose a brain disorder such as dyslexia, the changes that dyslexia causes in brain should be analysed in detail. Experts of this field can observe patients' behaviours to detect if patients are dyslexic or not. However, using an imaging modality such as EEG to diagnose dyslexic patients by obtaining multivariate time series data would be more effective if dyslexics and control group data could be distinguished with that data. Detection of faulty brain regions would be the ultimate aim, because it enables researches to focus on the distinguishing brain regions in order to create early diagnosis algorithms and methods.

The first step using the multivariate time series data might be the analysing of different brain regions in many aspects such as the communication networks of those regions with other parts of the brain. After revealing the connectivity networks of the brain regions, the next step would be the detailed analysis of the networks found. Graph theory is one of the most commonly used novel methods as its components aim to measure what is the efficiency of the connection network, therefore the speed of information flowing as well as the clustering ratio of information nodes and how do they formed can be found. Measuring those values may reveal differences between dyslexic and healthy brains; or between different conditions.

The purpose of the study is to contribute understanding of dyslexia by performing connectivity analyses to detect the main hub nodes of information flow. Further investigating the connectivity networks using graph theory components to see if there are differences between dyslexic and healthy people. Comparing the values of graph theory measures to see if there are any differences between the pre-stimulus (before stimulus) and reading conditions.

In this study, connectivity networks obtained by using partial directed coherence (PDC) algorithms, graph theory measures were calculated, hub nodes were found and statistical difference analyses were performed. The way of how those methods were used as well as how did the data gathered and pre-processed were described in Chapter 3. Results of the methods were also inserted after each related section in Chapter 3. Discussions were also made in Chapter 3. In Chapter 4, summary of the results with conclusions and comparison with literature can be read. The importance of this study and future work can also be found in Chapter 4. The following purposes will be answered through Chapter 3 and Chapter 4. Note that none of the results can be generalized for all dyslexic patients, but can be concluded and can be reproduced by using same methods, parameters and the data of this study. Purposes of the study are:

- To see if there are differences between control and dyslexic groups by comparing the values of graph theory measures. (Independent groups)
- To see if there are differences between before stimulus and reading state conditions by comparing the values of graph theory measures . (Dependent groups)
- To contribute understanding of dyslexia by performing connectivity analyses to detect the main hub nodes of information flow.

1.3. Why Was EEG Selected as Imaging Modality?

Mostly functional magnetic resonance imaging (fMRI) and positron emission tomography (PET) imaging techniques were used for studies. They provide quite useful results with their good spatial resolutions for analysing specific parts of the brain. However, they lack temporal resolution. On the other side, electroencephalography (EEG) has good temporal resolution with lack of a good spatial resolution. For connectivity analyses, having a good temporal resolution should be vital. Depending on the condition and location, brain neurons fire at rate of 2-1000 Hz [17] [18] [19]. Therefore, using an imaging modality with sampling rate lower than 2 Hz would cause a loss in valuable data. A typical fMRI device has a sampling rate of 0.2 Hz to 2 Hz while a typical EEG device has a sampling rate of 200 Hz to 2000 Hz. Nir et al (2008) also claims that fMRI recording is not suitable for analysing

higher rate of fluctuations [20]. Brain waves such as alpha (8Hz-13Hz), beta (13Hz-40Hz) etc. can only be investigated using an imaging modality having higher sampling rate than their frequency intervals. Therefore, using a fMRI device with 1Hz sampling rate to investigate such frequency waves is nothing but wasting time. All in all, in order to perform true connectivity analyses and frequency band analyses, researchers should use an imaging modality that provides higher sampling rate than the frequency bands that would be investigated.

A basic EEG device costs $200 to $3000 with add-ons [21]. However, the prices of EEG devices for medical purposes may be more expensive. This cost can be affordable compared with a typical MRI device's cost of $300000 to $3 million [22] and a typical PET device's cost of $1.3 million to $3.5 million [23]. So, if it is possible to obtain same or similar results with EEG, it would be better to choose EEG device as imaging modality due to its cost.

For studies with children, it may be hard to keep the child in MRI device due to its closed structure and the noises of magnets during data acquisition. Children are more likely to afraid of MRI device and they tend to move inside the machine. Data recording for fMRI requires the subject to be in closed environment. In contrast, most EEG devices allow an open measurement environment which is essential for children.

As a conclusion, for the studies require not high spatial resolution, using EEG as imaging modality would be wise due to it's easy to use, being a passive non-invasive device, fast data acquisition, not causing anxiety as other devices do and low cost.

1.4. Why Was PDC Selected as Connectivity Estimator Algorithm?

Partial directed coherence (PDC) is a recent technique to obtain connectivity networks of brain by using multivariate signals (see chapter 2.5.4.5 for more details about history and mathematical implementations). PDC algorithm uses combination of other techniques to obtain connectivity networks operating on frequency domain such as directed transfer function (DTF) (see chapter 2.5.4 for detailed information) as well as time domain multivariate estimators: Granger Causality (GC) and multivariate autoregressive models (MVAR). Granger Causality provides directionality information of connections between different datasets [24]. Therefore, direction of

connection makes PDC more suitable to be used for graph theory analyses (See Chapter 2.7).

PDC, by definition, measures only the direct causal relations between two datasets [24]. This property leads PDC to be immune to volume conduction effects. Some studies [25] [26] show PDC is not influenced by volume conduction and hence it can be used with EEG data in which electrode data may include unwanted signal parts of adjacency brain regions which is a result of volume conduction. According to Astolfi et al. (2007), PDC is an accurate functional connectivity estimator for EEG data [24]. However, some other studies [27] [28] showed PDC is eventually affected by volume conduction, but less than other estimators.

PDC analyses of multivariate time series result in directed and weighted connectivity adjacency matrices (see chapter 2.5.4.1) which carry information of the connected brain regions as well as the direction and the strength of the connection. Basic statistical approaches such as correlation and coherence can reveal the connection between two time series, but without the causal or directional information.

Since this study uses multivariate EEG data, requirement of no or less volume conduction, requirement of the directions of information flow for graph theory analyses and being a novel method for connectivity estimation, PDC was chosen to be the estimator for connectivity networks.

1.5. Literature Search

1.5.1. Dyslexia Studies with Brain Connectivity Analyses

The Table 1 includes the studies for connectivity analyses of dyslexia with important results to contribute dyslexia detection with the methods they use.

Table 1 – Literature search for studies which made connectivity analyses to find abnormal brain regions of dyslexic subjects.

Author	**Year**	**Method or Modality**	**Subjects**	**Result**
F. Ramus [29]	2014	Functional connectivity	Opinion paper	Importance of investigation of functional connectivity of temporoparietal area and frontal lobe for dyslexia detection.
Boets et al. [30]	2013	Functional connectivity, fMRI	22 normal readers, 23 adults with dyslexia	
Specht et al. [31]	2009	fMRI, functional connectivity	26 control group children, 26 children at-risk of dyslexia	Pre-reader children show more distributed functional connections especially for left occipitotemporal area and right hemispherical regions. Dyslexics have reduced functional activation in occipitotemporal area.
Raschle et al. [32]	2011	fMRI, functional connectivity	18 dyslexic and 18 control children	Hypoactivation in left temporoparietal and bilateral occipitotemporal area
Vandermosten et al. [33]	2015	DTI, functional connectivity	36 pre readers at risk of dyslexia and 35 healthy subjects without risk of dyslexia	At-risk of dyslexia group has reduced functional connections from occipitotemporal region to frontal regions.

Table 1 (Continued)

Black et. al. [34]	2012	fMRI, voxel based morphometry	51 children (5 to 6 years) at risk of dyslexia	Bilateral prefrontal and left temporoparietal grey matter volumes are associated with dyslexia.
Brown et. al. [35]	2001	MRI, voxel based analysis	16 dyslexic and 14 control	Dyslexics have grey matter reductions in frontal lobe, left temporal lobe and tempoparietoocipital juncture.
Hoeft et al. [36]	2007	fMRI, voxel based morphometry	19 control (age mean = 14.4) and 19 dyslexic (age mean = 14.4)	Dyslexics show hypoactivation in left frontal gyri, left parietal gyri and bilateral fusiform gyri.
Rimrodt et al. [37]	2010	DTI	14 dyslexic and 17 healthy children	Dyslexics show decreased fractional anisotropy in left inferior frontal gyrus and left temporoparietal white matter
Shaywitz and Shaywitz [38]	2005	Review	Review paper	Structural abnormalities for dyslexic groups are located in inferior frontal gyrus and occipitotemporal area.
Hosseini et al. [16]	2013	MRI, Graph theory	Beginner readers aged around 5: 22 with family history, 20 without family history of dyslexia	Dyslexic subjects show structural abnormalities and different connectivity networks in left inferior frontal gyrus and left supramarginal gyrus compared with control group.

Table 1 (Continued)

Vinckenbosch et al. [39]	2005	MRI	10 dyslexic and 14 control	Dyslexics show increased grey matter volume in bilateral precentral gyri and reduced grey matter volume in left inferior temporal gyri and left middle temporal gyrus.
Steinbrink et al. [40]	2008	DTI, voxel based morphometry	8 healthy (age mean = 23.7), 8 dyslexic (age mean = 20.1)	Dyslexics show decreased fractional anisotropy in white matter of bilateral frontotemporal area and left temporoparietal area. Dyslexics also show reduced grey matter volumes in superior temporal gyri.
Cui et al. [41]	2016	MRI, classification	School aged: 33 control, 28 dyslexic	Frontooccipital fasciculus and superior longitudinal fasciculus have different structural connectivity patterns for dyslexic subjects.
Kronbichler et al. [42]	2008	MRI, voxel based morphometry	Age range is 14 to 16: 13 dyslexic and 15 healthy	Less grey matter volume in right supramarginal gyrus, bilateral fusiform gyri and bilateral anterior cerebellum for dyslexic group.
Menghini et al. [43]	2008	fMRI, voxel based morphometry	10 normal readers (age mean = 40.7), 10 dyslexic (age mean = 40.8)	Less grey matter volume in right posterior superior parietal lobule for dyslexic group

Table 1 (Continued)

Clark et al. [44]	2014	MRI	3 MRI sessions with total of 39 controls and 27 dyslexics aged between 6 and 12	Neuroanatomical precursors of dyslexia in reading network are mostly located in primary sensory cortices which is located in the lateral postcentral gyrus of parietal lobe.
Beaulieu et al. [45]	2005	DTI	32 children (age mean = 11.1) with reading skills: 16 average, 12 above average and 4 below average readers	Left temporoparietal area dysfunction may cause reading disabilities for 8-12 years old children
Vandermosten et al. [46]	2016	Structural connectivities, MRI, meta-analysis	Meta-analysis study	Left tempoparietal area plays an important role in development of reading skills.
Deutsch et al. [47]	2005	DTI	14 reader children	Temporoparietal neural pathway is an important area for fluent reading.
Galaburda and Kemper [48]	1979	Longitudinal study	1 Dyslexic: Experiments at ages 13, 14, 15 and 19	Dyslexic subject has asymmetry between left and right parts of planum temporale
Silani et al. [49]	2005	MRI, voxel based morphometry	32 control, 32 dyslexic, aged between 20-30	Left inferior temporal gyri, left middle temporal gyri and left arcuate fasciculus show structural abnormalities for dyslexics.

Table 1 (Continued)

Richards et al. [50]	2008	DTI, tract based spatial statistics	7 control, 14 dyslexic, aged between 30 and 45	Structural connectivity results are consistent with functional connectivity results for the areas: Right frontal gyrus, right middle occipital gyrus, bilateral fusiform gyri, right inferior parietal gyrus and bilateral inferior temporal gyrus.
Krafnick et al. [51]	2011	Voxel based morphometry	11 dyslexic children	Reading training for eight weeks contributes an accelerated increase in grey matter volume in left fusiform gyrus.
Pernet et al. [52]	2009	MRI, voxel based morphometry	38 dyslexic (mean age = 27.25) and 39 control (mean age = 27.83)	Dyslexics show abnormalities in their left superior temporal gyrus and occipitotemporal gyrus.
Richlan et al. [13]	2013	meta-analysis	9 voxel based morphometry studies	Dyslexic group has less gray matter volume in right superior temporal gyrus and left superior temporal sulcus.
Linkersdörfer et al. [53]	2015	Longitudinal study, structural changes over time, MRI	22 normally developing children. Experiments at age means 7.5 and 8.4	Positive correlation between grey matter volume of left superior temporal gyrus and reading development.

Table 1 (Continued)

Wang et al. [54]	2016	Tract specific white matter study	78 healthy children at age between 59 to 150 months	White matter development in arcuate fasciculus is slower for poor-reading children compared with fluent reading children.
Carter et al. [55]	2009	DTI, voxel based morphometry	7 dyslexic and 6 control children aged between 10 to 14	Dyslexics show reduced fractional anisotropy in bilateral superior longitudinal fasciculus.
Frye et al. [56]	2011	DTI, white matter volume comparison	10 poor reader and 20 control (age range is 16 to 33 years)	Structural differences between poor readers and controls in superior longitudinal fasciculus.
Humphreys et al. [57]	1990	Structural, biopsy	3 subjects with difficulty in reading	Dysplasia (abnormal growth of cells) was found in dyslexic brains in left perisylvian regions.
Eliez et al. [58]	2000	MRI on subjects who had PET imaging previously	16 dyslexic and 14 control, aged between 18 to 40	Dyslexics show reduced grey matter volume in their left hemispheres.
Maisog et al. [59]	2008	Meta-study	15 dyslexia studies were investigated	Left inferior frontal area, inferior parietal lobule, left superior temporal gyrus and left ventral regions are underactivated during reading for dyslexics.

Table 1 (Continued)

Richlan et al. [11]	2009	Meta-study, Structural	17 structural dyslexia abnormalities studies	Less activation in left inferior frontal gyrus, left temporoparietal cortex and occipitotemporal cortex and higher activation in left precentral areas for dyslexic group.
Cao et al. [60]	2006	fMRI	14 control, 14 dyslexic children aged between 8 to 14	Underactivation in left inferior frontal gyrus
Booth et al. [61]	2007	fMRI, auditory and visual stimulli	Children aged between 9 to 15: 15 for auditory task and 13 for visual task for both groups	
Richlan et al. [62]	2010	fMRI, reading	18 healthy (age mean = 17.89) and 15 dyslexic (age mean = 18.09)	Overactivations in left precentral area for dyslexic subjects.
Wimmer et al. [63]	2010	fMRI, ortography	19 control, 20 dyslexic aged between 15 to 34	
Rumsey et al. [64]	1997	PET	17 dyslexics and 14 healthy children	

Table 1 (Continued)

Richlan et al. [12]	2011	Meta-analysis study to compare dyslexic adult and children studies	9 dyslexia dysfunctions studies with children (9-11 years old), 9 dyslexia dysfunctions studies with adults (18-30 years old)	Adults with dyslexia have underactivation in their left inferior frontal gyrus, left inferior temporal gyrus, left middle temporal gyrus and left superior temporal gyrus. Children with dyslexia have underactivation in bilateral inferior parietal lobe and left supramarginal gyrus. Both children and adults with dyslexia show overactivation in their left precentral gyrus and underactivation in left fusiform gyrus. Children with dyslexia show left temporoparietal dysfunction while adults with dyslexia show occipitotemporal dysfunction in orthographic task studies.
Yamada et al. [65]	2011	fMRI	5-year-old children	Children who are at-risk of dyslexia have less left temporoparietal area activity.

Table 1 (Continued)

Martin et al. [66]	2016	meta-analysis, functional connectivities	14 english word studies, 14 other languages studies about dyslexic brain abnormalities	Functional abnormalities for dyslexic group focus on left temporoparietal area.
Blau et al. [67]	2010	fMRI, word reading	16 healthy children (age mean = 9.43), 18 dyslexic children (age mean = 9.39)	Dyslexics have underactivation in left superior temporal sulcus during reading task.
Schulz et al. [68]	2009	fMRI	19 control 5^{th} grade, 19 control 2^{nd} and 3^{rd} grade, 19 dyslexic 5^{th} grade children	Underactivation of the left middle temporal gyrus for dyslexic children.
Maurer et al. [69]	2011	fMRI, event related potential data	19 control (mean age = 8.3), 13 dyslexic (mean age = 8.3)	Dyslexic subjects have reduced activation in their bilateral middle temporal area during reading.
Pugh et al. [70]	2000	Meta-analysis study, functional	Functional imaging (fMRI, PET, MEG) studies	Dyslexics have underactivation in left ventral occipitotemporal region during reading.
Schlaggar and McCandliss [71]	2007	fMRI, DTI, Functional changes during reading	Review article	Dyslexics have dysfunctionality in occipitotemporal area.

Table 1 (Continued)

Shaywitz et al. [72]	2007	fMRI	113 dyslexic and 119 control subjects aged between 7 and 18	Dyslexics showed less activation in left anterior lateral occipitotemporal region.
Church et al. [73]	2008	fMRI, reading, developmental study	25 children (age mean = 9.39), 25 adults (age mean = 25.22)	Angular and supramarginal gyrus have decreased activity compared with children
Richlan et al. [13]	2013	meta-analysis of voxel based morphometry studies	9 voxel based morphometry studies about grey matter abnormality for dyslexia	Both functional and structural abnormalities commonly appear in left temporal lobe and occipitotemporal area for dyslexics.

1.5.2. Brain Connectivity Studies with Graph Theory Analyses

Hosseini et al. (2013) [16] used graph theory and network hub analyses on structural brain networks to analyse familial risk for dyslexia in children. They performed the imaging with MRI on 22 children with and 20 children without familial dyslexia history. The hub nodes they found were mostly located on right hemisphere for subjects with familial history of dyslexia. However, main hub nodes for subjects without familial risk of dyslexia were mostly located in left hemisphere. They used statistical difference analysis (t-test) to find differences between graph theory measures between groups. The graph theory measures they have calculated were: Clustering coefficient, characteristic path length and small-world index. However, they failed to find statistical significant differences between groups ($0.12 < p < 0.40$). Huang et al. (2016) [74] combined PDC with graph theory to analyse brain networks for different mental tasks. However, this study had only one group that was healthy group with 19 subjects and two different mental tasks were stimulated. The common graph theory measures they computed with this study were global efficiency and degree (edge size). The most importance of this study is their stating that the global

efficiency measure can be used as characteristic quantity for attentional tasks which is reading task for my study. Therefore, global efficiency is needed to be investigated to compare healthy subjects' results with Huang et. al (2016).

Gonzalez et al. (2016) found lower network integration and communication of dyslexic group than control group with an EEG study [75]. The group sizes were 29 dyslexics and 15 controls. The experiments were performed on reading state. The graph theory measures were found using connectivity networks. One-way ANOVA was used to compare the values of both groups. They conclude that dyslexic group have less efficient network configuration than control group; this means that dyslexic group have lower global efficiency values.

CHAPTER 2

BACKGROUND METHODS

Some theoretical information is located in this section in order to support understanding of reader without putting the reader in need to search for specific terms and information.

2.1. Brain and Neuroplasticity

Central nervous system is made of spinal cord, brain stem, cerebrum and cerebellum [76]. Each part consists of specialized neural cells which are involved in keeping the body homeostasis.

2.1.1. Brain

Brain is the main organ that is regulating the neurologic and hormonal activities. Generally, brain is called for the structure consist of cerebrum, cerebellum, pons, mesencephalon and medulla. Brain is the controlling centre of central nervous system, so, consumes the most energy in percent that body produces. Therefore, requires a constant blood supply.

2.1.2. Cerebrum

Cerebrum is the largest part of the brain and is the main organ of central neural system for mammals [77]. Cerebrum is made of four main parts and they are: Frontal lobe, Parietal lobe, Temporal lobe and Occipital lobe [78].

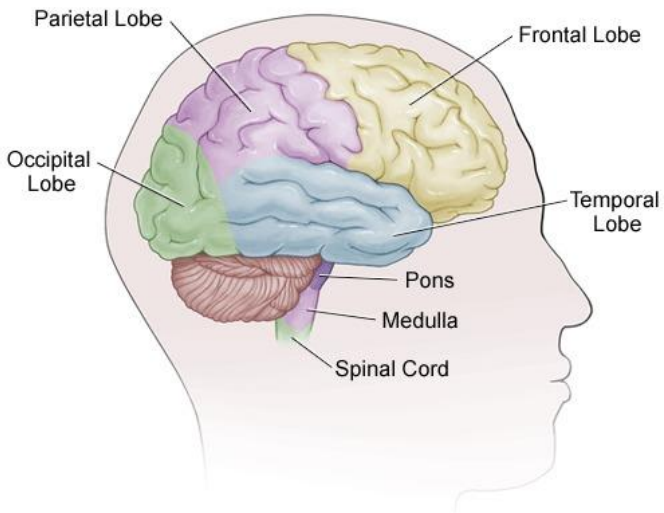

Figure 1 - Main parts of brain. Image was taken from [79]

Frontal lobe contains primary motor cortex which provides coordination of synergistic movements in collaboration with cerebellum [78]. Frontal lobe is also associated with attention, short term memory, planning and motivation [80]. Parietal lobe is the main somatosensory and association cortex, sensory inputs from all over the body passes through the thalamus to parietal lobe [78]. Parietal lobe has also language processing functions as reported by [81]. Temporal lobe plays a role in processing auditory input [82]. Medial temporal lobe located in temporal lobe, involved in long-term memory formation [83]. Occipital lobe is the visual processing centre, consists of primary visual centre and visual association cortex [78].

2.1.3. Gyri and Sulci

Cerebral cortex is made of gyri and sulci. Sulci are the fissures in the surface of the cerebrum. Gyri are ridges on the cerebrum surface. The figure below shows main shapes of gyrus and sulcus.

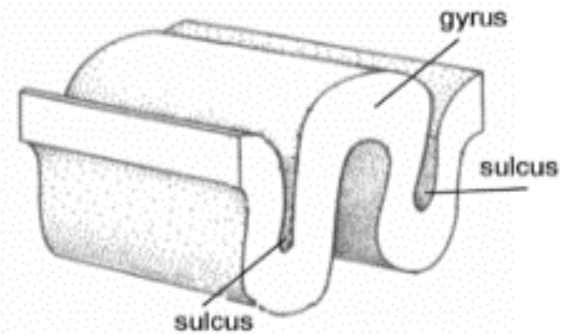

Figure 2 - Illustration of gyrus and sulcus. The image was taken from [84]

The biggest sulcus of cerebrum is interhemispheric fissure (medial longitudinal fissure), separates left and right hemispheres. The image below shows the main sulci and gyri as well as the lobes of cerebrum in a lateral view.

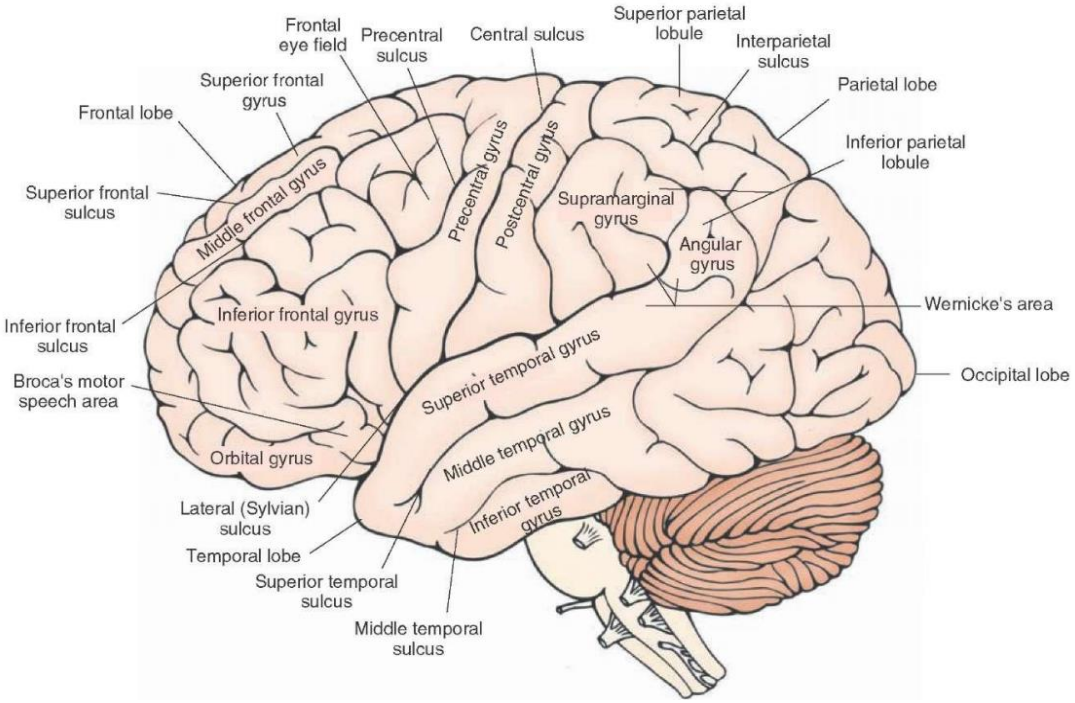

Figure 3 - Main gyri and sulci of the brain. Image was taken from [85]

The important areas for this study are [76] [78] [86]:

- Inferior frontal gyrus: A part of articulatory network which is involved in language processing, speech comprehension and production.
- Broca's area (Brodmann area 44): A part of inferior frontal gyrus involved in speech production and language processing.
- Superior temporal gyrus: Located in the top of temporal lobe, involved in sensation of sound and processing of speech.
- Wernicke's area (Brodmann area 22p): Located in the posterior part of superior temporal gyrus and involved in the comprehension of written and spoken language.
- Middle occipital gyrus: Located on the lateral surface of the occipital lobe which is secondary visual cortex and plays role in detection of visual patterns, word encoding and selective attention.
- Middle temporal gyrus: Middle gyrus of temporal lobe, involved in recognition of patterns and words while reading.
- Arcuate fasciculus: Bundle of axons that bidirectional connects Broca's and Wernicke's areas.
- Supramarginal gyrus: Located in the inferior portion of parietal lobe and plays role in language perception and processing.
- Inferior temporal gyrus: Associated with complex visual processing, object perception and number recognition.
- Angular gyrus: Located on the superior edge of the temporal lobe. Involved in language processes, spatial cognition, attention and memory recognition.
- Occipitotemporal sulcus: Visual word forming area and assumed to be an interface to phonology [87].
- Superior temporal sulcus: Assumed to play role in phoneme awareness [88] and integration of visual and auditory information.
- Left temporoparietal cortex: Considered to be a link between phonological processing and reading [89].
- Planum temporale: A cortical area in sylvian fissure and also forms Wernicke's area. Involved in auditory and language processing.

2.1.4. Neuroplasticity

Brain consists of neurons and clusters of neurons build parts that specialized in different functions. Every part of the brain communicates with each other directly or indirectly. Information flowing from one part should pass different nodes in the brain and the combination of the paths that an information follow makes connectivity maps of the brain. Every task or every connection maps that a person has may change through life due to neuroplasticity [90].

Brain is subjected to have neuroplastic change through organism's life. Activity dependent neuroplasticity causes rather significant neuroplastic changes and they are caused by organism's behaviour, emotions and external stimuli [91]. Neuroplasticity plays important roles in memory formation, learning and brain damage recovery which are important factors and their absence may cause brain disorders. Neuroplastic origins of brain disorders should be investigated for better definition of the disorders.

Brain connectivities are expected to change as a result of neuroplasticity. Therefore, analysing brain connectivity networks would provide information about neuroplasticity behaviour of brain.

2.2. Dyslexia

Approximately 144 million people suffered from brain disorders in Europa in 2010 and their cost was €798 billion according to [92]. Dyslexia was defined in 1989 by British Dyslexia Association as a specific difficulty in learning, spelling or written language [93], however, there are arguments about defining dyslexia [94]. In 1995, Elaine Miles asked if there can be a single definition of dyslexia and suggested, rather than a definition, description would be a better term to use [86]. In 2003, dyslexia were described as a brain disorder, characterized by poor word recognition, poor spelling and decoding abilities [95]. In 2010, Tunmer and Greaney defined dyslexia in four components: (1) persistency literacy learning difficulty, (2) despite to the high quality literacy instruction in (3) typically developing children (4) due to an impairment in the phonological skills required to learn read and write [96].

There are studies showing co-occurrence of some mental disorders such as dyslexia with ADHD [97] [98] [99] and dyslexia with developmental coordination disorder

(DCD) [100]. These co-occurrences may be due to abnormalities in functions of common specific brain areas for both disorders.

2.3. Brain Imaging Modalities

In order to explain what is happening in the brain, we need to know what is in there and how it works. Brain imaging modalities generate data according to the physical properties or activations of neurons by "forward modelling" of the brain. The main aim is to generate best approximate data without harming the organism (non-invasiveness).

2.3.1. Magnetic Resonance Imaging (MRI) – Functional MRI (fMRI)

fMRI is the extended form of MRI to observe functional changes in brain due to neuronal activity. The fMRI principle depends on observation of the excessive blood flow of active neurons. The idea of increasing of blood flow in active brain regions was first proposed in 1890 [101]. Neuronal activity in a brain region causes more blood flow to that part. This leads to rise in the dependency of oxygen in blood. In MRI terminology, it is called as blood oxygen level dependent (BOLD) signal. Red blood cells carry oxygen with the hemoglobin molecule (Hb). Deoxygenated hemoglobin (dHb) is more paramagnetic than oxygenated hemoglobin (oHb). This difference between dHb and oHb changes the raw MR signal to be collected from the body. Therefore, the mapping of the MRI signal in a brain shows which neurons are active at a time [102]. Although MRI imaging provides good spatial resolution, this modality has low temporal resolution. Therefore, using MRI modality for structural imaging which is generally independent of time is a good choice. However, low temporal resolution makes MRI not suitable for causality analyses which requires high temporal resolution.

Diffusion Weighted MRI (DWI): A modified MRI imaging which acquires image according to the contrast generated by diffusion of water molecules. DWI is used especially in tumour detection.

Diffusion Tensor MRI (DTI): Modified MRI that provides image according to the direction of diffusion of water molecules. It is possible to track fibres by using this method.

Figure 4 - A typical MRI device. Image was taken from [103]

2.3.1.1. Diffusion Tensor Imaging (DTI)

DTI is a specialized type of Diffusion weighted MRI (DWI). The scanning principle depends on the contrast generated by the diffusion of water molecules through tissues. DTI is mainly used to map white matter distribution in brain. It allows to examine fibre tract connections, in other words: structural images [104]. Water molecules diffuse faster as the tissue is aligned in the flow direction and slower as the tissue is perpendicular to the molecule flow. Therefore, for different speeds of diffusion, the amount of contrast changes.

The imaging theory of DTI is based on diffusion equation:

$$\frac{\partial \rho(x,t)}{\partial t} = D\nabla^2\rho(x,t) \qquad (1)$$

Where $\rho(x,t)$ is the diffusion concentration which is a function of length and time. D denotes the diffusion coefficient and ∇ stands for derivative.

2.3.1.2. Statistical Parametric Mapping and Voxel Based Morphometry

Statistical Parametric Mapping (SPM) is a technique developed by Worsley-Friston [105]based on the statistical tools such as:
The general linear model (GLM) for statistical estimation,

$$Y = X\beta + \epsilon \quad (2)$$

And random field theory (RFT) [106] for probabilistic statistical inferences. The most commonly used SPM algorithm is named as SPM and can be used following the link: http://www.fil.ion.ucl.ac.uk/.
Voxel-based morphometry (VBM) is a statistical neuroimaging analysis technique providing analysis of regional differences of brain volume images obtained generally by T1-weighted MRI. VBM is a specialized form of SPM that focuses on specified regions instead of whole brain. According to Ashburner-Friston (1999) a typical VBM algorithm based on SPM [107] include the following processes: Spatial normalization, image partitioning into grey and white matter, pre-processing of grey and white matter segments, statistical analysis, segmentation evaluation, evaluation of assumptions, testing the rate of false positives.
VBM is an efficient method to analyse in voxel-level of local grey matter (GM), white matter (WM) volume or density [108]. In 2005, by using voxel based morphometry on the data of 13 control and 13 dyslexic subjects, Eckert et al. suggests that voxel based morphometry results are consistent with DTI results to that time for many brain regions [109].

2.3.2. Positron Emission Tomography (PET)

Positron emission tomography imaging principle is based on the detection of the gamma rays which are emitted by positron emitting tracers. The tracers are injected into the body on several transporter molecules before the scanning. As tracer molecule, generally, fludeoxyglucose is used due to its replacing the glucose molecule which is used in metabolism. The scanner then detects the tracer uptake on regional body parts; therefore, measures metabolic activity on related tissues. As a brain imaging modality, PET can provide functional images proportional to the glucose uptake in different brain regions [110].

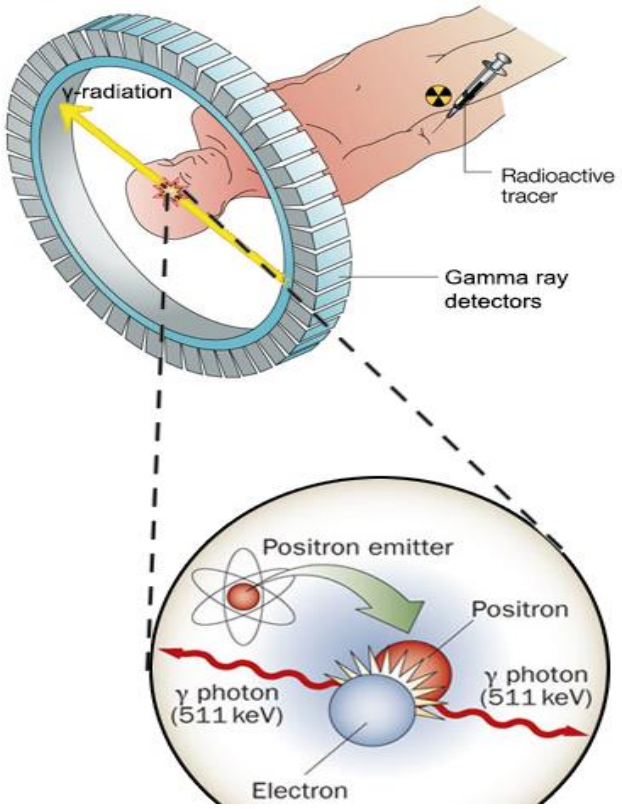

Figure 5 - Working principles of PET imaging. Image was taken from [111]

2.3.3. Functional Near Infrared Spectroscopy (fNIRS)

fNIRS is used to observe hemodynamic responses of brain. The fNIRS principle is based on the application of near infrared (700-900nm) wavelength of light onto tissue. Depending on the hemoglobin (Hb) and deoxyhemogloin (dHb) amount in the tissue, the absorption of the applied light changes. A photodetector measures the amount of scattered light. Both fNIRS and fMRI rely on the hemodynamic responses of tissue and therefore the measures of both methods can be compared.

A typical fNIRS system has sampling rate of 50-100Hz which makes fNIRS a preferable imaging modality to observe functional states of brain. Also its comparable low cost to MRI, again, puts it into advantageous position over fMRI.

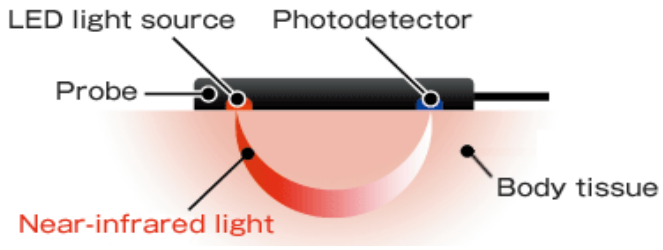

Figure 6 - fNIRS working principle. Image was taken from [112]

2.3.4. Transcranial Magnetic Stimulation (TMS)

Transcranial magnetic stimulation (TMS) is performed by electromagnetic coils which are placed near forehead. They stimulate or inhibit neurons in brain by delivering magnetic pulses.

TMS can be used for both diagnosis and treatment. For diagnosis, it is commonly used to measure brain-muscle interaction strengths. For treatment, several types of TMS are used to suppress effects of some brain disorders such as depression and migraine.

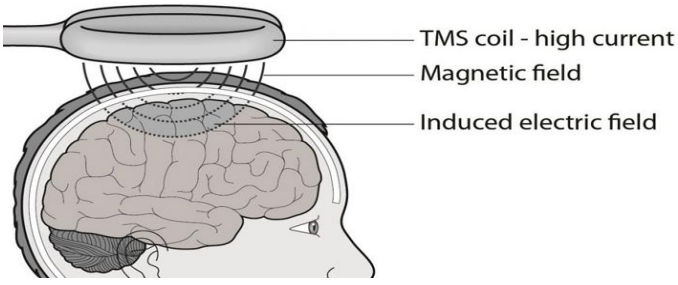

Figure 7 - TMS illustration. Image was taken from [113]

2.3.5. Magnetoencephalography (MEG)

Magnetoencephalography (MEG) is a passive imaging method to observe neuron activity using electromagnetic fields. The electromagnetic fields are generated by ionic current flow of axons and dendrites. MEG has good temporal resolution as well as has sufficient spatial resolution. It has high tolerance to motional artefacts and don't cause operational noises. Therefore, MEG can be a good choice for researches with children. However, having relatively higher cost than EEG, makes it harder to obtain for small research groups.

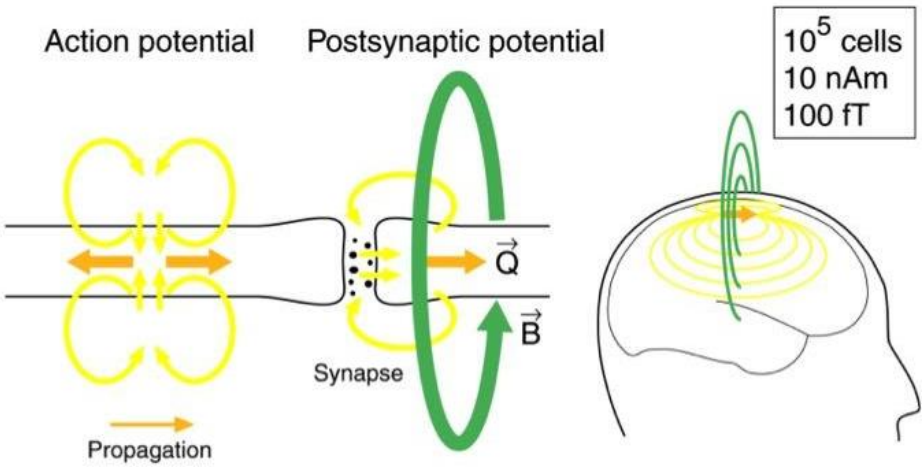

Figure 8 - MEG signal origin. The Image was taken from [114]

2.3.6. Electroencephalography (EEG)

EEG is a method to passively monitor bioelectrical activity of the brain. The monitoring is performed by electrodes which are placed on the predefined locations of scalp. Electrical activities are generated by the inhibitory and exhibitory post-synaptic potentials. The dipole is generated by intrinsic ionic currents of the cortical nerve cells [115]. Typical EEG data consist of voltage versus time measurements from different electrodes that are placed on the fixed standard locations on scalp. The measured voltage is mostly from the electrical activity of surface neurons and a small portion from electrical activity of neurons from deeper regions.

State of art EEG devices provide a good temporal resolution, but without a good spatial resolution. The bad spatial resolution is caused by the volume conduction and the limit

of electrodes that can be placed on the scalp. Large area of the cortical surface contributes to the signal picked up by each electrode. Therefore, adjacent two electrodes may have signal components which are originated from the same location. However, the temporal resolution of about 1000Hz sampling rate, enables to analyse electrical activity of brain in scale of milliseconds. These make EEG, a good imaging modality for brain studies such as brain connectivity [116].

Due to EEG's being a passive measurement method, it is non-invasive. EEG can be the best choice for brain studies which are investigating children brains. Because it allows open area measurement. Not only EEG is a non-invasive imaging method, but also it has low initial device and data acquisition costs.

High temporal resolution also makes EEG one of the important brain imaging modality to observe frequency domain representations. According to Nyquist sampling theorem, the maximum frequency value representation to be calculated uniquely can't exceed the half of sampling rate [117]. Then, ideally, to completely cover the 0-100Hz frequency representations of brain activity, the imaging modality should have at least 200Hz (Practically 400Hz) sampling rate. With higher than 1000Hz sampling rate of state of art EEG devices make EEG a suitable brain imaging modality to investigate higher frequency components of brain activity.

Figure 9 - A commercial EEG device (Nexus EEG)

2.4. Brain Connectivity

Brain connectivity, in general, refers to any interaction between different units or parts in cerebrum. Interactions can be either anatomical connections as structural connectivity or statistical dependencies as functional connectivity or causal relationships as effective connectivity [118]. Importance of brain connectivity researches are increasing since they are trying to reveal how neurons, brain parts or whole brain acts corresponding to any stimulus, condition or while resting.

Almost all central nervous system (CNS) disorders may have specific patterns in connections of brain regions. Most subjects have similar response in their brain connectivities if they have same disorder. Revealing those disorder specific patterns of brain, connectivities may be the key factor to early diagnose those disorders and connectivity can be modelled based on EEG or other imaging techniques.

2.4.1. Structural Connectivity

Structural connectivity provides information of which brain part is physically (anatomically) connected with another by neurons or neuron groups. Some brain imaging modalities such as MRI and DTI can be used to find structural connectivities by brain imaging while dissection can be performed by in-vitro studies to reveal physical structures. Voxel based analyses like morphometry, diffusion or tractography analyses are the most commonly used methods to reveal structural connectivities from brain imaging data.

Structural networks may be useful to detect faulty links between brain parts and may also be used to aid diagnosis of some brain disorders. Dyslexic brains are expected to show different structural networks from healthy brains (see Chapter 2.2).

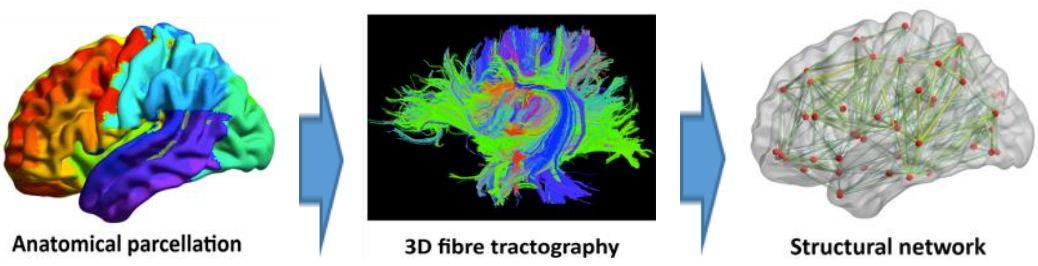

Figure 10 - Obtaining structural connectivity network from brain images. Image was taken from [119] and cropped for better understanding.

2.4.2. Effective Connectivity

Effective connectivity is defined as the causal relationships that different brain units exert over another [3]. Effective connectivity can be observed in multivariate time dependent systems, because it measures the causal influence that a brain unit cause on another brain unit. Brain is capable of performing billions of processes per second and in order not to lose any valuable information from brain activity, we need data with high temporal resolution for effective connectivity estimations. Therefore, the best modality can be used for effective connectivity estimation can be EEG which can provide high temporal estimations for very large range of time intervals. However, there are some methods implemented for imaging modalities with low sampling rate such as dynamical causal modelling (DCM) to produce effective connectivity maps on fMRI data [120]. But, using an imaging modality with low temporal resolution such as fMRI would yield a rough snapshot of effective connectivity.

Most commonly used effective connectivity estimators are Granger causality based directed transfer function (DTF), partially directed coherence (PDC); probabilistic methods such as Bayesian Networks (BN) and Dynamical Bayesian Networks (DBN); Kalman filtering based sliding window estimations; deterministic estimations such as dynamical causal modelling (DCM). These methods are summarized in Chapter 2.5.

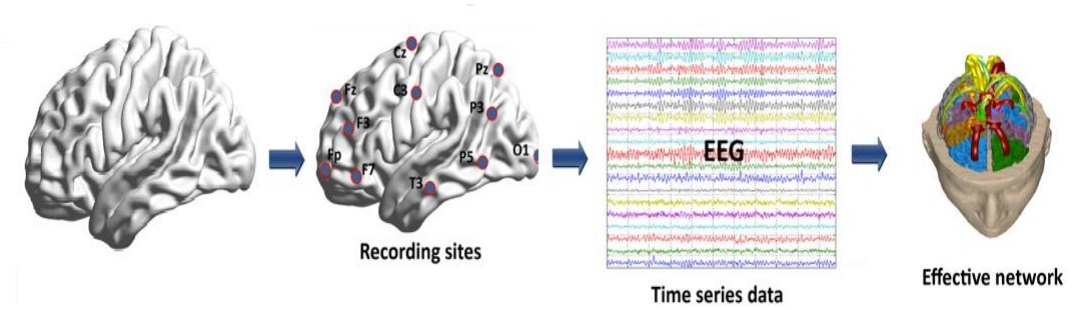

Figure 11 - Obtaining effective connectivity network from brain images. Image was taken from [119] and altered.

2.4.3. Functional Connectivity

Functional connectivity is used for finding the relations between brain regions at specific time slice. Most of the functional connectivity estimation methods (See Chapter 2.5) use statistical dependencies and relations of multivariate time series data.

DTF and PDC are the commonly used functional connectivity estimators (see Chapter 2.5) for time series data analyses, especially for EEG data [4].

Functional connectivity in frequency domain can be estimated by using data with enough sampling rate (See Nyquist theorem). Such functional connectivity maps can be used for spectral analyses of functional networks in brain.

Functional connectivity maps can be used to reveal task-related functional hubs in brain. A Functional hub is a critical region for sustaining information flow between different brain regions for different stimuli. Detecting a hub node for specific stimulus can be useful to reveal the functional activities that the stimulus can cause. Damaged hub nodes may not transmit or cause lag in transmission of the information which is received by the hub node [121]. Any distortion in the transmission line effects functions of whole brain. Brain disorders may cause damage in such hub nodes [121] and detecting those hubs therefore is a critical way to establish diagnosis techniques.

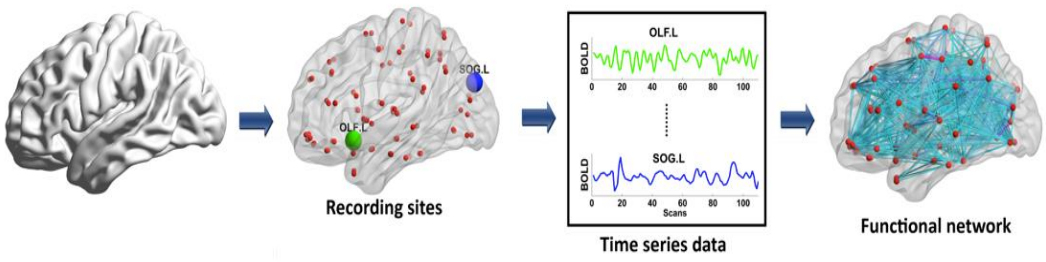

Figure 12 - Obtaining functional connectivity network from brain images. Image was taken from *[119]* and altered.

2.5. Brain Connectivity Estimators and Basics

2.5.1. Connectivity Adjacency Matrix

Connectivity adjacency matrix is a representation of connection values between different brain regions. In a 2D connectivity matrix, generally, columns indicate the connections “from” and rows indicate the connections “to” the nodes. Values of the matrix are generally normalized between 0 and 1. “0” indicates there is no connection and “1” indicates the highest connection value.

Connectivity adjacency matrices are like fingerprints of brain; different for every subject and also different for every condition/stimuli. Therefore, in order to reveal responses of brain to different stimuli, numerous connectivity adjacency matrices should be investigated by many methods [74].

An adjacency matrix can be weighted, unweighted; directed and undirected [16]. Weighting indicates the magnitude of connection. An unweighted matrix means that the values were discretized to have values of only 0's and 1's. On contrary, a weighted matrix can have all the values between 0 and 1 which indicate the connection strength. An undirected matrix is symmetric and represents the connections between nodes without indicating the connection direction. Oppositely, a directed matrix is generally not symmetric and contains the information of connection directions [9] (See Figure 13).

TO

	1	2	3	4	5	6	7	8	9	10	11	12	13	14
1	0	0	0	0	1	0	0	0	0	0	1	0	**1**	0
2	0	0	0	0	1	**1**	1	1	0	0	0	0	**1**	0
3	0	0	0	0	0	**1**	0	**1**	**1**	0	1	0	**1**	0
4	0	0	1	0	0	0	0	0	0	0	1	0	0	0
5	0	1	1	0	1	0	0	0	1	0	0	0	**1**	0
6	0	0	0	**1**	0	0	0	0	1	0	0	0	**1**	0
7	0	0	0	0	0	0	0	0	1	1	0	0	0	1
8	0	0	0	0	0	0	1	0	0	0	0	0	0	0
9	0	0	0	0	0	0	0	1	0	0	0	0	0	1
10	0	0	0	0	0	0	1	0	0	1	0	1	0	1
11	0	0	0	0	0	0	0	0	0	0	0	0	0	0
12	0	0	0	0	0	0	0	0	0	1	0	1	0	0
13	0	0	1	0	0	0	0	0	0	0	0	0	0	0
14	0	0	0	0	0	0	0	0	1	0	0	1	0	1

FROM

Figure 13 - A brain connectivity adjacency matrix; unweighted and directed. The value 1 in bold square indicates the connection from region 8 to region 3.

2.5.2. Granger Causality

Granger Causality was first introduced in 1969 to explain causal relations between econometric models [122]. Granger causality proposes that if some series Y(t) contain information in their past terms to predict the behaviour of series X(t), then series Y(t) are said to cause X(t) [123].

Let X(t) be a series that can be predicted from its p discrete past values with a mean square prediction error e_1, then X(t) can be written as:

$$X(t) = \sum_{j=1}^{p} \left(A_{11}(j)X(t-j)\right) + e_1(j) \tag{3}$$

Using discrete p previous values of series X and Y and a mean square prediction error e_2(j), the series X(t) can also be written as:

$$X(t) = \sum_{j=1}^{p} \left(A_{11}(j)X(t-j)\right) + \sum_{j=1}^{p} \left(A_{12}(j)Y(t-j)\right) + e_2(j) \tag{4}$$

According to the Granger causality principles, if var(e_1) > var(e_2), then series Y(t) cause series X(t). Where var(e_1) indicates the variance of the prediction error of original autoregressive model in Equation (3) and var(e_2) is the variance of the prediction error of Equation (4).

Granger causality index is a bivariate estimator that is operating in time domain and can be calculated as:

$$GCI_{1\to2} = \ln\left(\frac{var(e_1)}{var(e_2)}\right) \tag{5}$$

Where $GCI_{1\to2}$ is the Granger Causality index from first to second process and due to natural logarithm definition, its value can only be positive. The higher the value of Granger Causality index, the more the relation becomes causal.

2.5.3. Multivariate Autoregressive Model

Multivariate autoregressive models (MVAR) are generalized form of Granger causality for more than two time series, introduced in 1980 [124]. According to MVAR, a multichannel dataset with m channels $\mathbf{X}(t)$ where $\mathbf{X_1}(t),\ldots,\mathbf{X_m}(t)$ are time series data of different channels, can be represented as:

$$\mathbf{X}(t) = (\mathbf{X^{(1)}}(t), \mathbf{X^{(2)}}(t),\ldots, \mathbf{X^{(m)}}(t))^T \tag{6}$$

Then the MVAR model of each channel $\mathbf{X_i}(t)$ can be written in terms of coefficient matrix $\mathbf{A}(j)$ with sized (m x m), past values of time series $\mathbf{X}(t - j)$ with size (m x 1) and white noise representation $\mathbf{e}(t)$ with size (m x 1):

$$\boldsymbol{X}(t) = \sum_{j=1}^{p} (\mathbf{A}(j)\mathbf{X}(t-j)) + \boldsymbol{e}(t) \tag{7}$$

Where A(j) is the matrix containing the j^{th} order autoregressive model parameters (see Chapter 2.5.3.1 for calculation of A(j)). The number "p" indicates the model order of MVAR model.

There are several methods to find the model order "p". Generally Akaike Information Criteria (AIC) [125] is used to find the value of p for long multivariate datasets [24] [126]. According to AIC, the following formula is used to find model order "p":

$$\mathrm{AIC}(p) = \ln\left|\tilde{\Sigma}(p)\right| + \frac{2}{\hat{T}} pm^2 \tag{8}$$

Where $\tilde{\Sigma}$ is the estimated noise covariance of MVAR model for the value p. m is the number of channels and $\hat{T}$ is the number of data samples to fit the model [127]. The model order "p" is selected such as AIC(p) takes minimum value:

$$p_{selcted} = \arg\min_{p} AIC(p) \tag{9}$$

After a p value is selected, the next step of MVAR algorithm is to generate a valid multivariate autoregressive (MVAR) model by calculating the coefficients. This process is called as MVAR model fitting.

2.5.3.1. Multivariate Autoregressive Model Fitting

MVAR model fitting is the calculation of model coefficient matrix $\mathbf{A}(j)$ of an MVAR model (see Equation (7)). First of all, in order for a model to be able to be fitted, the inequality

$$n > m^2 p \tag{10}$$

should be satisfied [127]. In this inequality, n is the number of samples of a channel data (total samples per trial times number of trials), m is the number of channels and p is the model order. However, to be sure about having an unbiased and consistent MVAR model, [128] suggests that we would require 10 times more data samples for a better fitted model such as:

$$n > 10 * (m^2 p) \tag{11}$$

There are several MVAR model fitting methods. One of them, Vieira-Morf algorithm is a parametric autoregressive model fitting method and uses a multichannel non-least-squares lattice approach to estimate model coefficients [129]. Since Vieira-Morf algorithm is claimed to be estimating coefficients more accurately than other autoregressive model fitting methods and its being more suitable for multivariate data analyses according to Schlögl and Supp (2006) [130], Vieira-Morf algorithm was selected as a MVAR model fitting algorithm for this study.

Estimation of coefficients matrix A(j) of an MVAR model (see Equation (7)) by Vieira-Morf algorithm uses the following calculations [131]:

$$\widehat{\boldsymbol{A}} = \arg\min_{A} tr[(\boldsymbol{X} - \boldsymbol{AZ})' \sum^{-1} (\boldsymbol{X} - \boldsymbol{AZ})] \tag{12}$$

Where "tr" indicates the trace of the matrix, $\boldsymbol{Z} = \boldsymbol{X}(t-j)$ and "j" takes values from 1 to p where p is the model order. $\sum^{-1}$ indicates the inverse of the covariance matrix of noise. " ^ " operator indicates the estimated value of related variable. " $'$ " denotes the transpose operator. **X** is the raw dataset with channels m and samples n.
Using least squares estimator, Equation (12) can be rewritten as [126]:

$$\widehat{\boldsymbol{A}} = \boldsymbol{X}\boldsymbol{Z}'(\boldsymbol{Z}\boldsymbol{Z}')^{-\mathbf{1}} \tag{13}$$

In order to estimate model coefficients matrix as above, parameter of **Z** = **X**(t-p), t should be defined. Here, t is the total number of samples (time variant) of sliding window. The sliding window method has two parameters: Window length(t) and step size. For every step that window slides, a coefficient matrix $\widehat{\boldsymbol{A}}$ is estimated. If the window length was taken as the total sample size (n), then step size becomes trivial. This is due to the algorithm's calculating only one model coefficient matrix for whole samples of data.
According to Baccala and Sameshima (2001) [132], the frequency domain representation of $\mathbf{A}_{ij}(t)$ is $\mathbf{A}_{ij}(f)$ where i is the row and j is the column index and computed as follows for each discrete frequency values:

$$\mathbf{A}_{\boldsymbol{ij}}(f) = \begin{cases} 1 - \sum_{r=1}^{p} \boldsymbol{A}_r(i,j)e^{-i2\pi fr}, if\ i = j \\ -\sum_{r=1}^{p} \boldsymbol{A}_r(i,j)e^{-i2\pi fr}, otherwise \end{cases} \tag{14}$$

Some connectivity estimators such as partial directed coherence (PDC) directly uses $\mathbf{A}_{\boldsymbol{ij}}(f)$ to estimate connection networks (See chapter 2.5.4). However, some other estimators such as directed transfer function (DTF) (See chapter 2.5.5) uses the transfer function of the system, **H**:

$$\mathbf{H} = \mathbf{A}^{-\mathbf{1}}(f) \tag{15}$$

which contains all relation information between each data samples [123]. The error representation e(t) from Equation (7) is converted into frequency domain using Z transform:

$$\mathbf{e}(f) = \mathbf{A}(f)\mathbf{X}(f) \tag{16}$$

Then,

$$\mathbf{X}(f) = \mathbf{H}(f)\mathbf{e}(f) \tag{17}$$

As in Equation (15), $\mathbf{A}^{-1}(f) = \mathbf{H}(f)$ and $\mathbf{H}(f)$ indicates the transfer function of the system. $\mathbf{H}(f)$ is not a symmetrical matrix. Therefore, it can be used to find causal relations between channels of the multivariate dataset.

After the model coefficient matrix $\widehat{\boldsymbol{A}}$ is estimated, the next step is to validate the fitted model.

2.5.3.2. Multivariate Autoregressive Model Validation

Model validation is the testing of the fitted model in terms of whiteness, consistency and stability for each window of fitted MVAR model. A good model should pass all those tests. However, Equation (10) should be satisfied for those test to be applied properly. The inequality in Equation (10) can only be correct when there are sufficient data samples. If the data length is low, then, to perform validity tests, MVAR model order or the number of channels should be reduced.

The validation tests assume each of the sliding window data to be wide sense stationary (local WSS). However, for biological signals, wide sense stationarity can only be achieved within windows which have similar data behaviours. Similar data behaviours may occur for "no stimulus" (before stimulus) condition.

The following subsections explain the validation tests of the generated MVAR model.

2.5.3.2.1. Whiteness Test

Whiteness as a term, originated from white frequency which means having all frequency components equally, without any correlation. In other words: totally random. The better the model fitted, the smaller and more uncorrelated (more white) the residuals become. Considering the Equation (7), the general form of linear system of equations is:

$$\boldsymbol{Y} = \boldsymbol{AZ} + \boldsymbol{U} \tag{18}$$

"n" being the sample size, "m" being the channel size and "p" being the model order, in Equation (18), $\mathbf{Y} = [\mathbf{Y}(p+1) \ldots \mathbf{Y}(n)]$ is the [m x (n-p)] sized matrix indicating the complete dataset. $\mathbf{A} = [\mathbf{A}(1) \ldots \mathbf{A}(p)]$ is the m x (pm) sized coefficients matrix (See Chapter 2.5.3.1), $\mathbf{U} = [\mathbf{U}(p+1) \ldots \mathbf{U}(n)]$ is the m x (n-p) error matrix and $\mathbf{Z} = [\mathbf{Z}_1^T \ldots \mathbf{Z}_p^T]^T$ where $\mathbf{Z}_j$ is $\mathbf{Z}(p+1-j) = [\mathbf{Y}(p+1-j) \ldots \mathbf{Y}(n-j)]$ and j ranges from 1 to p. Using the estimated value of coefficients matrix $\widehat{\boldsymbol{A}}$ in Equation (18), the estimated error matrix (residuals) becomes:

$$\widehat{\boldsymbol{U}} = \widehat{\boldsymbol{A}}\boldsymbol{Z} - \boldsymbol{Y} \tag{19}$$

Recall Equation (13) for estimated coefficient matrix $\hat{A}$ in place of A in Equation (18). Then $\hat{U}$ becomes:

$$\widehat{\boldsymbol{U}} = \boldsymbol{XZ}'(\boldsymbol{ZZ}')^{-1}\boldsymbol{Z} - \boldsymbol{Y} \tag{20}$$

The main aim is to minimize the correlation between residuals of estimated error matrix $\widehat{\boldsymbol{U}}$. Residuals are the columns of $\widehat{\boldsymbol{U}}$. In this study, autocorrelation function (ACF) was used to test the residual correlations. For stationary processes, ACF measures the dependencies between residuals ($\widehat{\boldsymbol{U}_t}$) in terms of the lag "h" value where $\widehat{\boldsymbol{U}_t}$ indicates the t'th column of $\widehat{\boldsymbol{U}}$ of Equation (20). The AFC of a residual matrix $\widehat{\boldsymbol{U}}$ can be found by dividing the autocovariance value of $\hat{U}$ up to lag "h" (γ(h)) by the autocovariance value at zero lag (variance) (γ(0)). The Equation (21) below is the formulation for ACF which results in a normalized value between 0 and 1. The value "1" indicates the residuals are completely white while "0" indicates the complete dependency.

$$\rho(h) = \frac{\gamma(h)}{\gamma(0)} \tag{21}$$

The Equation (21) can be extended as:

$$\rho(h) = \frac{Cov(\widehat{\boldsymbol{U}}_{t+h}, \widehat{\boldsymbol{U}}_t)}{Cov(\widehat{\boldsymbol{U}}_{t+0}, \widehat{\boldsymbol{U}}_t)} = \frac{E[(\widehat{\boldsymbol{U}}_{t+h} - \mu)(\widehat{\boldsymbol{U}}_t - \mu)]}{E[(\widehat{\boldsymbol{U}}_{t+0} - \mu)(\widehat{\boldsymbol{U}}_t - \mu)]} \tag{22}$$

where E[] indicates the estimated value operator and μ is the mean value of $\widehat{\boldsymbol{U}}_t$.
The test uses χ^2 (Chi-Square) distribution under null hypothesis which assumes the data distribution is uncorrelated (white) as long as the inequality in Equation (23) is satisfied.

$$\rho(h) > \chi^2_{1-\alpha} \tag{23}$$

Where $\rho(h)$ is the test statistic and α is the significance level. Significance level (α = 0.05) represents the probability of null hypothesis rejection of a normal distribution. Since whiteness test uses significance level (α) as 0.05, whiteness test values should exceed 95%, in order to say the model is "white".

2.5.3.2.2. Consistency test

Consistency can be defined as the uniformity of the smaller parts of a MVAR model. Consistency is measured as percent consistency (PC) which gives the portion of the correlation structure of raw data which has been fitted by the MVAR model [128].
With the estimated components of MVAR model (See Chapter 2.5.3.1) i.e. using $\widehat{\boldsymbol{U}}$ and $\widehat{\boldsymbol{A}}$ in Equation (18), a pseudo dataset is generated having same dimensions with original raw data. Then for both real and pseudo datasets, all auto-correlations and cross-correlations between matrices were calculated up to a lag value (h). The lag value was set to be equal to the model order for this study. Then, the percent consistency value can be found by the following formula:

$$PC = 100 * \left(1 - \frac{\|R_p - R_r\|}{\|R_r\|}\right) \tag{24}$$

Where PC indicates the percent of consistency, R_p is the correlation matrix of estimated coefficients of MVAR model, R_r is the correlation matrix of real dataset and $\|.\|$ denotes the L_2 norm.
The higher the PC value, the higher the similarity between the correlation structures of modelled and real data becomes. Delorme et. al (2011) suggests PC > 85% for a good model [128]. However, this ratio can only be achieved by using long samples of data and with large sample sizes. According to Cronbach's alpha [133] reliability test, the consistency value acceptance table is as follows [134]:

Table 2 – Percent Consistency acceptance table according to Cronbach's alpha reliability test.

Cronbach's alpha (PC)	Consistency
PC ≥ 90	Excellent
90 > PC ≥ 80	Good
80 > PC ≥ 70	Acceptable
70 > PC ≥ 60	Questionable
60 > PC ≥ 50	Poor
50 > PC	Unacceptable

2.5.3.2.3. Stability test

Stability of the fitted model means that the model is locally stationary in sliding time windows (see Chapter 2.5.3.1 for sliding time window) [25]. Most of the statistical analyses assume the data are stationary. Hence, the variances in specified windows of data are not expected to be changing over samples. To check if the generated MVAR model was stable, all the eigenvalues of the estimated coefficient matrix (see Equation (13)) should have modulus (See Equation (25)) smaller than 1 [127]. In order to check if this condition held, the largest eigenvalue can be put into modulus equation:

$$SI = \ln|\lambda_{max}| \tag{25}$$

Where SI is the stability index value and λ_{max} is the largest eigenvalue of estimated coefficient matrix $\widehat{\boldsymbol{A}}$. According to this equation, the MVAR model is stable only when "SI" is smaller than 0 (where $\lambda_{max} < 1$). So, an MVAR model is acceptable when it is stable.

2.5.4. Partial Directed Coherence (PDC) Estimation

Defined first in 2001 by Baccala and Sameshima [132] using the formulations depending on the MVAR model (see Chapter 2.5.3). According to Astolfi et. al (2007) PDC has better accuracy in generating connectivity networks and discriminating direct information flows from indirect flows compared with other connectivity estimation

methods [24]. As defined by Baccala and Sameshima (2001) [132], using MVAR model coefficient matrix $\boldsymbol{A}(f)$ (See Equation (14)) directly, the Partial Directed Coherence formula can be written as:

$$PDC_{ij}(f) = \frac{\boldsymbol{A}_{ij}(f)}{\sqrt{\boldsymbol{A}_j^*(f)\boldsymbol{A}_j(f)}} \tag{26}$$

Where $\boldsymbol{A}_{ij}(f)$ is ith row and jth column and $\mathbf{A}_j$ is the jth column of MVAR coefficient matrix in frequency domain. $PDC_{ij}(f)$ gives the connection strength from the node j to i. PDC value of closer to zero means there is less direct causal influence and vice versa for values getting closer to 1.

Apparently, PDC calculation is performed in frequency domain. But, since no autocorrelation or variance values were used in calculations, it has no direct relation with power spectrum. The denominator part of the formula normalizes the PDC value of a sink channel "i". PDC only calculates the direct relationships between nodes j and i, without considering other nodes [24].

PDC is a multivariate approach and that enables it to be used in analyses of multichannel data such as EEG [135]. Main PDC formula (Equation (26)) is operated in frequency domain. Therefore, the calculations are frequency variant. However, using MVAR modelling on time domain makes PDC also time variant. Thus, PDC values may change through time and frequency.

Similar to PDC, partial coherence (PC) can also be used as a connectivity estimator. Using the transfer function $\boldsymbol{H}(f)$ from Equation (15), and error matrix $\boldsymbol{e}(f)$ from Equation (16), it is possible to define the power spectra **S**(f) as:

$$\boldsymbol{S}(f) = \boldsymbol{H}(f)var(\boldsymbol{e}(f))\boldsymbol{H}^*(f) \tag{27}$$

Where $\mathbf{H}(f) = \mathbf{A}^{-1}(f)$, variance of the Fourier Transform of noise matrix **e**(t) represented by var(**e**(f)) and * denotes the complex conjugate transpose operation. From this equation, coherence which expresses the simultaneous activation of channels i and j can be calculated as:

$$Coh_{ij}(f) = \frac{|\boldsymbol{S}_{ij}(f)|^2}{\boldsymbol{S}_{ii}(f)\boldsymbol{S}_{jj}(f)} \tag{28}$$

Simultaneous activation of channels i and j results in a symmetric coherence matrix. Using the symmetric coherence matrix, partial coherence can be calculated by considering minors of $\mathbf{S}_{ij}(f)$ values, $\mathbf{M}_{ij}(f)$:

$$PC_{ij}(f) = \frac{\boldsymbol{M}_{ij}(f)}{\sqrt{\boldsymbol{M}_{ii}(f)\boldsymbol{M}_{jj}(f)}} \tag{29}$$

Earlier studies [25] [123] claimed that DTF and PDC weren't affected by volume conduction and suggested that performing excessive pre-processing is unnecessary. However, a recent study [28] shows that DTF results are affected by volume conduction. From their claim, it can be concluded that PDC may also be in condition of volume conduction.

2.5.5. Directed Transfer Function (DTF)

First introduced by Kaminski and Blinowska in 1991 [136] and derived from Granger Causality.

The unnormalized directed transfer function (DTF) is simply the power of transfer function found in MVAR calculations (Equation (15)) for specific frequency values:

$$\boldsymbol{\theta}_{ij}(f) = \boldsymbol{H}_{ij}(f) \tag{30}$$

In order to be able to compare results, normalization is required. The normalized DTF was defined by dividing DTF value of a channel by the total of outgoing DTF values from that channel. In other words, the normalized DTF is a representation for the ratio of the DTF between two channels to one channels total DTF. Then, normalized DTF can be formulated as:

$$DTF_{ij}(f) = \frac{\boldsymbol{H}_{ij}(f)}{\sqrt{\sum_{j=1}^{N} \left|\boldsymbol{H}_{ij}(f)\right|^2}} \tag{31}$$

DTF_{ij} includes both direct and indirect relations unlike PDC. However, this property of DTF corrects the results of [28] which claims that DTF is affected by volume conduction. Therefore, DTF may result in wrong connectivity results when channels are close to each other.

2.5.6. Dynamic Bayesian Networks (DBN)

DBN algorithms are first developed in early 1990s for forecasting researches by Dagum et al. [137] using Bayesian Algorithms (BN). Computations mainly depend on probabilistic calculations of effective connectivity between two time slices of each channels time series data. Each connection between two different channel at different time slices are represented by the magnitude of probability in range from 0 to 1 which indicates the probability that a channel at state t has causal influence on different channel at state t+1. Therefore, it can be said that DBN algorithms can be used to build probabilistic temporal networks.

In 2006 Smith et al. [82] published a study involving application of DBN algorithm on EEG data first time. Later on many studies were conducted on neuroscience using DBN algorithms [138]. DBN maps represent discrete time stochastic processes for each channel time series data X(t):

$$\boldsymbol{X}(t) = (\boldsymbol{X}(t)^{(1)}, \boldsymbol{X}(t)^{(2)}, \dots, \boldsymbol{X}(t)^{(\mathrm{m})}) \tag{32}$$

There are some assumptions to be made in order to perform DBN calculations. For example, the data is assumed to be stationarity which claims that causal relations don't depend on t. States on time slices are assumed to be observed or partially observed and process is assumed to be first order Markovian transition model i.e. [138]:

$$p(\boldsymbol{X}(t)|\boldsymbol{X}(t-1), \dots, \boldsymbol{X}(1)) = p(\boldsymbol{X}(t)|\boldsymbol{X}(t-1)) \tag{33}$$

Then, taking MVAR process into account, the probabilities which a channel's different time slices have causal influence on itself or other channels activities:

$$p(\mathbf{X}_{\mathrm{i}}(1),\ldots,\mathbf{X}_{\mathrm{i}}(t)) = p(\mathbf{X}_{\mathrm{i}}(1))\prod_{i=1}^{n}\prod_{j=1}^{t}\prod_{t=1}^{t} p(\mathbf{X}_{\mathrm{i}}(t+1)\,|\mathbf{X}_{j}(t)) \qquad (34)$$

Where $\mathbf{X}_{\mathrm{i}}(t)$ and $\mathbf{X}_{\mathrm{j}}(t)$ indicates arbitrary channel time series data as i and j refer to channel number and t refers to the time slice number. The following figure is an example of a dynamic Bayesian network representation for 14 channel EEG data.

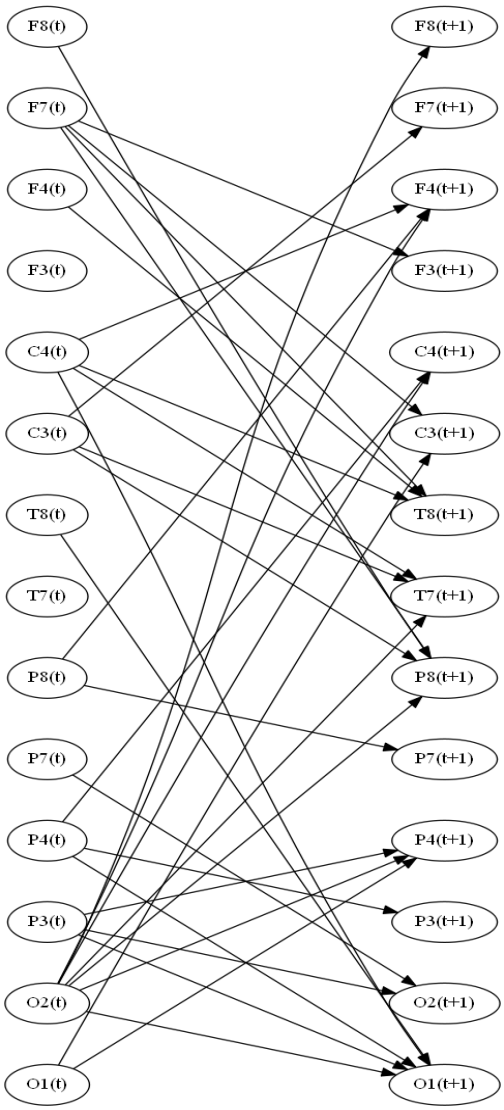

Figure 14 - An example of two time slices DBN effective connectivity map for 14 channel EEG data.

2.5.7. Dynamic Causal Modelling (DCM)

For effective connectivity analyses, DCM is a common method used with generally MRI based modality data. First developed by K.J. Friston et.al in 2003 [139]. This method theoretically computes many effective connectivity maps and selects highest probable one through estimation [140].

Computation process involves bilinear model as in the formula:

$$\dot{\boldsymbol{z}} = (\mathbf{A} + \sum_{j=1}^{k} \boldsymbol{u}_j \boldsymbol{B}^j)\boldsymbol{z} + \boldsymbol{C}\boldsymbol{u} \tag{35}$$

Here, **A** indicates the effective connectivity matrix, $\mathbf{u}_j$ is system input, $\mathbf{B}^j$ stands for the matrix of external modulation of connectivity, **C** is for direct inputs to neuronal activity states (**z**). With such parameters, DCM model provides information about future neuronal activity $\dot{\boldsymbol{z}}$ by using previous states of neuronal activities (**z**) through building effective connectivity maps between two temporal states.

2.6. Analyses of Statistical Difference Between Two Groups of Samples

t-test is a parametric test which aims to determine whether group means are significantly different ($p \leq 0.05$) by comparing group means of two independent or dependent groups, relative to group variances. t-test is a parametric method which assumes the variances of two groups are equal to each other [141].

Assuming the following null (H_0) and alternative (H_1) hypotheses:

$$\begin{aligned} H_0&: \mu_1 = \mu_2 \text{ ("Population means are equal")} \\ H_1&: \mu_1 \neq \mu_2 \text{ ("Population means are not equal")} \end{aligned} \tag{36}$$

where μ_1, μ_2 refers to the population means of first and second groups, respectively, and assuming variances are not equal according to Levene's test:

$$H_0: \sigma_1^2 - \sigma_2^2 = 0$$
$$H_1: \sigma_1^2 - \sigma_2^2 \neq 0 \quad (37)$$

If the variances are equal i.e. H_0 accepted and $p > 0.05$: parametric t-test can be used. If variances are not equal non-parametric tests should be used. In this cases, for independent groups Mann-Whitney U-Test can be used; similarly, for dependent groups Wilcoxon Signed Rank Test can be used [141].

2.6.1.1. Difference Between Two Independent Groups: Independent Samples t-Test and Mann-Whitney U-Test

Independent samples t-test was used to find the difference between means of two independent datasets. The independent datasets, ideally, are expected to have no correlation between any random pair of variables, one from each dataset. For example: Male and female; experimental and control.

For independent groups which have been assumed to have statistically equal variances, t-test can be used to find statistical differences. Considering σ_1^2, σ_2^2 are variances μ_1 and μ_2 are mean values, n_1 and n_2 are sample sizes for groups 1 and 2 respectively, the test statistic t (t-value) can be calculated as [141]:

$$t = \frac{\mu_1 - \mu_2}{\sqrt{\frac{\sigma_1^2}{n_1} + \frac{\sigma_2^2}{n_2}}} \quad (38)$$

The Equation (38) results in the test statistic t which is the normalization of difference between mean values with respect to sums of variances divided by sample sizes. See Chapter 2.6.2 for p-value calculation using t-value.

For independent groups which have statistically different variances, instead of t-test, a non-parametric Mann-Whitney U-Test can be used. Considering n_1 and n_2 are sample sizes and R_1 and R_2 are the sum of the ranks for groups 1 and 2 respectively, the test statistic U value of first group can be found as [141]:

$$U_1 = R_1 - \frac{n_1(n_1 + 1)}{2} \tag{39}$$

Similarly, for second group:

$$U_2 = R_2 - \frac{n_2(n_2 + 1)}{2} \tag{40}$$

The calculation of values R_1 and R_2 can be done by, first combining both groups' samples and giving the ranks starting from 1 to total sample size to each sample. The smallest sample value takes the rank of 1 and it continues till all the samples have a rank. For p-value calculation, the smallest of U value is used (See Chapter 2.6.2).

2.6.1.2. Between Two Dependent Groups: Paired Samples t-Test and Wilcoxon Signed Rank Test

Paired samples t-test is used to compare two, dependent data sets which have statistically equal variances. The data are generally collected from same subjects for different conditions or time intervals. The two dependent datasets are expected to have correlation and for this reason the two datasets should have same sample sizes. For example, pre-test and post-test.

Since the two datasets are dependent, they have same variable for different conditions. Then, the difference between two paired sample can be calculated. Let D be the difference vector between two dependent datasets with samples d_i (indicating the difference between i^{th} pair of two datasets), then $D = [d_1 \dots d_n]$, where n is the size of a dataset.

For groups with statistically equal variances, the t-test statistic "t" (t-value) can be found by using the formula below:

$$t = \frac{\bar{d} - 0}{\hat{\sigma}/\sqrt{n}} \tag{41}$$

Here, $\bar{d}$ is the mean of the difference vector D, $\hat{\sigma}$ is the standard deviation of the difference vector D and n is the sample size of D. See Chapter 2.6.2 for p-value calculation using t-value.

For groups with statistically not equal variances, a non-parametric, Wilcoxon Signed Ranks Test can be used. The test statistic W can be calculated as [141]:

$$W = \sum_{i=1}^{n_r} \left[sgn\left(\mathrm{x_{1,i}} - \mathrm{x_{2,i}}\right) R_i \right] \tag{42}$$

Where $x_{1,i}$ and $x_{2,i}$ are samples of groups 1 and 2 respectively, n_r is the reduced sample size and can be found by removing the same magnitude pairs of samples from both groups such as $\left|\mathrm{x_{1,i}} - \mathrm{x_{2,i}}\right| = 0$. sign () is the sign function and R_i is the rank sum. Calculation of rank sum (R_i) is same as explained in Chapter 2.6.1.1.

To calculate p values from Wilcoxon Signed Ranks Test statistic, z values are calculated using the formula [141]:

$$z = \frac{W}{\sqrt{\frac{n_r(n_r+1)(2n_r+1)}{6}}} \tag{43}$$

Using the critical z distribution table, p-values can be found.

2.6.2. Calculation of p-values

Now, observed t-value can be calculated using the t-value of Equation (38). According to the t distribution critical values table, the calculated t-values were compared with the values in the table. The null hypothesis (H_0) (see Equation (36)) is rejected (it means that the difference is significant for the comparison between groups), if the calculated t-value exceeds the critical t-value for that test's degree of freedom value (df) and p-value (Type I error level: 95% confidence level = significance level (0.05 for this study)). Degree of freedom is the number of independent parts of data that can be used in estimating the statistical test. The following equation is used to find two-tailed p-value [141]:

$$p = 2 \cdot Prob(t > T) \quad (44)$$

Where "T" is the value from critical t-distribution table (see the paragraph below) and "t" is the t-value that has been calculated in Equation (38).

This comparison is automatically done in statistical programmes, and p-value (Type I error level) is written in output. However, for manual calculations, the t distribution table can be found on web, e.g.:

(http://sites.stat.psu.edu/~ajw13/stat200/tables/Table_A3.pdf)

Similarly, the critical p value distribution table for Mann-Whitney U-Test can also be found on web, e.g:

(http://www.psychologywizard.net/mann-whitney-u-test-ao1-ao2.html)

Critical p-value table for Wilcoxon Signed Ranks Test can be found using the following link, similar to the tables above:

(http://onlinepubs.trb.org/onlinepubs/nchrp/cd-22/v2appendixc_files/image038.gif)

2.7. Graph Theory

According to Brandes and Erlebach (2005) brain connectivity graphs can be examined by some graph theory properties such as connection degrees, strengths, motifs, clustering coefficients, path lengths, network global efficiencies, hubs and edges and some other graph theory components [142].

For the calculations of graph theory components (Chapter 2.7), either the discretized (Appendix 1) or weighted form of the connectivity adjacency matrix (See Chapter 2.5.1) can be used.

2.7.1. Global Efficiency

Global efficiency is a measure of "how efficiently the information is flowing in a network" [143]. The higher the global efficiency is, theoretically, the faster the information can flow. In other words, information transmitted from a node passes fewer nodes before reaches its destination. This measurement is commonly used in neuroscience for structural connectivities [7]. The formulation for global efficiency

was first defined by [143]. Global efficiency value (E_{glo}) of a network can be calculated as:

$$E_{glo} = \frac{1}{n(n-1)} \sum_{i \neq j} \frac{1}{d_{i,j}} \tag{45}$$

Where n is the total number of nodes and d(i,j) denotes the length of the shortest path (number of edges to go from i to j) between arbitrary nodes i and j.

"m" being the number of subjects in a group, averaging E_{glo} values of Equation (45), the formula below yields the average for all subjects of a group:

$$E_{glo,avg} = \frac{1}{m} \sum_{m} \left(\frac{2}{n(n-1)} \sum_{i \neq j} \frac{1}{d(i,j)} \right) \tag{46}$$

2.7.2. Clustering Coefficient

Clustering coefficient represent the clustering tendency of nodes in a network. Large clustering coefficient indicates that the network was made of highly clustered nodes. Clustering coefficient value (C) can be calculated as:

$$C = \frac{1}{n} \sum_{i=1}^{n} \frac{2e_i}{k_i(k_i - 1)} \tag{47}$$

n is the total number of nodes. k_i is the total number of first degree neighbours (nodes that have one edge between the node i) and e_i is the total number of edges of the node which is being iterated.

"m" being the number of subjects in a group, by using averaging operator ($\frac{1}{m} \sum_m ()$) for averaging all C values for groups, in Equation (47), the formula below yields the average for all subjects of a group:

$$C_{avg} = \frac{1}{m} \sum_{m} \left(\frac{1}{n} \sum_{i=1}^{n} \frac{2e_i}{k_i(k_i - 1)} \right) \tag{48}$$

2.7.3. Characteristic Path Length

Characteristic path length refers to the expected value of the steps to get from one arbitrary node to any other node in a network. It was calculated by finding the shortest path between all different pairs of electrodes and averaging the value for each node-node pairs. The lower the characteristic path length, more compact the network becomes [144]. Characteristic path length value (L) of a network can be found as:

$$L = \frac{\sum_i \sum_j d_{i,j}}{n(n-1)} \tag{49}$$

Where $d_{i,j}$ indicates the shortest path length between node i and j. n is the number of nodes.

To average the value L for all the subjects in a group, the formula below yields the average characteristic path length value for all subjects of a group:

$$l_{avg} = \frac{1}{m} \sum_{m} \left(\frac{1}{n(n-1)} \sum_{i,j} d_{i,j} \right) \tag{50}$$

Where m indicates the number of subjects in an experimental group.

2.7.4. Small World Measure

Small world networks are special forms of graphs and defined as in a network. In a small world network, not every node is connected to each other, each node is accessible from every other node by at most a few steps. Small world networks are characterized by large clustering coefficient (C) and small characteristic path length (L) according to Watts and Strogatz (1998) [144]. Functional brain networks show small-world properties [121] and detailed analyses of brain connectivity networks can be used to identify hub nodes of brain which are centres of information flow and integration [118].

Since small world measure (S) is depending on large clustering coefficient (C) and low characteristic path length (L). As Supekar et al. (2008) used in their study, S can be calculated as [145]:

$$S \sim \frac{C}{L} \tag{51}$$

Small world measure values can be used to compare connectivity networks of subjects in terms of "small-worldness".

The formula below yields the average small world measure (S_{avg}) value for "m" subjects of a group:

$$S_{avg} = \frac{1}{m} \sum_{m} \frac{C}{L} \tag{52}$$

Figure 15 is an example representation for small world connections. The small world values were also calculated using the same network.

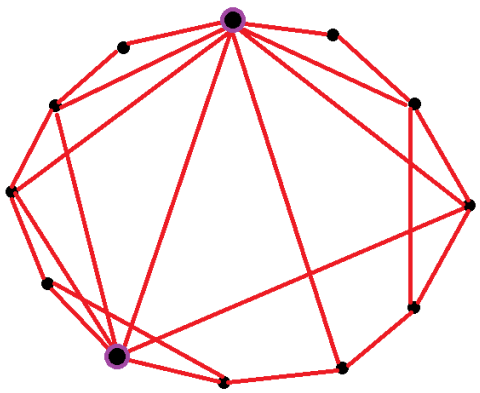

Figure 15 - A small-world network example, Bold nodes indicate hubs, Characteristic path length = 1.803, Clustering coefficient = 0.522. Image retrieved from [146].

2.8. Hub Node Occurrences and Hub Nodes of Groups

Incoming and outgoing hub nodes represent hub nodes which have the highest occurrence of incoming and outgoing connections, respectively. They can be calculated by finding the nodes which have maximum incoming or outgoing connections among all the nodes. Therefore, it is possible to find the highest occurrence of such nodes for all subjects within groups. The following Equations (53) and (54), can be used to calculate incoming and outgoing hub node occurrences using the connectivity adjacency matrices.

$$x_{i_{hub}} = \sum_{m|\sum row_i = max} 1 \tag{53}$$

$$x_{o_{hub}} = \sum_{m|\sum col_o = max} 1 \tag{54}$$

2.9. Test to Compare Proportions of Two Groups: Chi-square Test

Chi-square (χ^2) test [147] is a non-parametric test for nominal (categorical) variables. It can be used when the observations are occurrences in terms of %, frequencies in categories -or ratio values-. It tests whether the observed values differ from the expected values. There are two types of χ^2 test: First one is to compare the categorical groups of one variable. This is called as goodness of fit test. Second one is to compare the frequencies (occurrence) of values of two variables and called as chi-square independency test. If one variable is correlated with other variable (if change of one variable depends on another), then contingency coefficient is calculated. The test statistic (χ^2) can be calculated using the following formula [147]:

$$\chi^2 = \sum \frac{f_o - f_e}{f_e} \tag{55}$$

Where f_e is the expected frequency of the variable and f_o is the observed frequency of the variable. Then, the test statistic χ^2 is compared with the critical value of χ^2_α (α = 0.05) and the null hypothesis (See Chapter 2.6) is rejected if $\chi^2 > \chi^2_\alpha$. The p value can be found using the χ^2 distribution table [147].

The χ^2distribution changes with the number of categories of a variable. As the number of categories increases, the distribution approaches to the normal distribution. In this case, z-test can be made.

Chi-square test (Equation (55)) can also be used to compare two proportions (n-1 degree of freedom and for proportions calculated form 2x2 contingency table for small sample) as recommended by Campbell (2007) [148] and Richardson (2011) [149].

CHAPTER 3

EXPERIMENTS, RESULTS AND DISCUSSION

3.1. Data Acquisition and Preprocessing

Data were collected under the project with the information given in acknowledgement chapter, mainly conducted in Ankara University. Electroencephalogram (EEG) was used as imaging modality. Total of 58 subjects' data were collected from 7-12 years old children: 27 from control group and 31 from dyslexic group. The permission was taken from ethics committee of Ankara University. The report is available for the project "Developmental Dyslexia: Defining the relations between linguistics and EEG data" See ACKNOWLEDGEMENTS for detailed information.

Children who were using medicines to suppress attention deficit hyperactivity disorder (ADHD) stopped medicine intake for at most 24 hours before EEG recording, since most of the dyslexia patient also show attention deficit hyperactivity disorder as mentioned in [150].

All electroencephalography recordings were performed by a 32-channel BrainAmp electroencephalogram. 14 of 32 electrodes were used in analyses; the two electrodes were reference electrodes and they were located on left and right earlobes. Grounding lead was placed on left eye. There were also two electrodes which were located above and side of right eye to track eye artefacts. Therefore, they provided artefact elimination caused by eye movement. The electrodes which were used for analyses were placed according to 10-20 standard locations as shown in Figure 16.

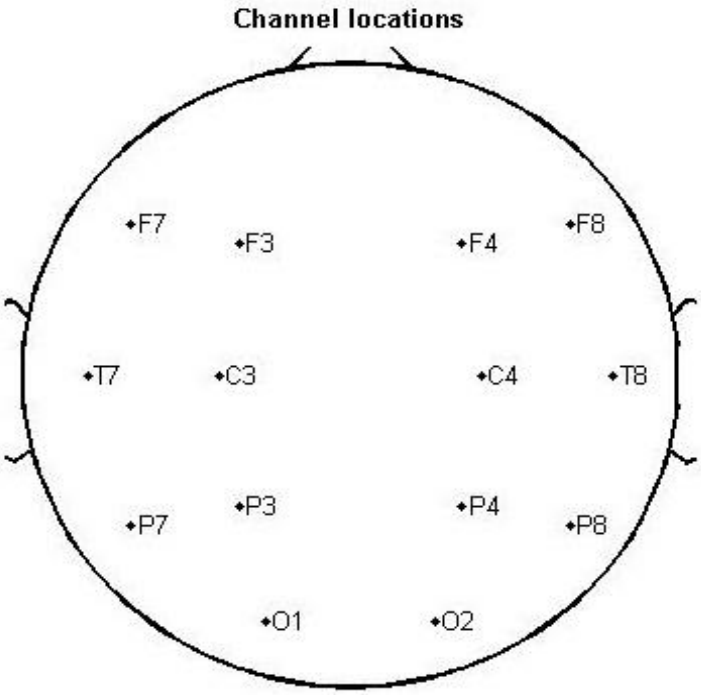

Figure 16 - Electrode locations used for this study

The sampling frequency for all data were 1000 hertz(Hz) and the impedance of all the electrodes were lower than 20 kilo-ohm(kΩ). Data recording was performed in a shielded room like Faraday Cage which eliminates environmental electromagnetic interferences by passing no outside electrical field inside the cage.

While recording, all children were sitting 114 centimetres(cm) away from the screen. Experimental setup was consisting of some meaningful words which were all Turkish words without any foreign language origin. Subjects were asked to read each word silently. Each word could be considered as a stimulus for each epoch and they all were represented in the middle of the computer screen one by one. The durations of the words to appear on the screen were determined by the reading speed of the subject, typically 1500-2500ms. There were a total of 50 pseudo-words and 50 regular words which were listed randomly for each subject. Subjects read each word twice, therefore, a total of 200 reading was performed.

EEG recording was performed independently for reading section of each word. Figure 17 represents the experimental setup for averaged data generation. Only regular word reading data were used for this thesis study.

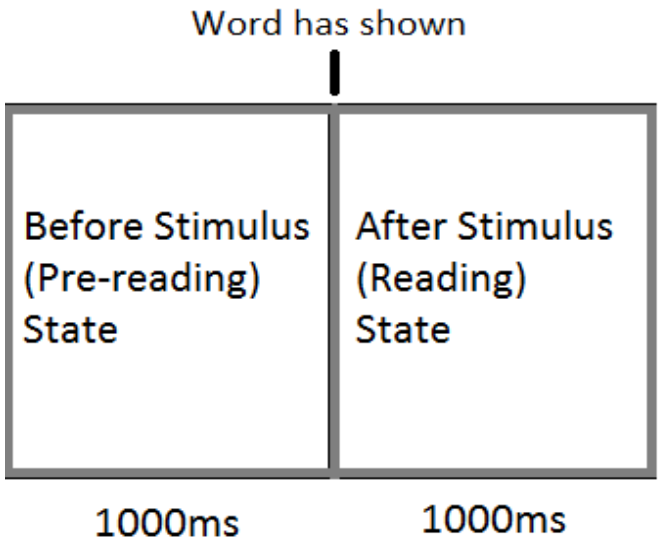

Figure 17 - Experimental setup

Recorded data was filtered between 0.5-100Hz and 50Hz notch filter which is a band-stop filter with a narrow stopband at 50Hz was also applied in order to eliminate main hum from the 50Hz power line. In order to eliminate eye movement artefacts, independent component analysis was applied. The trials with artefacts were discarded and the remaining trials were averaged in time.

The data for each electrode and for each subject then were divided into two parts: Before stimulus (pre-reading) and after stimulus (reading) parts. Figure 18 represents the data of a subject from all channels. x-axis represents the time where 0-1000ms is before stimulus and 1000-2000ms is after stimulus durations.

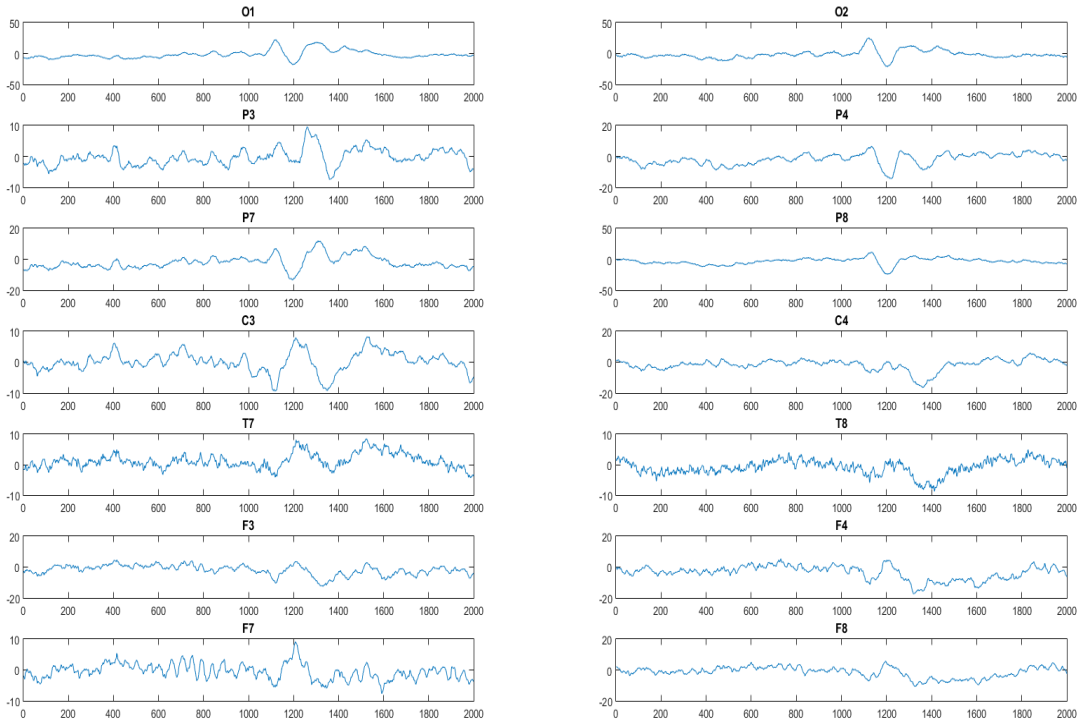

Figure 18 - A sample representation of raw data for all channels of a subject from dyslexic group.

3.1.1. Channel Reduction

In order to successfully validate an MVAR model, Delorme et al. (2011) suggests that the ratio of number of samples to number of channels should be high enough to satisfy Equation (11) [128]. According to Equation (11), with the dataset with number of samples n=1000 the number of channels (m) should be smaller than $\sqrt{100/p}$ to successfully validate the MVAR model where p is the MVAR model order (See Chapter 2.5.3.1). According to Equation (11), even with p=2, for better model validation, the number of channels (m) can take values at most up to 6.

Some channels which were behaving similarly and adjacent to each other were merged by averaging two channel data. Initially, there were 14 channels: F3, F4, F7, F8, P3, P4, P7, P8, C3, C4, T7, T8, O1 and O2 (See Chapter 3.1). By comparing the channel behaviours of after stimulus conditions of grand average of control subjects as in Figure 20, Figure 21, Figure 22, Figure 23, Figure 24, Figure 25 in Appendix B, channels with similar behaviours were determined. Averaging those channels in time, resulted in the merged channels. Channel merging was performed between channels with similar behaviours as following:

- F3-F7 to represent left frontal node (FL)
- F4-F8 to represent right frontal node (FR)
- P7-O1 to represent left occipito-parietal node (OPL)
- P8-O2 to represent right occipito-parietal node (OPR)

Two channels were taken as they were:

- P3 to represent left parietal node (PL)
- P4 to represent right parietal node (PR)

Four channels were discarded as in study [151]: C3, C4, T7 and T8.

The new nodes (FL, FR, OPL, OPR, PL and PR) now form the new dataset for each subject. The representation of the new nodes on the original electrode locations can be found in Figure 19. The following analyses were performed using the new dataset with the order of nodes: FL, FR, PL, PR, OPL, OPR. The order was determined by the locations of each node, from ante to dorsum.

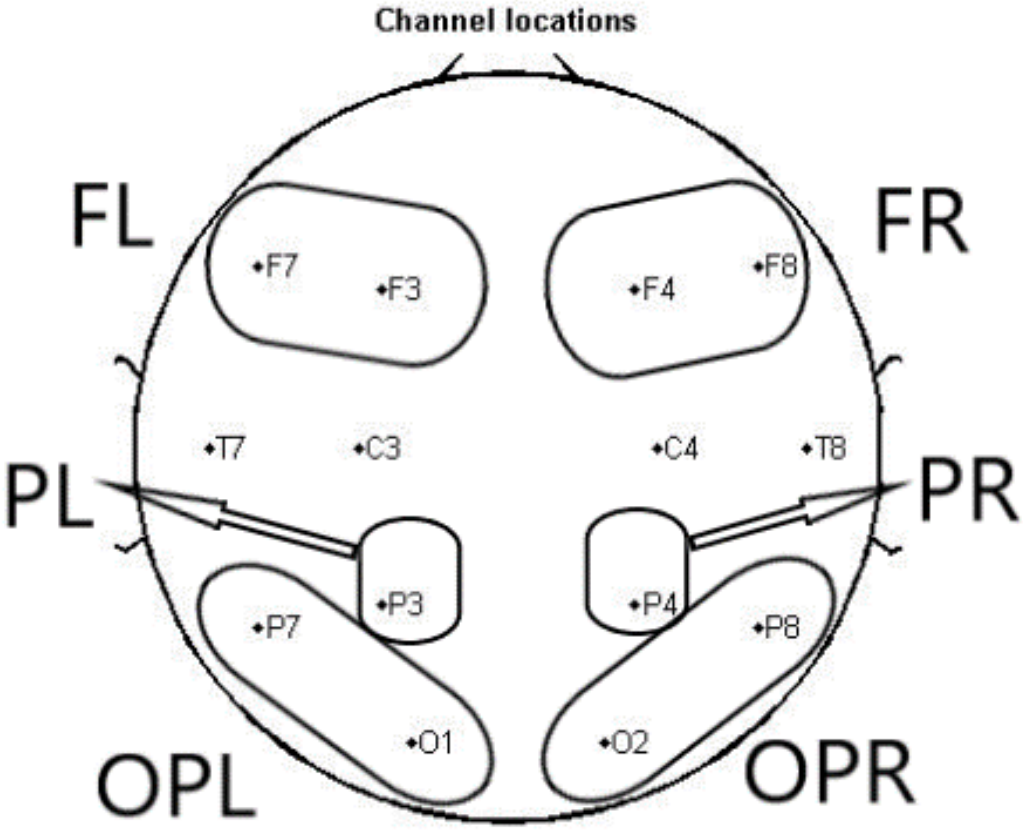

Figure 19 - Representation of new channel nodes and locations.

3.2. Multivariate Autoregressive Model Fitting

The main MVAR model equation (See Equation (7)), requires model order (p) value definition. In order to fit and validate an MVAR model successfully, model order should be selected properly. Using the Equation (11) with sample size n = 1000 and number of channels m = 6, the value of model order should be smaller than 2.778 (See Chapter 2.5.3.2). Then, to satisfy this, model order "p" should be selected as 2 which is the largest integer to satisfy p < 2.778. However, selecting p as 2 generates a poor MVAR model (See Chapter 2.5.3.2). Therefore, a larger model order is required to be selected. Model order values p = 3 and p = 4 were used in pre-analyses and p = 4 was selected which was satisfying the acceptable values for MVAR model validation as mentioned in Chapter 2.5.3.2. p = 4 doesn't satisfy Equation (11) which grants a good model validation. But, satisfies Equation (10) which is sufficient for acceptable model validation. The validation results were given in Chapter 3.3, in Table 3.

Model fitting is the estimation of model coefficients matrix (A) of MVAR model (See Equation (3)). To fit the model, Vieira-Morf MVAR model fitting algorithm [131] was used. The reason of selecting this algorithm is Vieira-Morf algorithm's capability of estimating coefficient matrix more accurately for multivariate data than other algorithms according to Schlögl and Supp (2006) [130]. Using the Equation (12) where Z = X(t-p) and p = 4, the model coefficient matrix $\widehat{A}$ was estimated. In Equation (12), X is the data to be fitted. For this study, X(t) is a 6x1000 (Channels x Data Samples) sized matrix.

The window length was selected as 1000 samples (=1.000 seconds of time series where sampling rate is 1000Hz (See Chapter 3.1) to cover all the samples of data. One MVAR model was fitted for the whole data samples.

3.3. Multivariate Autoregressive Model Validation

MVAR model validation was done in three parts: Whiteness test (Chapter 2.5.3.2.1), consistency test (Chapter 2.5.3.2.2) and stability test (Chapter 2.5.3.2.3). The parameters were set to satisfy the inequality in Equation (10) (Also see Chapter 3.2).

Whiteness test (Chapter 2.5.3.2.1) checks if the residuals of fitted model were correlated or not. According to the Equation (19), the residuals ($\widehat{U}_j$) for each fitted model ($\hat{A}$) can be calculated where "j" indicates the columns. Autocorrelation function (ACF) method was used to perform whiteness test. The residuals matrix $\widehat{U}$ was estimated using Equation (19) (Also see Chapter 3.2). The size of $\widehat{U}$ was 6 x 1000 where 6 is the number of channels (m = 6) and 1000 is the number of samples (n = 1000). $\widehat{U}_t$ were indicating the columns (residuals) and μ was the mean value of $\widehat{U}_t$. Here, the maximum lag amount that the autocovariances to be estimated was selected as h = 4 which is same as the MVAR model order. Using the ratio between autocovariance values of lag 4 and lag 0 in Equation (21), ACF value was found. The mean and standard deviation of ACF values in the form of "mean ± standard deviation" can be found in Table 3 under whiteness row as % percent values for both groups and both conditions. Since whiteness values in Table 3 exceeds 95%, MVAR models can be considered as white (See Chapter 2.5.3.2.1).

Consistency test (Chapter 2.5.3.2.2) was performed by calculation of percent consistency values (PC) for each subject using the Equation (24). In Equation (24), R_p is the correlation matrix of estimated coefficients of MVAR model and R_r is the correlation matrix of real dataset. Average PC value of individuals were located in good to questionable scale according to Table 2. As explained in previous paragraph, the selection of model order as 4 caused a drop in those values. The test results can be found in Table 3 for groups and conditions. According to those values, overall PC values of before stimulus conditions for both groups were located in "good" while after stimulus condition of control group was located in "acceptable" and after stimulus condition of dyslexic group was located in "questionable" consistency scale of Table 2. Therefore, most of the MVAR models have passed the consistency test. The models which were failed at consistency test were not discarded, but used as if they were

passed the test. The reason of doing this is not to reduce the number of subjects for remaining analyses.

Table 3 – MVAR model validation results for consistency and whiteness tests as % percentage values. First term indicates the mean and second term indicates the standard deviation.

	Control (n = 27)		**Dyslexic (n = 31)**	
	BS	**AS**	**BS**	**AS**
Mean Consistency (%)	89.346±5.563	73.568±23.326	87.426±7.052	66.518±25.935
Whiteness (%)	96.073±1.949	95.953±2.512	95.922±2.642	95.398±3.154

Stability test (Chapter 2.5.3.2.3) was performed using the stability index values (SI) using Equation (25). The only parameter of the equation "λ_{max}" is the maximum eigenvalue of the estimated coefficient matrix which is expected to have modulus less than 1. The mean values of stability test results of subjects can be found in Table 4. According to this table, all MVAR models of before stimulus condition have passed the stability test. On the other hand, for after stimulus conditions, MVAR models of some subjects (1 control subject for after stimulus condition and 5 dyslexic subjects for after stimulus condition) have poor stability values.

Table 4 - MVAR model validation results for stability test as number of models which passed the test.

	Control (n = 27)		**Dyslexic (n = 31)**	
	BS	**AS**	**BS**	**AS**
Stable models (#)	27	26	31	26

As a conclusion, for before stimulus condition, MVAR models for all subjects have been validated. For after stimulus condition, 1 subject from control group and 5 subjects from dyslexic group failed at MVAR model validation. For the analyses onwards, all subjects were used, no matter how their validation results were. The reason is not to reduce degree of freedom values for statistical analyses (See Chapter 2.6). But, for future studies, by collecting data from more subjects which increases the degree of freedom for statistical analyses, MVAR models with poor validation results can be discarded.

3.4. Connectivity Analysis with PDC

After MVAR models have been fit and most of them (58/58 for before stimulus, 52/58 for after stimulus) have been validated, the next step was to estimate connectivity networks of each subject using partial directed coherence (PDC) algorithm. A connectivity network of a subject should have 6x6 matrix representation for this study. Here 6 indicates the node size (See Chapter 3.1.1). The values of MVAR model coefficient matrix in the form of Equation (14) were used to find PDC connection values. Each value (PDC_{ij}) of these connectivity matrices was calculated using the Equation (26). In this equation, the inputs are i^{th} row and/or j^{th} column values of estimated MVAR coefficient matrix (See Chapter 3.2).

One MVAR model has been generated for each subject as described in Chapter 3.2. This was due to the time window which was selected to cover all the samples (n = 1000) of the data. Since the time window covers all the data samples, the middle point of total data points (n = 500) became the sample which the connectivity was estimated at.

Considering the initial experimental setup, for after stimulus condition, the time slice corresponding to this sample becomes t = 1500ms (1000ms + 500ms) for data of a subject where 500ms corresponds to the middle point for n = 1000 samples (See Chapter 3.1). Similarly, for before stimulus condition, the time slice which the connectivity was estimated was t = 500ms (1000ms – 500ms). Those time points are the points where the data were modelled in terms of connectivity.

Equation (26) performs calculations for discrete f values which are corresponding to the model order, up to p = 4. To find a model to represent all discrete f values (1 to 4), the connectivity matrices for discrete frequencies were averaged. Averaging yielded a 6 x 6 connectivity network matrix for each subject.

The estimated 6x6 sized matrices hold the information of connectivity strengths from node j to node i. The order of nodes which form the rows and columns were described in Chapter 3.1.1. Table 5 is an example of an estimated weighted connectivity matrix of a subject from control group.

Table 5 – An example representation of an estimated weighted connectivity matrix.

Nodes	**FL**	**FR**	**PL**	**PR**	**OPL**	**OPR**
FL	0.393	0.021	0.029	0.032	0.026	0.046
FR	0.000	0.208	0.007	0.075	0.019	0.050
PL	0.001	0.016	0.178	0.033	0.033	0.022
PR	0.003	0.009	0.026	0.290	0.055	0.027
OPL	0.003	0.011	0.085	0.024	0.501	0.010
OPR	0.003	0.011	0.046	0.002	0.074	0.170

According to Table 5, for example, the value of the cell in 2nd column and 5th row indicates the connectivity strength from node FR to node OPL. The representation of the value of this cell in Equation (26) is "PDC_{52}".

Table 6 consists of the connectivity networks which values were averaged for groups and conditions to give a rough representation to compare groups and conditions.

In Table 6, the highest connection strength values were generally located on the diagonals of the matrices. This is an expected situation since nodes have more causal relationship with their past-future values than other nodes' past-future values.

Table 6 – The averaged weighted connectivity network results for groups and conditions.

	Nodes	**FL**	**FR**	**PL**	**PR**	**OPL**	**OPR**
Before Stimulus Condition of Control Group	**FL**	0.205	0.005	0.057	0.057	0.040	0.074
	FR	0.008	0.200	0.058	0.122	0.040	0.087
	PL	0.007	0.002	0.333	0.043	0.017	0.029
	PR	0.007	0.003	0.032	0.374	0.014	0.043
	OPL	0.005	0.002	0.020	0.052	0.249	0.033
	OPR	0.006	0.002	0.028	0.040	0.014	0.251
	Nodes	**FL**	**FR**	**PL**	**PR**	**OPL**	**OPR**
After Stimulus Condition of Control Group	**FL**	0.226	0.007	0.103	0.145	0.061	0.108
	FR	0.008	0.198	0.072	0.106	0.045	0.087
	PL	0.015	0.004	0.323	0.056	0.035	0.069
	PR	0.017	0.005	0.033	0.419	0.036	0.068
	OPL	0.007	0.002	0.016	0.042	0.242	0.037
	OPR	0.007	0.002	0.018	0.041	0.020	0.295
	Nodes	**FL**	**FR**	**PL**	**PR**	**OPL**	**OPR**
Before Stimulus Condition of Dyslexic Group	**FL**	0.225	0.024	0.188	0.076	0.076	0.033
	FR	0.006	0.249	0.115	0.040	0.037	0.028
	PL	0.005	0.020	0.446	0.062	0.029	0.028
	PR	0.006	0.012	0.039	0.291	0.017	0.022
	OPL	0.010	0.026	0.084	0.033	0.265	0.023
	OPR	0.010	0.029	0.071	0.060	0.029	0.230
	Nodes	**FL**	**FR**	**PL**	**PR**	**OPL**	**OPR**
After Stimulus Condition of Dyslexic Group	**FL**	0.260	0.017	0.190	0.049	0.125	0.051
	FR	0.013	0.218	0.097	0.047	0.052	0.0400
	PL	0.007	0.021	0.446	0.043	0.070	0.031
	PR	0.013	0.020	0.044	0.251	0.029	0.024
	OPL	0.010	0.017	0.049	0.014	0.265	0.009
	OPR	0.008	0.010	0.039	0.026	0.025	0.253

3.5. Calculation of Graph Theory Measures

After connectivity matrices were obtained for each subject, graph theory measures can be calculated. Calculations of graph theory measures can either be operated with weighted or discretized binary connectivity matrices. Discretizing a data causes loss in valuable information. Therefore, weighted connectivity matrices (Chapter 3.4) were directly used for the calculation of graph theory measures.

Global efficiency (Chapter 2.7.1), clustering coefficient (Chapter 2.7.2), characteristic path length (Chapter 2.7.3), and small world measure (Chapter 2.7.4) are the graph theory measures which were used in further analyses of this thesis study.

3.5.1. Global Efficiency Calculation

Global efficiency (see Chapter 2.7.1 for theory) values of each subject were calculated by using the Equation (45).The parameter “n” indicates the node size which is 6 for this experiment. Since the weighted connectivity matrices were used in calculation of Equation (45), the shortest path between node i and j “d_(i,j)” took decimal values, i.e. sum of related values of weighted matrix. The decimal values which are close to zero caused the equation to result in higher values, i.e. on the order of 102 which is not possible to be achieved for binary connectivity matrices.

For group averages, Equation (46) was used where “m” is the group size which is 27 for controls and 31 for dyslexics.

Table 7– Global efficiency values of subjects.

Control Group Subjects	Condition		Dyslexic Group Subjects	Condition	
	Before Stimulus	After Stimulus		Before Stimulus	After Stimulus
CS1	189.7	96.0	**DS1**	135.9	32.6
CS2	127.2	198.3	**DS2**	84.3	68.4
CS3	329.5	224.5	**DS3**	118.9	66.4
CS4	140.2	85.2	**DS4**	62.8	49.9
CS5	437.5	657.6	**DS5**	47.2	188.2
CS6	299.4	143.4	**DS6**	588.5	88.4
CS7	39.7	95.7	**DS7**	181.3	314.0
CS8	244.2	59.6	**DS8**	63.4	215.3
CS9	42.6	76.8	**DS9**	157.7	59.6
CS10	159.9	107.0	**DS10**	148.7	31.2
CS11	52.8	102.4	**DS11**	76.9	208.7
CS12	351.7	208.3	**DS12**	67.2	206.1
CS13	785.9	168.8	**DS13**	295.3	140.8
CS14	177.3	93.5	**DS14**	497.5	105.3
CS15	210.1	37.1	**DS15**	75.2	164.7
CS16	24.8	68.3	**DS16**	136.4	450.7
CS17	47.1	31.6	**DS17**	250.0	82.2
CS18	78.1	98.1	**DS18**	166.7	155.1
CS19	234.9	163.6	**DS19**	307.3	261.7
CS20	1109.1	141.3	**DS20**	126.0	316.1
CS21	69.8	45.4	**DS21**	366.0	349.2
CS22	24.4	97.8	**DS22**	53.9	109.4
CS23	293.1	80.0	**DS23**	139.9	119.2
CS24	108.6	71.4	**DS24**	23.6	17.0
CS25	225.9	3997.6	**DS25**	64.2	50.9
CS26	28.0	26.3	**DS26**	21.5	84.1
CS27	118.3	43.8	**DS27**	908.4	501.5
-	-	-	**DS28**	112.9	168.5
-	-	-	**DS29**	298.9	121.1
-	-	-	**DS30**	82.2	22.1
-	-	-	**DS31**	82.7	64.9

3.5.2. Clustering Coefficient Calculation

Clustering coefficient (see Chapter 2.7.2 for theory) values of each subject were calculated using the Equation (47). The values of parameters of Equation (47) are as follows: "n" is the number of nodes which was 6; "k_i" is the first degree neighbours of node i and "e_i" is the total number of edges the node i have. k_i and e_i took decimal values from weighted connectivity matrices. Therefore, the output of Equation (47) results in the order of 10^{-1} to 10^{-2}. For group averages, Equation (48) was used where "m" is the group size which is 27 for controls and 31 for dyslexics.

Table 8 – Clustering coefficient values of subjects.

Control Group Subjects	Condition		Dyslexic Group Subjects	Condition	
	Before Stimulus	After Stimulus		Before Stimulus	After Stimulus
CS1	0.099	0.073	**DS1**	0.121	0.177
CS2	0.100	0.118	**DS2**	0.091	0.091
CS3	0.078	0.093	**DS3**	0.095	0.089
CS4	0.065	0.087	**DS4**	0.102	0.153
CS5	0.085	0.076	**DS5**	0.099	0.079
CS6	0.059	0.118	**DS6**	0.080	0.084
CS7	0.112	0.094	**DS7**	0.064	0.060
CS8	0.086	0.111	**DS8**	0.085	0.085
CS9	0.127	0.110	**DS9**	0.103	0.133
CS10	0.080	0.084	**DS10**	0.113	0.151
CS11	0.084	0.094	**DS11**	0.086	0.081
CS12	0.099	0.079	**DS12**	0.089	0.069
CS13	0.070	0.075	**DS13**	0.068	0.070
CS14	0.066	0.061	**DS14**	0.091	0.083
CS15	0.082	0.182	**DS15**	0.137	0.173
CS16	0.177	0.131	**DS16**	0.096	0.099
CS17	0.122	0.178	**DS17**	0.054	0.090
CS18	0.120	0.125	**DS18**	0.090	0.064
CS19	0.063	0.075	**DS19**	0.052	0.063
CS20	0.097	0.075	**DS20**	0.062	0.088
CS21	0.127	0.147	**DS21**	0.075	0.054
CS22	0.189	0.114	**DS22**	0.172	0.139
CS23	0.088	0.077	**DS23**	0.090	0.136
CS24	0.079	0.093	**DS24**	0.173	0.182
CS25	0.084	0.087	**DS25**	0.118	0.121
CS26	0.219	0.184	**DS26**	0.162	0.189
CS27	0.119	0.125	**DS27**	0.037	0.036
-	-	-	**DS28**	0.074	0.082
-	-	-	**DS29**	0.077	0.069
-	-	-	**DS30**	0.154	0.211
-	-	-	**DS31**	0.171	0.157

3.5.3. Characteristic Path Length Calculation

Characteristic path length (see Chapter 2.7.3 for theory) values of each subject were calculated using the Equation (49). The node size (n) is 6 (see Chapter 3.1.1). As described in Chapter 3.5.1, due to the small, decimal values of $d_{i,j}$, characteristic path length value (L) of a subject takes the values on the order of 10^{-2}. For group averages, Equation (50) was used where "m" is the group size which is 27 for controls and 31 for dyslexics.

Table 9 – Characteristic path length values of subjects.

Control Group Subjects	Condition		Dyslexic Group Subjects	Condition	
	Before Stimulus	After Stimulus		Before Stimulus	After Stimulus
CS1	0.043	0.019	**DS1**	0.064	0.083
CS2	0.073	0.059	**DS2**	0.026	0.021
CS3	0.019	0.047	**DS3**	0.066	0.051
CS4	0.012	0.033	**DS4**	0.025	0.049
CS5	0.027	0.016	**DS5**	0.034	0.017
CS6	0.011	0.060	**DS6**	0.030	0.024
CS7	0.053	0.057	**DS7**	0.012	0.007
CS8	0.023	0.047	**DS8**	0.022	0.016
CS9	0.047	0.054	**DS9**	0.026	0.040
CS10	0.016	0.016	**DS10**	0.030	0.053
CS11	0.028	0.034	**DS11**	0.022	0.023
CS12	0.042	0.034	**DS12**	0.026	0.032
CS13	0.010	0.016	**DS13**	0.021	0.022
CS14	0.028	0.019	**DS14**	0.022	0.030
CS15	0.041	0.121	**DS15**	0.042	0.056
CS16	0.112	0.048	**DS16**	0.029	0.044
CS17	0.084	0.160	**DS17**	0.015	0.028
CS18	0.056	0.055	**DS18**	0.023	0.026
CS19	0.029	0.033	**DS19**	0.009	0.013
CS20	0.063	0.022	**DS20**	0.012	0.021
CS21	0.032	0.029	**DS21**	0.021	0.010
CS22	0.109	0.065	**DS22**	0.087	0.102
CS23	0.034	0.030	**DS23**	0.018	0.070
CS24	0.017	0.024	**DS24**	0.107	0.087
CS25	0.054	0.043	**DS25**	0.029	0.032
CS26	0.143	0.113	**DS26**	0.094	0.114
CS27	0.043	0.057	**DS27**	0.007	0.007
-	-	-	**DS28**	0.027	0.024
-	-	-	**DS29**	0.018	0.018
-	-	-	**DS30**	0.085	0.126
-	-	-	**DS31**	0.107	0.119

3.5.4. Small World Measure Calculation

Small world measure (see Chapter 2.7.4 for theory) of a subject can be calculated with previously calculated values of clustering coefficient (C) using Equation (47) (see Chapter 3.5.2) and characteristic path length (L) using Equation (49) (see Chapter 3.5.3). With the known C and L values, Equation (51) yields small world network measure (S). Small world measure values were calculated for each subject, independently. For group averages, Equation (52) was used where "m" is the group size which is 27 for controls and 31 for dyslexics.

Table 10 – Small world measure values of subjects

Control Group Subjects	Condition		Dyslexic Group Subjects	Condition	
	Before Stimulus	After Stimulus		Before Stimulus	After Stimulus
CS1	2.321	3.823	**DS1**	1.900	2.144
CS2	1.364	1.999	**DS2**	3.487	4.402
CS3	4.128	1.969	**DS3**	1.443	1.748
CS4	5.539	2.672	**DS4**	3.995	3.102
CS5	3.187	4.662	**DS5**	2.900	4.659
CS6	5.321	1.972	**DS6**	2.698	3.450
CS7	2.116	1.662	**DS7**	5.330	8.191
CS8	3.687	2.333	**DS8**	3.914	5.459
CS9	2.700	2.038	**DS9**	3.973	3.291
CS10	5.126	5.337	**DS10**	3.715	2.849
CS11	2.989	2.739	**DS11**	3.978	3.460
CS12	2.367	2.287	**DS12**	3.400	2.177
CS13	6.942	4.591	**DS13**	3.252	3.144
CS14	2.367	3.114	**DS14**	4.098	2.763
CS15	2.015	1.501	**DS15**	3.243	3.108
CS16	1.580	2.712	**DS16**	3.310	2.232
CS17	1.440	1.111	**DS17**	3.578	3.242
CS18	2.145	2.258	**DS18**	3.969	2.476
CS19	2.185	2.276	**DS19**	5.729	4.872
CS20	1.553	3.370	**DS20**	5.003	4.163
CS21	3.972	5.006	**DS21**	3.494	5.310
CS22	1.735	1.753	**DS22**	1.978	1.364
CS23	2.576	2.516	**DS23**	5.016	1.934
CS24	4.579	3.937	**DS24**	1.621	2.088
CS25	1.552	2.019	**DS25**	4.086	3.728
CS26	1.531	1.632	**DS26**	1.718	1.663
CS27	2.740	2.199	**DS27**	5.225	5.478
-	-	-	**DS28**	2.734	3.417
-	-	-	**DS29**	4.379	3.902
-	-	-	**DS30**	1.814	1.675
-	-	-	**DS31**	1.594	1.313

3.6.Statistical Difference Analyses

The statistical differences were tested using the t-test for the two conditions: Between the datasets of independent groups and between the datasets of dependent groups. The tests were made separately for each dependent variables (Clustering coefficient, global efficiency, characteristic path length and small-world measure) and for before stimulus and after stimulus conditions.

Independent samples t-test was used to investigate the differences between two experimental groups: Controls and dyslexics when equality of variances was satisfied. Otherwise, Mann-Whitney U Test was used to investigate group differences when equality of variances was not satisfied.

To analyse the differences between two stimulus conditions: Before stimulus and after stimulus, paired samples t-test was used when equality of variances was satisfied or the data have normal distribution. When equality of variances was not satisfied or data distribution is not normal, Wilcoxon Test was used.

For all of the tests, the significance level was taken as $p < 0.05$.

3.6.1. Statistical Analyses Between Dyslexic and Control Groups

Dyslexic and control groups have different subjects, and therefore, their measurements are independent. Independent samples t-test (see Chapter 2.6.1.1 for theory) was used to find the differences in datasets of controls and dyslexics between each graph theory measures (see Chapter 2.7).

The calculations of graph theory measures: Global efficiency (Chapter 3.5.1), clustering coefficient (Chapter 3.5.2), characteristic path length (Chapter 3.5.3) and small world measure (Chapter 0) were made for each subject of both groups and for both conditions (BS-AS) as described in Chapter 3.5. The mean values and variances of graph theory components datasets were calculated for Controls ($n_1 = 27$) and dyslexics ($n_2 = 31$). Using Equation (38), where μ_1 and μ_2 are the mean values; σ_1^2 and σ_2^2 are the variance values of graph theory measures for control and dyslexic groups respectively, the t-values were found for each graph theory component and for each condition (BS-AS) between independent groups: Controls and dyslexics.

After the t-values were found, p-values were calculated using Equation (41). For calculation of p-values, the critical t-value distributions were used (See Chapter 2.8.1).

Table 11 - Independent samples t-test results of graph theory properties for connectivity maps obtained by PDC algorithm based on independent groups: Controls and dyslexics.

Condition	Graph Theory Property	Group	n	Mean	St. dev.	t	df	p (one-tailed)
Before Stimulus	Characteristic Path Length	Control Dyslexic	27 31	,046 ,037	,033 ,029	1.085	56	,141
	Clustering Coefficient	Control Dyslexic	27 31	,103 ,099	,039 ,037	,348	56	,364
	Global Efficiency	Control Dyslexic	27 31	220.4 185.2	241.9 190.2	,619	56	,269
	Small World Measure	Control Dyslexic	27 31	2.954 3.438	1.479 1.189	- 1.381	56	,086
After Stimulus	Characteristic Path Length	Control Dyslexic	27 31	,049 ,044	,034 ,035	,511	56	,305
	Clustering Coefficient	Control Dyslexic	27 31	,106 ,108	,034 ,046	Variances are not equal. Mann-Whitney U Test was made. (See Table 12)		
	Global Efficiency	Control Dyslexic	27 31	267.4 155.3	755.0 124.1	,815	56	,209
	Small World Measure	Control Dyslexic	27 31	2.722 3.316	1.137 1.506	- 1.676	56	,049

Note that although the standard deviation values look different, especially for global efficiency values of after stimulus condition which has significance < 0.092, all graph theory components but clustering coefficient of after stimulus condition have statistically indifferent variances according to Levene's Test (Results can be accessed by asking the researcher). For clustering coefficient of after stimulus condition, variances were not assumed to be equal according to Levene's test for Equality of Variances ($p < 0.027$). Therefore, Mann Whitney U Test was needed to be made for clustering coefficient of after stimulus conditions. Table 12 contains the Mann Whitney U Test results for clustering coefficient of after stimulus conditions of independent groups.

Table 12 – Mann-Whitney U Test result for graph theory property which has not equal variances.

Condition	Graph Theory Property	Group	n	Mean	Mann-Whitney U	p (one-tailed)
After Stimulus	Clustering Coefficient	Control Dyslexic	27 31	0.049 0.044	402.0	,399

According to Table 11:

1. For before stimulus condition, no graph theory component show significant difference ($p < 0.05$) between control and dyslexic groups for effective connectivity networks.
2. For after stimulus condition,
    a. Small world measure ($p < 0.049$) have significant difference between groups.

There was no significant difference between control and dyslexic groups during pre-stimulus in terms of graph theory measures such as characteristic path length, clustering coefficient and global efficiency as in the study of Hosseini et al. (2013) [16]. But the results show that, the small world index values are significantly different between groups. Considering the t values (negative) in Table 11, for both before and after stimulus conditions, small world measures are larger for dyslexic group.

Significant values for small world index for after stimulus condition are important. Dyslexic group has higher small world index values. Using the small-worldness definition [144] [152], dyslexic group has more “directly connected” nodes in small clusters. This may be causing disorientation in forwarding the information to correct destination.

According to Table 12, clustering coefficient for after stimulus condition has no significant difference between groups.

3.6.2. Statistical Analyses for Before and After Stimulus Conditions

Paired samples t-test (Chapter 2.6.1.2) was used to find the differences in distributions of two dependent datasets: Before and after stimulus data of same subjects. Before and after stimulus observations are an example of longitudinal experiment. In other words, data for both cases were obtained from the same subject for different conditions. For this analysis, instead of comparing two experimental groups, two conditions of same groups were compared.

The dependent pairs of before and after stimulus samples are the graph theory measures of same subject for before and after stimulus conditions. The calculations of graph theory components: Global efficiency (Chapter 3.5.1), clustering coefficient (Chapter 3.5.2), characteristic path length (Chapter 3.5.3) and small world measure (Chapter 0) were made for each subject of both groups and for both conditions (BS-AS).

The distribution of the graph theory values (separately) for before stimulus condition of control group is compared with the distribution of the graph theory values (separately) for after stimulus condition of control group. Similarly, the distribution of the graph theory values (separately) for before stimulus condition of dyslexic group is compared with the distribution of the graph theory values (separately) for after stimulus condition of dyslexic group.

Using the Equation (41); the differences between each samples of graph theory components for before and after stimulus values (d_i) forms a set of vector (D_j). Where i is the subject number of a group (from 1 to 27 for control subjects and from 1 to 31 for dyslexic subjects) and j is the group number (0: Controls, 1: Dyslexics). $\hat{\sigma}$ is the variance and $\bar{d}$ is the mean of D_j. Calculation of the test statistic (t-value) were performed using the Equation (41).

After the calculation of t-value, p-value was found using the Equation (44) (Chapter 2.6.1.2).

The process of comparing before and after stimulus cases was repeated for both groups, for each graph theory component, separately.

Table 13 - Paired samples t-test results of graph theory properties for connectivity maps obtained by PDC algorithm based on dependent paired conditions for same subjects: Before and after stimulus conditions.

Group	Graph Theory Property	Condition	n	Mean	St. dev.	t	df	p (one-tailed)
Controls	Characteristic Path Length	Before St. After St.	27	,046 ,049	,033 ,034	-,393	26	,349
	Clustering Coefficient	Before St. After St.		Failed at normalization test (sig<0.05). Non-parametric Wilcoxon Signed Ranks Test was used. Results can be found in Table 14.				
	Global Efficiency	Before St. After St.						
	Small World Measure	Before St. After St.		2.954 2.722	1.479 1.137	,936	26	,179
Dyslexics	Characteristic Path Length	Before St. After St.	31	,037 ,044	,0294 ,0346	-2.384	30	,012
	Clustering Coefficient	Before St. After St.		,099 ,108	,0366 ,0464	-1.985	30	,028
	Global Efficiency	Before St. After St.		Failed at normalization test (sig<0.05). Non-parametric Wilcoxon Signed Ranks Test was used. Results can be found in Table 14.				
	Small World Measure	Before St. After St.		3.438 3.316	1.189 1.506	,589	30	,280

For the graph theory measures which failed at normality test (as indicated in Table 13), Wilcoxon Signed Ranks Test was performed. The results can be found in Table 14.

Table 14 – Wilcoxon Signed Ranks Test for graph theory components of dependent groups which failed at normality test.

Group	Graph Theory Property	Condition	n	Mean	Z	Asymp. p (one-tailed)
Controls	Clustering Coefficient	Before St. After St.	27	0.102 0.106	-,312	,378
	Global Efficiency	Before St. After St.		220.4 267.4	-1.874	,031
Dyslexics	Global Efficiency	Before St. After St.	31	185.2 155.3	-,705	,241

According to Table 13 and Table 14, the following were observed for connectivity networks between before and after stimulus conditions of:

1. For control group, global efficiency values of control group are statistically different for before and after stimulus conditions ($p < ,031$).
2. For dyslexic group:

a. Characteristic path length has significant ($p < 0.012$) difference between before and after stimulus conditions.
b. Clustering coefficient has significant ($p < 0.028$) difference between before and after stimulus conditions.

While control group has significant difference between global efficiency values, dyslexic group has significant difference in characteristic path length and clustering coefficient values. This may show that reading stimulus causes control group connections to be more efficient in information transmission (negative Z value for global efficiency); a better task-oriented shape. On the other hand, reading stimulus causes connections of dyslexic subjects to be more compact, but with reduced directness. Reading stimuli may be causing dyslexic nodes to form small clusters, but with low connectivity between clusters.

3.7. Hub Node Occurrences and Detection of Hub Nodes of Groups

Incoming and outgoing hub node occurrence values (Chapter 2.8) for each subject were calculated using Equation (53) and Equation (54), respectively. As described in Chapter 2.5.1, columns of a connectivity adjacency matrix indicate the nodes which have the outgoing connections and rows indicate the incoming connections. Therefore, in Equation (53) and Equation (54), the terms "row_i" and "col_o" were used to identify incoming and outgoing connections. For connectivity matrices which have more than one maximum incoming or outgoing hub nodes, multiple nodes were considered to be hub nodes of that subject.

To detect overall hub node for a group, the hub nodes of each connectivity map were counted. Thus, the node which has the maximum hub node occurrence was considered as the hub node for the overall group. To count the hub node occurrences, the weighted connectivity matrices (see Chapter 3.4) were discretized to generate unweighted connectivity adjacency matrices (See Appendix A for discretization process). Then, using Equation (53) and Equation (54) on unweighted connectivity matrices; incoming connection hub nodes and outgoing connection hub nodes were found, respectively.

Analyses were made for both before and after stimulus cases and for control and dyslexic groups, separately. Table 15 shows the occurrence values for before and after stimulus conditions of both groups.

Table 15 – Normalized occurrence values of "being the node with highest connections" in a connectivity network of each subject as % percent. Grey shaded cell-lines indicate important results.

Group	**Node**	Controls		Dyslexics	
Condition		BS	AS	BS	AS
Number of being outgoing connection hub node	FL	0.0%	3.7%	0.0%	6.5%
	FR	0.0%	0.0%	9.7%	12.9%
	PL	29.6%	33.3%	48.4%	45.2%
	PR	40.7%	33.3%	35.5%	25.8%
	OPL	14.8%	40.7%	16.1%	35.5%
	OPR	44.4%	44.4%	16.1%	19.4%
Number of being incoming connection hub node	FL	55.6%	55.6%	58.1%	51.6%
	FR	63.0%	55.6%	29.0%	25.8%
	PL	3.7%	14.8%	16.1%	25.8%
	PR	18.5%	18.5%	12.9%	22.6%
	OPL	11.1%	11.1%	6.5%	3.2%
	OPR	7.4%	3.7%	22.6%	6.5%
Number of subjects (n):		27		31	
Outgoing Connection Hub Node		OPR	OPR	PL	PL
Incoming Connection Hub Node		FR	FL,FR	FL	FL

Note that, the number of hub nodes exceed the number of total subjects in a group for some cases according to Table 15. The reason is, there may be multiple hub nodes for each subject, e.g., two or more nodes may have equal hub node appearance value which is higher than the values of other nodes.

According to the hub node analysis shown in Table 15; following results were found and comments were made for the control and dyslexic groups for this study:

1. Before stimulus condition of control group
    a. The node OPR (Right occipito-parietal area) is the main hub for transmitting information. The node PR (Right parietal area) is also minor hub node for transmitting the information.
    b. FR (Right frontal) node is the main hub node which the information flow is focused to. FL (Left frontal node) has also high incoming connection hub node occurrences.

2. After stimulus condition of control group
    a. The nodes OPR (Right occipito-parietal area) and OPL (Left occipito-parietal area) are the two main hubs for transmitting information.
    b. FL (Left frontal area) and FR (Right frontal area) are the main hub nodes which have highest incoming connections occurrences.
3. Before stimulus condition of dyslexic group
    a. PL (Left parietal area) is the main hub node which the information is emitted from. PR (Right parietal area) is also hub node for some subjects.
    b. The node FL (Left frontal area) is the main hub node for collection of information while other nodes have hub node occurrences but values are not close to FL.
4. After stimulus condition of dyslexic group
    c. PL (Left parietal area) and OPL (Left occipito-parietal area) are hub nodes for dyslexic group.
    d. The node FL (Left frontal area) is the main hub node for information collection in dorsal region.

According to the results above, several conclusions can be made. First, before stimulus condition of control group has their hub nodes distributed mostly in right hemispheres (Result 1-a, 1-b). However, hub nodes of dyslexics were located mostly on left hemisphere for before stimulus condition (Result (3-a, 3-b).

During reading state, control group outgoing connection hub nodes were collected mostly on occipital lobe, on the other hand, left side of dyslexic brains have hub nodes for outgoing connections (Results 2-a and 4-a). This may conclude that the occipital region is important for proper reading.

Information mainly flows to frontal region for both groups. The results are as expected: Increased frontal region activity during reading task, since frontal lobe is directly related with conscious and thinking related tasks (Chapter 2.1).

Chi-square test was made between groups and conditions in order to compare proportions in Table 15 (See Chapter 2.9). Using the Equation (55), chi-square test for proportions were made for the following groups: before stimulus - after stimulus condition of control group for outgoing connection hub nodes (See Table 16), before stimulus - after stimulus condition of dyslexic group for outgoing connection hub

nodes (See Table 17), before stimulus - after stimulus condition of control group for incoming connection hub nodes (See Table 18), before stimulus - after stimulus condition of dyslexic group for incoming connection hub nodes (See Table 19), control group - dyslexic group for outgoing connection hub nodes of before stimulus condition (See Table 20), control group - dyslexic group for outgoing connection hub nodes of after stimulus condition (See Table 21), control group - dyslexic group for incoming connection hub nodes of before stimulus condition (See Table 22), control group - dyslexic group for incoming connection hub nodes of after stimulus condition (See Table 23).

Table 16 – Results of Chi-square test for proportions for before stimulus - after stimulus condition of control group for outgoing connection hub nodes.

Nodes	**Control group, Before stimulus, Outgoing connections occurrences in %**	**Control group, After stimulus, Outgoing connections occurrences in %**	**Chi-square (χ^2)**	**p (two-tailed)**
FL	0.0	3.7	0.999	0.32
FR	0.0	0.0	---	1.00
PL	29.6	33.3	0.084	0.77
PR	40.7	33.3	0.311	0.58
OPL	14.8	40.7	4.433	0.03
OPR	44.4	44.4	---	1.00

Table 17 – Results of Chi-square test for proportions for before stimulus - after stimulus condition of dyslexic group for outgoing connection hub nodes

Nodes	Dyslexic group, Before stimulus, Outgoing connections occurrences in %	Dyslexic group, After stimulus, Outgoing connections occurrences in %	Chi-square ($\chi 2$)	p (two-tailed)
FL	0.0	6.5	2.049	0.15
FR	9.7	12.9	0.156	0.69
PL	48.4	45.2	0.063	0.80
PR	35.5	25.8	0.675	0.41
OPL	16.1	35.5	2.998	0.08
OPR	16.1	19.4	0.114	0.74

Table 18 – Results of Chi-square test for proportions for before stimulus - after stimulus condition of control group for incoming connection hub nodes

Nodes	Control group, Before stimulus, Incoming connections occurrences in %	Control group, After stimulus, Incoming connections occurrences in %	Chi-square ($\chi 2$)	p (two-tailed)
FL	55.6	55.6	---	1.00
FR	63.0	55.6	0.301	0.58
PL	3.7	14.8	1.945	0.16
PR	18.5	18.5	---	1.00
OPL	11.1	11.1	---	1.00
OPR	7.4	3.7	0.346	0.56

Table 19 – Results of Chi-square test for proportions for before stimulus - after stimulus condition of dyslexic group for incoming connection hub nodes

Nodes	Dyslexic group, Before stimulus, Incoming connections occurrences in %	Dyslexic group, After stimulus, Incoming connections occurrences in %	Chi-square ($\chi 2$)	p (two-tailed)
FL	58.1	51.6	0.260	0.61
FR	29.0	25.8	0.079	0.78
PL	16.1	25.8	0.866	0.35
PR	12.9	22.6	0.983	0.32
OPL	6.5	3.2	0.360	0.55
OPR	22.6	6.5	3.179	0.07

Table 20 – Results of Chi-square test for proportions for control group - dyslexic group for outgoing connection hub nodes of before stimulus condition.

Nodes	Control group, Before stimulus, Outgoing connections occurrences in %	Dyslexic group, Before stimulus, Outgoing connections occurrences in %	Chi-square ($\chi 2$)	p (two-tailed)
FL	0.0	0.0	---	1.00
FR	0.0	9.7	2.715	0.09
PL	29.6	48.4	2.095	0.15
PR	40.7	35.5	0.163	0.69
OPL	14.8	16.1	0.018	0.89
OPR	44.4	16.1	5.486	0.02

Table 21 – Results of Chi-square test for proportions for control group - dyslexic group for outgoing connection hub nodes of after stimulus condition.

Nodes	Control group, After stimulus, Outgoing connections occurrences in %	Dyslexic group, After stimulus, Outgoing connections occurrences in %	Chi-square ($\chi 2$)	p (two-tailed)
FL	3.7	6.5	0.226	0.63
FR	0.0	12.9	3.676	0.05
PL	33.3	45.2	0.839	0.36
PR	33.3	25.8	0.385	0.53
OPL	40.7	35.5	0.163	0.68
OPR	44.4	19.4	4.141	0.04

Table 22 - Results of Chi-square test for proportions for control group - dyslexic group for incoming connection hub nodes of before stimulus condition.

Nodes	Control group, Before stimulus, Incoming connections occurrences in %	Dyslexic group, Before stimulus, Incoming connections occurrences in %	Chi-square ($\chi 2$)	p (two-tailed)
FL	55.6	58.1	0.036	0.85
FR	63.0	29.0	6.629	0.01
PL	3.7	16.1	2.355	0.12
PR	18.5	12.9	0.339	0.56
OPL	11.1	6.5	0.380	0.54
OPR	7.4	22.6	2.499	0.11

Table 23 – Results of Chi-square test for proportions for control group - dyslexic group for incoming connection hub nodes of after stimulus condition.

Nodes	Control group, After stimulus, Incoming connections occurrences in %	Dyslexic group, After stimulus, Incoming connections occurrences in %	Chi-square ($\chi 2$)	p (two-tailed)
FL	55.6	51.6	0.091	0.76
FR	55.6	25.8	5.262	0.02
PL	14.8	25.8	1.046	0.30
PR	18.5	22.6	0.145	0.70
OPL	11.1	3.2	1.382	0.24
OPR	3.7	6.5	0.226	0.63

1. By comparing for before stimulus - after stimulus condition of control group for outgoing connection hub nodes, according to Table 16;

OPL (Left occipito-parietal area) causes significant ($p < 0.03$) difference between before and after stimulus conditions. Outgoing hub node occurrences of OPL drastically increases from before stimulus to after stimulus conditions. This is an expected result, since the reading circuity in brain is mainly located at left occipito-temporal and occipito-parietal regions [152].

2. By comparing control group - dyslexic group for outgoing connection hub nodes of before stimulus condition, according to Table 20;

OPR (Right occipito-parietal area) causes significant ($p < 0.02$) difference between control and dyslexic groups. This may show that dyslexic group has lesser information transmission from right dorsal regions on pre-stimulus state.

3. By comparing control group - dyslexic group for outgoing connection hub nodes of after stimulus condition, according to Table 21;

Both FR (Right frontal area) ($p < 0.05$) and OPR (Right occipito-parietal area) ($p < 0.04$) have significant differences between control and dyslexic groups. Together with the significant result in Table 20, such differences can be important for comparing groups and may be a sign for "suppressed right dorsal activity in dyslexic subjects".

4. By comparing control group - dyslexic group for incoming connection hub nodes of before stimulus condition, according to Table 22;

FR (Right frontal area) shows significant ($p < 0.01$) difference between groups. This may be an indicator for lesser information transmission to right frontal regions for dyslexic group.

5. By comparing control group - dyslexic group for incoming connection hub nodes of after stimulus condition, according to Table 23;

FR (Right frontal area) shows significant ($p < 0.02$) difference between groups. Similar to before stimulus condition (Table 22), this result may show a lesser information transmission to right frontal regions for dyslexic subjects.

CHAPTER 4

CONCLUSION

4.1. Summary of the Results and Relation with Literature

The aim of the study was to find differences between connectivity networks of control and dyslexic groups with graph theory measures, if exist (Chapter 1, Chapter 3.1). This was achieved by making connectivity analyses (Chapter 3.4), calculating the graph theory properties from connectivity maps (Chapter 3.5) and detection of hub nodes (Chapter 3.7) as well as statistically analysing those graph theory values for independent (Controls - Dyslexics) and dependent (Before stimulus – After Stimulus) groups (Chapter 0).

As explained in Chapter 1.4, PDC is one of the popular algorithms to estimate brain connectivities [25] [74] [153]. This idea can be supported by the connectivity results of group averages in Table 6 such that the connectivity values of group averages contain higher connectivity values for diagonal elements which is an expected outcome. To analyse connectivity networks, graph theory analyses are useful to reveal the connectivity behaviours of networks [74]. The values for global efficiency (Table 7), clustering coefficient (Table 8), characteristic path length (Table 9) and small-world measure (Table 10) were calculated using PDC connectivity matrices. Statistical analysis of small-world measure yielded significant difference ($p < 0.049$) between control and dyslexic group (Chapter 3.6.1). Similarly, global efficiency is found to be significant ($p < 0.031$) for control group and characteristic path length ($p < 0.012$) and clustering coefficient ($p < 0.028$) are found to be significant for dyslexic group between before stimulus and after stimulus conditions (Chapter 3.6.2).

According to Table 11, statistical analyses of graph theory properties between control and dyslexic group had no significant difference for before stimulus condition for characteristic path length, clustering coefficient, global efficiency and small world measure. For after stimulus condition: Characteristic path length, clustering coefficient and global efficiency values had no significant difference. These findings are similar with the study of Hosseini et al. (2013) [16] as they had no significant differences between control and dyslexic groups in terms of characteristic path length and clustering coefficient. However, small-world measure values have significantly different ($p < 0.049$) results. To our knowledge, there is no study which investigated small-world measure between control and dyslexic subjects for reading stimuli to compare. But, by small-worldness definition (see Chapter 2.7.4), we can conclude, dyslexic group have more direct connections with more clustering tendency between nodes with significantly higher small-world measures. This may mean that the information between nodes would flow faster. Therefore, we may conclude that, dyslexic subjects have more direct connections between nodes, but without efficient transmission of information.

Statistical analyses (Table 13, Table 14) between dependent samples show that global efficiency ($p < 0.031$) is an important variable for control subjects; characteristic path length ($p < 0.012$) and clustering coefficient ($p < 0.028$) are important variables for dyslexic subjects to cause differences between before and after stimulus conditions. According to Table 14, global efficiency for control group with statistically different significance value ($p < 0.031$) may show that efficiency in connections increases with a visual stimulus (word) and reading process. Comparing of this result with dyslexic subjects in Table 14, may show: Control group brains have better task orientation than dyslexic brains in reading task. This conclusion may support the results of [154] in terms of their findings for non-dyslexic readers about better adaptation to reading task and results of [10] which says that dyslexic subjects have disruption in the organisation of the brain for reading task. Several studies [155] [156] also point out the deficiency in orientation to the task of dyslexic subjects during reading tasks. And there are many studies [44] [59] [62] [67] [69] [70] [71] [73] [75] which have investigated the abnormalities (functional, structural or effective) during reading task of dyslexic group

Results from Table 13 may also show that, applying stimulus distorts the direct connections and causes more clustering in dyslexic brains. Considering the conclusion in second paragraph of this chapter, this result may also point the problem in connections between clusters, instead of connections between individual nodes. This conclusion is supporting the results of an fMRI voxel-cluster studies [50] [157] in terms of the differences in clusters of dyslexic and control brains, but not the same due to the methods which have been used.

Hub node analyses in Chapter 3.7 have both expected and interesting results. An expected result is the increasing of hub occurrence frequency of OPL (Left occipito-parietal area) for after stimulus compared to before stimulus condition for both groups. This is an expected result, because the reading circuitry is located in left hemisphere, starting from left dorsal regions (left occipito-temporal region) to medial regions [158] [159]. An interesting result from Table 15 is incoming connection hub node differences between control and dyslexic groups. For control group, whole frontal lobe acts as hub node. However, for dyslexic group, left frontal lobe is a dominant hub node. Therefore, there might be a disorientation between left-right hemispheres of dyslexic group, especially at frontal region. A study [33] had similar result which tells dyslexic group has reduced functional connections from occipitotemporal region to frontal regions. Many studies [11] [12] [59] [60] [61] found less activations in frontal lobe for dyslexics which support our results. Some studies [29] [30] point out the importance of investigating connectivities in the frontal regions for dyslexics.

4.2. Importance of the Study and Future Work

According to our information, this is the first study that is making hub analysis for incoming and outgoing information in EEG data for dyslexia. To our information, this study is also the first study which made graph theory analyses on connectivity networks for reading stimulus.

The study can be repeated with longer EEG data in order to prevent MVAR validation problems as described in Chapter 2.5.3.2 and Chapter 3.3. Longer EEG data can also provide opportunity to work with more electrodes to successfully perform MVAR model validation. Using an EEG device which has more channels also enables to analyse more detailed areas. The more electrode number means the more spatial resolution. Therefore, the determination of abnormal brain regions becomes more accurate.

The hub node analyses can be extended in order to find differences between regions on left and right hemispheres. To make such comparisons, chi-square test can be used. Comparing left and right hemispheres may yield differences between before and after stimulus as well as control and dyslexic groups.

The analyses was made by using data from relatively low subjects (27 controls and 31 dyslexics) compared with related studies in literature [33] [52] [54] [72]. Using data from more subjects would yield more reliable and more statistically different results. Moreover, more data can be collected from children aged 2-7 (pre readers) and same analyses should be performed to compare results in terms of similarities or differences. Doing so, it may be easier to create early diagnosis algorithms for detection of dyslexia, before dyslexic children experience negative psychological and social factors.

REFERENCES

[1] R. L. Peterson and B. Pennington, "Developmental dyslexia," *Annual Review of Clinical Psychology,* vol. 11, pp. 283-307, 2015.

[2] E. Paulesu, U. Frith, M. Snowling, A. Gallagher, J. Morton, R. S. J. Frackowiak and C. D. Frith, "Is developmental dyslexia a disconnection syndrome? Evidence from PET scanning," *Brain,* vol. 119, pp. 143-157, 1996.

[3] K. J. Friston, "Functional and Effective Connectivity in Neuroimaging: A Synthesis," *Human Brain Mapping,* vol. 2, pp. 56-78, 1994.

[4] V. Sakkalis, "Review of advanced techniques for the estimation of brain connectivity measured with EEG/MEG," *Computers in Biology and Medicine,* vol. 41, pp. 1110-1117, 2011.

[5] J. F. Geweke, "Measures of Conditional Linear Dependence and Feedback Betvveen Time Series," *Journal of the American Statistical Association,* vol. 79, no. 388, pp. 907-915, 1984.

[6] I. N. C. Lawes, T. R. Barrick, V. Murugam and N. Spierings, "Atlas-based segmentation of white matter tracts of the human brain using diffusion tensor tractography and comparison with classical dissection," *NeuroImage,* vol. 39, no. 1, pp. 62-79, 2008.

[7] E. Bullmore, M. Brammer, S. Rabe-Hesketh, V. Curtis, R. Morris, S. Williams, T. Sharma and P. McGuire, "Methods for Diagnosis and Treatment of Stimulus-Correlated Motion in Generic Brain Activation Studies Using fMRI," *Human Brain Mapping,* vol. 7, no. 1, p. 38–48, 1999.

[8] D. J. A. Smit, C. J. Stam and D. Posthuma, “Heritability of ‘‘Small-World’’ Networks in the Brain: A Graph Theoretical Analysis of Resting-State EEG Functional Connectivity,” *Human Brain Mapping,* vol. 29, p. 1368–1378, 2008.

[9] J. Li, “Dynamic Bayesian Networks Modeling and Analysis of Neural Signals,” The University of British Columbia, Vancouver, 2009.

[10] S. E. Shaywıtz, B. A. Shaywıtz, K. R. Pugh, R. K. Fulbrıght, R. T. Constable, W. Mencl, D. P. Shankweıler, A. M. Lıberman, P. Skudlarskı, J. M. Fletcheri, L. Katz, K. E. Marchıone, C. Lacadıe, C. Gatenby and J. C. Gore, “Functional disruption in the organization of the brain for reading in dyslexia,” *Neurobiology,* vol. 95, p. 2636–2641, 1998.

[11] F. Richlan, M. Kronbichler and H. Wimmer, “Functional Abnormalities in the Dyslexic Brain: A Quantitative Meta-Analysis of Neuroimaging Studies,” *Human Brain Mapping,* vol. 30, p. 3299–3308, 2009.

[12] F. Richlan, M. Kronbichler and H. Wimmer, “Meta-analyzing brain dysfunctions in dyslexic children and adults,” *NeuroImage,* vol. 56, p. 1735–1742, 2011.

[13] F. Richlan, M. Kronbichler and Heinz Wimmer, “Structural Abnormalities in the Dyslexic Brain: A Meta-Analysis of Voxel-Based Morphometry Studies,” *Human Brain Mapping,* vol. 34, p. 3055–3065, 2013.

[14] M. Cole, S. Pathak and W. Schneider, “Identifying the brain's most globally connected regions,” *NeuroImage,* vol. 49, p. 3132–3148, 2010.

[15] M. Rubinov and O. Sporns, “Complex network measures of brain connectivity: uses and interpretations,” *NeuroImage,* vol. 52, p. 1059–1069, 2010.

[16] S. H. Hosseini, J. M. Black, T. Soriano, N. Bugescu, R. Martinez, M. M. Raman, S. R. Kesler and F. Hoeft, “Topological properties of large-scale structural brain networks in children with familial risk for reading difficulties,” *NeuroImage,* vol. 71, pp. 260-274, 2013.

[17] “AI Impacts,” 14 04 2015. [Online]. Available: http://aiimpacts.org/rate-of-neuron-firing/. [Accessed 2016].

[18] D. R. Cleary, A. M. Raslan, J. E. Rubin, D. Bahgat and A. Viswanathan, “Deep brain stimulation entrains local neuronal firing in human globus pallidus internus,” *J Neurophysiol,* vol. 109, p. 978–987, 2012.

[19] G. A. Ojemann, “Human Temporal Cortical Single Neuron Activity during Language: A Review,” *Brain Sci.,* vol. 3, pp. 627-641, 2013.

[20] Y. Nir, R. Mukamel, I. Dinstein, E. Privman, M. Harel, L. Fisch, H. Gelbard-Sagiv, S. Kipervasser, F. Andelman, M. Y. Neufeld, U. Kramer, A. Arieli, I. Fried and R. Malach, “Interhemispheric correlations of slow spontaneous neuronal fluctuations revealed in human sensory cortex,” *Nat Neurosci,* vol. 11, no. 9, p. 1100–1108, 2008.

[21] “Cost Helper,” [Online]. Available: http://health.costhelper.com/eeg.html. [Accessed 2016].

[22] “Quora,” 21 5 2012. [Online]. Available: https://www.quora.com/How-much-does-an-fMRI-machine-cost. [Accessed 2016].

[23] R. C. Chu, “Positron Emission Tomography: An Emerging Technology,” *Proc Annu Symp Comput Appl Med Care,* vol. 1, pp. 469-475, 1980.

[24] L. Astolfi, F. Cincotti, D. Mattia, M. G. Marciani, L. A. Baccala, F. d. V. Fallani, S. Salinari, M. Ursino, M. Zavaglia, L. Ding, J. C. Edgar, G. A. Miller, B. He and F. Babiloni, “Comparison of Different Cortical Connectivity Estimators for High-Resolution EEG Recordings,” *Human Brain Mapping,* vol. 28, p. 143–157, 2007.

[25] M. Kaminski and K. J. Blinowska, “Directed Transfer Function is not influenced by volume conduction—inexpedient pre-processing should be avoided,” *Frontiers in Computational Neuroscience,* vol. 8, no. 61, 2014.

[26] A. Omidvarnia, G. Azemi, B. Boashash, J. M. O’Toole, P. B. Colditz and S. Vanhatalo, “Measuring Time-Varying Information Flow in Scalp EEG Signals: Orthogonalized Partial Directed Coherence,” *IEEE Transactions on Biomedical Engineering ,* vol. 61, no. 33, pp. 680 - 693, 2013.

[27] L. Leistritz, B. Pester, A. Doering, K. Schiecke, F. Babiloni, L. Astolfi and H. Witte, "Time-variant partial directed coherence for analysing connectivity: a methodological study," *Phil. Trans. R. Soc. A,* vol. 371, no. 1997, 2013.

[28] C. Brunner, M. Billinger, M. Seeber, T. R. Mullen and S. Makeig, "Volume Conduction Influences Scalp-Based Connectivity Estimates," *Front. Comput. Neurosci.,* vol. 10, no. 121, pp. 1-4, 2016.

[29] F. Ramus, "Neuroimaging sheds new light on the phonological deficit in dyslexia," *Trends in Cognitive Sciences,* vol. 18, no. 6, pp. 274-275, 2014.

[30] B. Boets, H. P. O. d. Beeck, M. Vandermosten, S. K. Scott, C. R. Gillebert, D. Mantini, J. Bulthé, S. Sunaert, J. Wouters and P. Ghesquière, "Intact But Less Accessible Phonetic Representations in Adults with Dyslexia," *Science,* vol. 342, pp. 1251-1254, 2013.

[31] K. Specht, K. Hugdahl, S. Ofte, M. Nygård, A. Bjørnerud, E. Plante and T. Helland, "Brain activation on pre-reading tasks reveals at-risk status for dyslexia in 6-year-old children," *Scand J Psychol,* vol. 50, no. 1, pp. 79-91, 2009.

[32] N. M. Raschle, J. Zuk and N. Gaab, "Functional characteristics of developmental dyslexia in left-hemispheric posterior brain regions predate reading onset," *PNAS,* vol. 109, no. 6, pp. 2156-2161, 2012.

[33] M. Vandermosten, J. Vanderauwera, C. Theys, A. D. Vos, S. Vanvooren, S. Sunaert and P. G. Jan Wouters, "A DTI tractography study in pre-readers at risk for dyslexia," *Developmental Cognitive Neuroscience,* vol. 14, pp. 8-15, 2015.

[34] J. M. Black, H. Tanaka, L. Stanley, M. Nagamine, N. Zakeran, A. Thurston, S. Kesler, C. Hulme, H. Lyytinen, G. H. Glover, C. Serrone, M. M. Raman, A. L. Reiss and F. Hoeft, "Maternal History of Reading Difficulty is Associated with Reduced Language-Related Grey Matter in Beginning Readers," *Neuroimage,* vol. 59, no. 3, p. 3021–3032, 2012.

[35] W. E. Brown, S. Eliez, V. Menon, J. Rumsey, C. White and A. Reiss, "Preliminary evidence of widespread morphological variations of the brain in dyslexia," *Neurology,* vol. 56, no. 6, pp. 781-784, 2001.

[36] F. Hoeft, A. Meyler, A. Hernandez, C. Juel, H. Taylor-Hill, J. L. Martindale, G. McMillon, G. Kolchugina, J. M. Black, A. Faizi, G. K. Deutsch, W. T. Siok, A. L. Reiss, S. Whitfield-Gabrieli and J. D. E. Gabrieli, "Functional and morphometric brain dissociation between dyslexia and reading ability," *PNAS,* vol. 104, no. 10, pp. 4234-4239, 2007.

[37] S. L. Rimrodt, D. J. Peterson, M. B. Denckla, W. E. Kaufmann and L. E. Cutting, "White matter microstructural differences linked to left perisylvian language network in children with dyslexia," *Cortex,* vol. 46, no. 6, p. 739–749, 2010.

[38] S. E. Shaywitz and B. A. Shaywitz, "Dyslexia (Specific Reading Disability)," *Biol Psychiatry,* vol. 57, pp. 1301-1309, 2005.

[39] E. Vinckenbosch, F. Robichon and S. Eliez, "Gray matter alteration in dyslexia: converging evidence from volumetric and voxel-by-voxel MRI analyses," *Neuropsychologia,* vol. 43, no. 3, p. 324–331, 2005.

[40] C. Steinbrink, K. Vogt, A. Kastrup, H.-P. Müller, F. Juengling, J. Kassubek and A. Riecker, "The contribution of white and gray matter differences to developmental dyslexia: Insights from DTI and VBM at 3.0 T," *Neuropsychologia,* vol. 46, p. 3170–3178, 2008.

[41] Z. Cui, Z. Xia, M. Su, H. Shu and G. Gong, "Disrupted White Matter Connectivity Underlying Developmental Dyslexia: A Machine Learning Approach," *Human Brain Mapping,* vol. 37, p. 1443–1458, 2016.

[42] M. Kronbichler, H. Wimmer, W. Staffen, F. Hutzler, A. Mair and G. Ladurner, "Developmental Dyslexia: Gray Matter Abnormalities in the Occipitotemporal Cortex," *Human Brain Mapping,* vol. 29, p. 613–625, 2008.

[43] D. Menghini, G. E. Hagberg, L. Petrosini, M. Bozzali, E. Macaluso, C. Caltagirone and S. Vicari, "Structural Correlates of Implicit Learning Deficits in Subjects with Developmental Dyslexia," *Ann. N.Y. Acad. Sci,* vol. 1145, pp. 212-221, 2008.

[44] K. A. Clark, T. Helland, K. Specht, K. L. Narr, F. R. Manis, A. W. Toga and K. Hugdahl, "Neuroanatomical precursors of dyslexia identified from pre-reading through to age 11," *Brain,* vol. 137, p. 3136–3141, 2014.

[45] C. Beaulieu, C. Plewes, L. A. Paulson, D. Roy, L. Snook, L. Concha and L. Phillips, “Imaging brain connectivity in children with diverse reading ability,” *NeuroImage,* vol. 25, p. 1266– 1271, 2005.

[46] M. Vandermosten, F. Hoeft and E. S. Norton, “Integrating MRI brain imaging studies of pre-reading children with current theories of developmental dyslexia: a review and quantitative meta-analysis,” *Current Opinion in Behavioral Sciences,* vol. 10, pp. 155-161, 2016.

[47] G. Deutsch, R. Dougherty, R. Bammer, W. Siok, J. Gabrieli and B. Wandell, “Children's reading performance is correlated with white matter structure measured by diffusion tensor imaging,” *Cortex,* vol. 41, no. 3, pp. 354-63, 2005.

[48] A. M. Galaburda and T. L. Kemper, “Cytoarchitectonic Abnormalities in Developmental Dyslexia: A Case Study,” *Ann Neurol,* vol. 6, pp. 94-100, 1979.

[49] G. Silani, U. Frith, J.-F. Demonet, F. Fazio, D. Perani, C. Price, C. D. Frith and E. Paulesu, “Brain abnormalities underlying altered activation in dyslexia: a voxel based morphometry study,” *Brain,* vol. 128, pp. 2453-2461, 2005.

[50] T. Richards, J. Stevenson, J. Crouch, L. Johnson, K. Maravilla, P. Stock, R. Abbott and V. Berninger, “Tract-Based Spatial Statistics of Diffusion Tensor Imaging in Adults with Dyslexia,” *AJNR Am J Neuroradiol,* vol. 29, no. 6, p. 1134–1139, 2008.

[51] A. J. Krafnick, D. L. Flowers, E. M. Napoliello and G. F. Eden, “Gray matter volume changes following reading intervention in dyslexic children,” *Neuroimage,* vol. 57, no. 3, p. 733–741, 2011.

[52] C. Pernet, J. Andersson, E. Paulesu and J. F. Demonet, “When All Hypotheses are Right: A Multifocal Account of Dyslexia,” *Human Brain Mapping,* vol. 30, p. 2278–2292, 2009.

[53] J. Linkersdörfer, A. Jurcoane, S. Lindberg, J. Kaiser, M. Hasselhorn, C. J. Fiebach and J. Lonnemann, “The Association between Gray Matter Volume and Reading Proficiency: A Longitudinal Study of Beginning Readers,” *Journal of Cognitive Neuroscience,* vol. 27, no. 2, p. 308–318, 2014.

[54] Y. Wang, M. V. Mauer, T. Raney, B. Peysakhovich, B. L. C. Becker, D. D. Sliva and N. Gaab, "Development of Tract-Specific White Matter Pathways During Early Reading Development in At-Risk Children and Typical Controls," *Cerebral Cortex,* pp. 1-17, 2016.

[55] J. C. Carter, D. C. Lanham, L. E. Cutting, A. M. Clements-Stephens, X. Chen, M. Hadzipasic, J. Kim, M. B. Denckla and W. E. Kaufmann, "A dual DTI approach to analyzing white matter in children with dyslexia," *Psychiatry Res,* vol. 172, no. 3, p. 215–219, 2009.

[56] R. E. Frye, J. Liederman, K. M. Hasan, A. Lincoln, B. Malmberg, J. McLean and A. Papanicolaou, "Diffusion Tensor Quantification of the Relations Between Microstructural and Macrostructural Indices of White Matter and Reading," *Human Brain Mapping,* vol. 32, p. 1220–1235, 2011.

[57] P. Humphreys, W. E. Kaufmann and A. M. Galaburda, "Developmental Dyslexia in Women: Neuropathological Findngs in Three Patients," *Ann Neurol,* vol. 28, pp. 727-738, 1990.

[58] S. Eliez, J. M. Rumsey, J. N. Giedd, J. E. Schmitt, A. J. Patwardhan and A. L. Reiss, "Morphological Alteration of Temporal Lobe Grey Matter in Dyslexia: An MRI Study," *J. Child Psychol. Psychiat.,* vol. 41, no. 5, pp. 637-644, 2000.

[59] J. M. Maisog, E. R. Einbinder, D. L. Flowers, P. E. Turkeltaub and G. F. Eden, "A Meta-analysis of Functional Neuroimaging Studies of Dyslexia," *Ann. N.Y. Acad. Sci.,* vol. 1145, p. 237–259, 2008.

[60] F. Cao, T. Bitan, T.-L. Chou, D. D. Burman and J. R. Booth, "Deficient orthographic and phonological representations in children with dyslexia revealed by brain activation patterns," *J Child Psychol Psychiatry,* vol. 47, no. 10, p. 1041–1050, 2006.

[61] J. R. Booth, G. Bebko, D. D. Burman and T. Bitan, "Children with reading disorder show modality independent brain abnormalities during semantic tasks," *Neuropsychologia,* vol. 45, no. 4, p. 775–783, 2007.

[62] F. Richlan, D. Sturm, M. Schurz, M. Kronbichler, G. Ladurner and H. Wimmer, "A Common Left Occipito-Temporal Dysfunction in Developmental Dyslexia

and Acquired Letter-By-Letter Reading?," *PLoS ONE,* vol. 5, no. 8, p. e12073, 2010.

[63] H. Wimmer, M. Schurz, D. Sturm, F. Richlan, J. Klackl, M. Kronbichler and G. Ladurner, "A dual-route perspective on poor reading in a regular orthography: An fMRI study," *Cortex,* vol. 46, pp. 1284-1298, 2010.

[64] J. M. Rumsey, B. Horwitz, B. C. Donohue, K. Nace, J. M. Maisog and P. Andreason, "Phonological and orthographic components of word recognition A PET-rCBF study," *Brain,* vol. 120, p. 739–759, 1997.

[65] Y. Yamada, C. Stevens, M. Dow, A. H. B., J. C. D. and J. N. H., "Emergence of the neural network for reading in five-year-old beginning readers of different levels of pre-literacy abilities: an fMRI study," *Neuroimage,* vol. 57, p. 704–713, 2011.

[66] A. Martin, M. Kronbichler and F. Richlan, "Dyslexic Brain Activation Abnormalities in Deep and Shallow Orthographies: A Meta-Analysis of 28 Functional Neuroimaging Studies," *Human Brain Mapping,* vol. 37, p. 2676–2699, 2016.

[67] V. Blau, J. Reithler, N. v. Atteveldt, J. Seitz, P. Gerretsen, R. Goebel and L. Blomert, "Deviant processing of letters and speech sounds as proximate cause of reading failure: a functional magnetic resonance imaging study of dyslexic children," *Brain,* vol. 133, pp. 868-879, 2010.

[68] E. Schulz, U. Maurer, S. v. d. Mark, K. Bucher, S. Brem, E. Martin and D. Brandeis, "Reading for meaning in dyslexic and young children: Distinct neural pathways but common endpoints," *Neuropsychologia,* vol. 47, p. 2544–2557, 2009.

[69] U. Maurer, E. Schulz, S. Brem, S. v. d. Mark, K. Bucher, E. Martin and D. Brandeis, "The development of print tuning in children with dyslexia: Evidence from longitudinal ERP data supported by fMRI," *NeuroImage,* vol. 57, p. 714–722, 2011.

[70] K. R. Pugh, W. E. Mencl, A. R. Jenner, L. Katz, S. J. Frost, J. R. Lee, S. E. Shaywitz and B. A. Shaywitz, "Functional Neuroimaging Studies of Reading

adn Reading Disability (Developmental Dyslexia)," *Mental Retardation and Developmental Disabilities,* vol. 6, pp. 207-213, 2000.

[71] B. L. Schlaggar and B. D. McCandliss, "Development of Neural Systems for Reading," *Annu. Rev. Neurosci,* vol. 30, p. 475–503, 2007.

[72] B. A. Shaywitz, P. Skudlarski, J. M. Holahan, K. E. Marchione, R. T. Constable, R. K. Fulbright, D. Zelterman, C. Lacadie and S. E. Shaywitz, "Age-Related Changes in Reading Systems of Dyslexic Children," *Ann Neurol,* vol. 61, p. 363–370, 2007.

[73] J. A. Church, R. S. Coalson, H. M. Lugar, S. E. Petersen and B. L. Schlaggar, "A Developmental fMRI Study of Reading and Repetition Reveals Changes in Phonological and Visual Mechanisms Over Age," *Cerebral Cortex,* vol. 18, pp. 2054-2065, 2008.

[74] D. Huang, A. Ren, J. Shang, Q. Lei, Y. Zhang, Z. Yin, J. Li, K. M. v. Deneen and L. Huang, "Combining Partial Directed Coherence and Graph Theory to Analyse Effective Brain Networks of Different Mental Tasks," *Frontiers in Human Neuroscience,* vol. 10, no. 235, 2016.

[75] G. F. González, M. V. d. Molen, G. Žarić, M. Bonte, J. Tijms, L. Blomert, C. Stam and M. V. d. Molena, "Graph analysis of EEG resting state functional networks in dyslexic readers," *Clinical Neurophysiology,* vol. 127, no. 9, p. 3165–3175, 2016.

[76] P. Brodal, The Central Nervous System: Structure and Function, Oxford University Press, 2010.

[77] A. Schüz and H. Preissl, "Basic Connectivity of the Cerebral Cortex and some Considerations on the Corpus Callosum," *Neuroscience and Biobehavioral Reviews,* vol. 20, no. 4, pp. 567-570, 1996.

[78] H. M. Duvernoy, P. Bourgouin, E. A. Cabanis, F. Cattin, J. Guyot, M. T. Iba-Zizen, P. Maeder, B. Parratte, L. Tatu and F. Vuillier, The Human Brain: Surface, Three-Dimensional Sectional Anatomy with MRI, and Blood Supply, SpringerWienNewYork, 1999.

[79] “Upright Health,” Upright Health, [Online]. Available: http://www.upright-health.com/lateral-ventricles. [Accessed 2016].

[80] A. Nieoullon, “Dopamine and the regulation of cognition and attention,” *Progress in Neurobiology*, vol. 67, pp. 53-83, 2002.

[81] S. L. E. Brownsett and R. J. S. Wise, “The Contribution of the Parietal Lobes to Speaking and Writing,” *Cerebral Cortex*, vol. 20, pp. 517-523, 2010.

[82] E. E. Smith and S. M. Kosslyn, Cognitive psychology: Mind and brain, Upper Saddle River, N.J: Pearson/Prentice Hall, 2007.

[83] A. Jeneson and L. R. Squire, “Working memory, long-term memory, and medial temporal lobe function,” *Learning and Memory*, vol. 19, pp. 15-25, 2012.

[84] Wikipedia, “Wikipedia - Sulcus (neuroanatomy),” Wikipedia, [Online]. Available: https://en.wikipedia.org/wiki/Sulcus_(neuroanatomy). [Accessed 2016].

[85] U. o. Tulane, “The macrostructure of the brain,” University of Tulane, [Online]. Available: http://www.tulane.edu/~howard/BrLg/t3-BrainMacro.html. [Accessed 2016].

[86] A. A. Beaton, Dyslexia, Reading and the Brain, Hove and NY: Psychology Press, 2004.

[87] C. J. Price and J. T. Devlin, “The Interactive Account of ventral occipitotemporal contributions to reading,” *Trends in Cognitive Sciences*, vol. 15, no. 6, pp. 246-253, 2011.

[88] F. R. Vellutino and J. M. Fletcher, “Developmental Dyslexia,” in *The Science of Reading: A Handbook*, Oxford, UK, Blackwell Publishing Ltd, 2008, p. ch19.

[89] M. Vigneau, V. Beaucousin, P. Herve, H. Duffau, F. Crivello, O. Houde, B. Mazoyer and N. Tzourio-Mazoyer, “Meta-analyzing left hemisphere language areas: Phonology, semantics, and sentence processing,” *NeuroImage*, vol. 30, p. 1414 – 1432, 2006.

[90] T. J. v. Hartevel, J. Cabral, G. Deco, A. Møller, A. L. Green, T. Z. Aziz and M. L. Kringelbach, "Neural Plasticity in Human Brain Connectivity: The Effects of Long Term Deep Brain Stimulation of the Subthalamic Nucleus in Parkinson's Disease," *PLoS ONE,* vol. 9, no. 1, 2014.

[91] A. Pascual-Leone, C. Freitas, L. Oberman, J. C. Horvath, M. Halko, M. Eldaief, S. Bashir, M. Vernet, M. Shafi, B. Westover, A. M. Vahabzadeh-Hagh and A. Rotenberg, "Characterizing Brain Cortical Plasticity and Network Dynamics Across the Age-Span in Health and Disease with TMS-EEG and TMS-fMRI," *Brain Topogr,* vol. 24, p. 302–315, 2011.

[92] J. Olesen, A. Gustavsson, M. Svensson, H.-U. Wittchen and B. Jönsson, "The economic cost of brain disorders in Europe," *European Journal of Neurology,* vol. 19, p. 155–162, 2012.

[93] P. Thomson and P. Gilchrist, "Dyslexia - A Multidisciplinary Approach," in *Dyslexia - A Multidisciplinary Approach*, Nelson Thornes, 2000, p. 5.

[94] F. E. Tønnessen, "How Can We Best Define 'Dyslexia'?," *Dyslexia,* vol. 3, pp. 78-92, 1997.

[95] G. R. Lyon, S. E. Shaywitz and B. A. Shaywitz, "A Definition of Dyslexia," *Annals of Dyslexia*, vol. 53, pp. 1-14, 2003.

[96] W. Tunmer and K. Greaney, "Defining Dyslexia," *Journal of Learning Disabilities,* vol. 43, no. 3, pp. 229-243, 2010.

[97] L. J. Seidman, M. C. Monuteaux, A. Doyle, J. Biederman and S. V. Faraone, "Learning disabilities and executive dysfunction in boys with attention-deficit/hyperactivity disorder," *Neuropsychology,* vol. 15, no. 4, pp. 544-556, 2001.

[98] G. Russell and Z. Pavelka, "Co-Occurrence of Developmental Disorders: Children Who Share Symptoms of Autism, Dyslexia and Attention Deficit Hyperactivity Disorder," in *Recent advances in Autism Spectrum Disorders*, InTech, 2013, p. Ch17.

[99] C. C. Sexton, H. L. Gelhorn, J. A. Bell and P. M. Classi, "The Co-occurrence of Reading Disorder and ADHD: Epidemiology, Treatment, Psychosocial

Impact, and Economic Burden," *Journal of Learning Disabilities,* vol. 45, no. 6, pp. 538-564, 2012.

[100] B. Kadesjö and C. Gillberg, "The Comorbidity of ADHD in the General Population of Swedish School-age Children," *J. Child Psychol. Psychiat.,* vol. 42, no. 4, pp. 487-492, 2001.

[101] C. S. Roy and C. S. Sherrington, "On the Regulation of the Blood Supply of the Brain," pp. 85-108, 1890.

[102] S. A. Huettel, A. W. Song and G. McCarthy, "Spatial and Temporal Properties of fMRI," in *Functional Magnetic Resonance Imaging*, Sunderland, Massachusetts, Sinauer Associates, Inc, 2004, pp. 198-200; 208-211.

[103] H. M. Doss, "fMRI – The Future Mind Reader?," Physics Central, [Online]. Available: http://physicscentral.com/explore/action/fmri.cfm. [Accessed 2016].

[104] P. J. Basser, J. Mattiello and D. LeBihan, "MR Diffusion Tensor Spectroscopy and Imaging," *Biophysical Journal,* vol. 66, pp. 259-267, 1994.

[105] K. Worsley and K. Friston, "Analysis of fMRI Time-Series Revisited," *NeuroImage,* vol. 2, pp. 173-181, 1995.

[106] K. Worsley, S. Marrett, P. Neelin, A. Vandal, K. Friston and A. Evans, "A Unified Statistical Approach for Determining Significant Signals in Images of Cerebral Activation," *Human Brain Mapping,* vol. 4, pp. 58-73, 1996.

[107] J. Ashburner and K. J. Friston, "Voxel-Based Morphometry—The Methods," *NeuroImage,* vol. 11, p. 805–821, 2000.

[108] C. Hutton, B. Draganski, J. Ashburner and N. Weiskopf, "A comparison between voxel-based cortical thickness and voxel-based morphometry in normal aging," *Neuroimage,* vol. 48, no. 2-8, pp. 371-380, 2009.

[109] M. Eckert, C. Leonard, M. Wilke, M. Eckert, T. Richards, A. Richards and V. Berninger, "Anatomical signatures of dyslexia in children: unique information from manual and voxel based morphometry brain measures.," *Cortex,* vol. 41, no. 3, pp. 304-315, 2005.

[110] D. Bailey, D. Townsend, P. Valk and M. Maisey, Positron Emission Tomography: Basic Sciences, London: Springer Science & Business Media, 2005.

[111] "Positron Emission Tomography," Multimodal NeuroImaging Analysis, 28 April 2015. [Online]. Available: https://multimodalneuroimaging.wordpress.com/. [Accessed 2016].

[112] "Principle of NIRS (near-infrared spectroscopy)," Hamamatsu, [Online]. Available: https://www.hamamatsu.com/us/en/technology/.

[113] "New guidance on transcranial magnetic stimulation echoes Council's call for more evidence collection," Nuffield Council on Bioethics, 23 January 2014. [Online]. Available: http://nuffieldbioethics.org/news/2014/. [Accessed 2016].

[114] "Origin of the Magnetic Field," University of Washington, [Online]. Available: http://ilabs.washington.edu/sites/default/files/magneticfield-origin.jpg. [Accessed 2016].

[115] F. L. d. Silva and D. L. Schomer, Niedermeyer's Electroencephalography: Basic Principles, Clinical Applications, and Related Fields, Lippincott Williams & Wilkins, 2011.

[116] S. Haufe, V. Nikulin and G. Nolte, "Identifying brain effective connectivity patterns from EEG: performance of Granger Causality, DTF, PDC and PSI on simulated data," *Neuroscience,* vol. 12, no. 1, p. 141, 2011.

[117] H. Nyquist, "Certain Topics in Telegraph Transmission Theory," *Proceedings of the IEEE,* pp. 13-17, 1928.

[118] O. Sporns, "Brain Connectivity," *Scholarpedia,* vol. 2, no. 10, p. 4695, 2007.

[119] "Cognitive Engineering," Sinapse Institute, [Online]. Available: http://www.sinapseinstitute.org/projects/cognitiveengr/connectivity.php. [Accessed 2016].

[120] K. Stephan, W. Penny, R. Moran, H. d. Ouden, J. Daunizeau and K. Friston, "Ten simple rules for dynamic causal modeling," *NeuroImage,* vol. 49, p. 3099–3109, 2010.

[121] S. Achard, R. Salvador, B. Whitcher, J. Suckling and E. Bullmore, "A Resilient, Low-Frequency, Small-World Human Brain Functional Network with Highly Connected Association Cortical Hubs," *The Journal of Neuroscience,* vol. 26, no. 1, pp. 63-72, 2006.

[122] C. W. J. Granger, "Investigating Causal Relations by Econometric Models and Cross-spectral Methods," *Econometrica,* vol. 37, no. 3, pp. 424-438, 1969.

[123] K. J. Blinowska, "Review of the methods of determination of directed connectivity from multichannel data," *Med Biol Eng Comput,* vol. 49, pp. 521-529, 2011.

[124] C. Granger, "Testing for causality: A personal viewpoint," *Journal of Economic Dynamics and Control,* vol. 2, no. 1, pp. 329-352, 1980.

[125] H. Akaike, "A new look at the statistical model identification," *IEEE Transactions on Automatic Control,* vol. 19, no. 6, pp. 716-723, 1974.

[126] H. Lütkepohl, "VAR Analysis in JMulTi," in *Handbook of Economic Forecasting*, Elsevier, 2006.

[127] T. Mullen, "Source Information Flow Toolbox (SIFT)," Swartz Center for Computational Neuroscience, California, San Diego, 2010.

[128] A. Delorme, T. Mullen, C. Kothe and e. al, "EEGLAB, SIFT, NFT, BCILAB, and ERICA: New Tools for Advanced EEG Processing," *Computational Intelligence and Neuroscience,* no. 2011, p. 12, 2011.

[129] M. Morf, A. Vieira and T. Kailath, "Covariance Characterization by Partial Autocorrelation Matrices," *The Annals of Statistics,* vol. 6, no. 3, pp. 643-648, 1978.

[130] A. Schlögl and G. Supp, "Analyzing event-related EEG data with multivariate autoregressive parameters.," *Prog Brain Res,* vol. 159, pp. 135-147, 2006.

[131] T. Kailath, A. Vieira and M. Morf, "Inverses of Toeplitz operators, innovations, and orthogonal polynomials," *SIAM Rev.,* no. 20, pp. 106-119, 1978.

[132] L. A. Baccalá and K. Sameshima, "Partial directed coherence: a new concept in neural structure determination," *Biological Cybernetics,* vol. 84, no. 6, pp. 463-474, 2001.

[133] C. L.J., “Coefficient alpha and the internal structure of tests,” *Psychometrika,* vol. 16, no. 3, pp. 297-334, 1951.

[134] D. George and P. Mallery, SPSS for Windows step by step: A simple guide and reference, Boston: Allyn & Bacon, 2003.

[135] J. Toppi, F. D. V. Fallani, G. Vecchiato, A. G. Maglione, F. Cincotti, D. Mattia, S. Salinari, F. Babiloni and L. Astolfi, “How the Statistical Validation of Functional Connectivity Patterns Can Prevent Erroneous Definition of Small-World Properties of a Brain Connectivity Network,” *Computational and Mathematical Methods in Medicine,* no. 130985, 2012.

[136] M. J. Kaminski and K. J. Blinowska, “A new method of the description of the information flow in the brain structures,” *Biological Cybernetics,* vol. 65, no. 203, pp. 203-210, 1991.

[137] P. Dagum, A. Galper and E. Horvitz, “Dynamic Network Models for Forecasting,” in *UAI'92 Proceedings of the Eighth international conference on Uncertainty in artificial intelligence,* Stanford, 1992.

[138] C. Bielza and P. Larrañaga, “Bayesian networks in neuroscience: a survey,” *Frontiers in Computational Neuroscience,* vol. 8, no. 131, pp. 1-23, 2014.

[139] K. J. Friston, L. Harrison and W. Penny, “Dynamic causal modelling,” *NeuroImage,* vol. 19, no. 4, pp. 1273-1302, 2003.

[140] A. R. McIntosh, “Moving between functional and effective connectivity,” in *Society for Neuroscience,* Washington, D.C., 2010.

[141] B. G. Tabachnick and L. S. Fidell, Using Multivariate Statistics, Northridge: Pearson Education, 2013.

[142] U. Brandes and T. Erlebach, Network Analysis. Methodological Foundations, Berlin: Springer-Verlag, 2005.

[143] V. Latora and M. Marchiori, “Efficient Behavior of Small-World Networks,” *Physical Review Letters,* vol. 87, no. 19, 2001.

[144] D. J. Watts and S. H. Strogatz, “Collective dynamics of 'small-world' networks,” *Nature* , vol. 393, pp. 440-442, 1998.

[145] K. Supekar, V. Menon, D. Rubin and M. Musen, "Network Analysis of Intrinsic Functional Brain Connectivity in Alzheimer's Disease," *PLoS Computational Biology,* vol. 4, no. 6, 2008.

[146] Wikipedia, "Small-world network," [Online]. Available: https://en.wikipedia.org/wiki/Small-world_network. [Accessed 2016].

[147] G. W. Snedecor and W. G. Cochran, Statistical Methods, Iowa: Iowa State University Press, 1989.

[148] C. I., "Chi-squared and Fisher-Irwin tests of two-by-two tables with small sample recommendations," *Statistics in Medicine,* vol. 26, pp. 3661-3675, 2007.

[149] R. J.T.E., "The analysis of 2 x 2 contingency tables - Yet again," *Statistics in Medicine,* vol. 30, p. 890, 2011.

[150] G. F. Eden and C. J. Vaidya, "ADHD and Developmental Dyslexia Two Pathways Leading to Impaired Learning," *Ann. N.Y. Acad. Sci.,* vol. 1145, p. 316–327, 2008.

[151] S. Brambati, C. Termine, M. Ruffino, G. Stella, F. Fazio, S. Cappa and D. Perani, "Regional reductions of gray matter volume in familial dyslexia," *Neurology,* vol. 63, no. 4, pp. 742-745, 2004.

[152] S. F. Muldoon, E. W. Bridgeford and D. S. Bassett, "Small-World Propensity and Weighted Brain Networks," *Scientific Reports,* vol. 6, 2016.

[153] J.-Y. Chang, A. Pigorini, M. Massimini, G. Tononi, L. Nobili and B. D. V. Veen, "Multivariate autoregressive models with exogenous inputs for intracerebral responses to direct electrical stimulation of the human brain," *Frontiers in Human Neuroscience,* vol. 6, no. 317, pp. 1-14, 2012.

[154] A. Buchweitz, R. A. Mason, L. M. B. Tomitch and M. A. Just, "Brain activation for reading and listening comprehension: An fMRI study of modality effects and individual differences in language comprehension," *Psychol. Neurosci.,* vol. 2, no. 2, pp. 111-123, 2009.

[155] W. Backes, EricVuurman, R. Wennekes, P. Spronk, M. Wuisman, J. v. Engelshoven and J. Jolles, "Atypical Brain Activation of Reading Processes in

Children With Developmental Dyslexia," *Journal of Child Neurology,* vol. 17, no. 12, pp. 867-871, 2002.

[156] I. Lundberg and G. Sterner, "Reading, arithmetic, and task orientation—How are they related?," *Annals of Dyslexia,* vol. 56, no. 2, pp. 361-377, 2006.

[157] M. v. Ermingen-Marbach, M. Grande, J. Pape-Neumann, K. Sass and S. Heim, "Distinct neural signatures of cognitive subtypes of dyslexia with and without phonological deficits," *Neuroimage: Clinical,* vol. 2, pp. 477-490, 2013.

[158] B. A. Wandell and J. D. Yeatman, "Biological development of reading circuits," *Curr Opin Neurobiol,* vol. 23, no. 2, p. 261–268, 2013.

[159] T. Horowitz-Kraus, J. J. Vannest, D. Kadis, N. Cicchino, Y. Y. Wang and S. K. Holland, "Reading acceleration training changes brain circuitry in children with reading difficulties," *Brain and Behavior,* vol. 4, no. 6, pp. 886-902, 2014.

[160] R. d. Oliveira-Souza, R. D. Hare, I. E. Bramati, G. J. Garrido, F. A. Ignácio, F. Tovar-Moll and J. Moll, "Psychopathy as a disorder of the moral brain: Fronto-temporo-limbic grey matter reductions demonstrated by voxel-based morphometry," *NeuroImage,* vol. 40, no. 3, p. 1202–1213, 2008.

[161] E. Paulesu, J.-F. Demonet, F. Fazio, E. McCrory, V. Chanoine, N. Brunswick, S. F. Cappa, G. Cossu, M. Habib, C. D. Frith and U. Frith, "Dyslexia: Cultural Diversity and Biological Unity," *Science,* vol. 291, no. 5511, pp. 2165-2167, 2001.

[162] Z. M. Saygin, E. S. Norton, D. E. Osher, S. D. Beach, A. B. Cyr, O. Ozernov-Palchik, A. Yendiki, B. Fischl, N. Gaab and J. D. Gabrieli, "Tracking the Roots of Reading Ability: White Matter Volume and Integrity Correlate with Phonological Awareness in Prereading and Early-Reading Kindergarten Children," *The Journal of Neuroscience,* vol. 33, no. 33, pp. 13251-13258, 2013.

[163] A. Galaburda, G. Sherman, G. Rosen, F. Aboitiz and N. Geschwind, "Developmental dyslexia: four consecutive patients with cortical anomalies," *Ann Neurol,* vol. 18, no. 2, pp. 222-233, 1985.

[164] N. Geschwind and W. Levitsky, “Human Brain: Left-Right Asymmetries in Temporal Speech Region,” *Science*, vol. 161, no. 3837, pp. 186-187, 1968.

[165] C. A. Myers, M. Vandermosten, E. A. Farris, R. Hancock, P. Gimenez, J. M. Black, B. Casto, M. Drahos, M. Tumber, R. L. Hendren, C. Hulme and F. Hoeft, “White Matter Morphometric Changes Uniquely Predict Children’s Reading Acquisition,” *Psychological Science*, vol. 25, no. 10, p. 1870–1883, 2014.

[166] A. Meyler, T. A. Keller, V. L. Cherkassky, D. Lee, F. Hoeft, S. Whitfield-Gabrieli, J. D. E. Gabrieli and M. A. Just, “Brain Activation during Sentence Comprehension among Good and Poor Readers,” *Cereb Cortex*, vol. 17, no. 12, pp. 2780-2787, 20098.

[167] R. Ptak, MarieDiPietro and Jean-MichelPignat, “The role of parieto-temporal connectivity in pure neglect dyslexia,” *BrainResearch,* vol. 1648, p. 144–151, 2016.

[168] F. Morken, T. Helland, K. Hugdahl and K. Specht, “Reading in Dyslexia across Literacy Development: A Longitudinal Study of Effective Connectivity,” *NeuroImage*, vol. 144, pp. 92-100, 2017.

[169] S. Achal, F. Hoeft and S. Bray, “Individual Differences in Adult Reading Are Associated with Left Temporo-parietal to Dorsal Striatal Functional Connectivity,” *Cerebral Cortex*, pp. 1-13, 2015.

[170] L. Reed-Guy, “Brain Disorders,” Healthline, 22 December 2015. [Online]. Available: http://www.healthline.com/health/brain-disorders#Overview1. [Accessed 2016].

[171] K. Yong, K. Rajdev, E. Warrington, J. Nicholas, J. Warren and S. Crutch, “A longitudinal investigation of the relationship between crowding and reading: A neurodegenerative approach,” *Neuropsychologia,* vol. 85, pp. 127-136, 2016.

[172] J. R. C. Marques, “À procura do perfil molecular que caracteristico da Perturbação de Hiperatividade e Défice de Atenção e da Dislexia,” Universidade de Aveiro Departamento de Biologia, Aveiro, 2015.

[173] T. C. Ferree, P. Luu, G. S. Russell and D. M. Tucker, "Scalp electrode impedance, infection risk, and EEG data quality," *Clinical Neurophysiology,* vol. 112, pp. 536-544, 2001.

[174] G. F. Woodman, "A Brief Introduction to the Use of Event-Related Potentials (ERPs) in Studies of Perception and Attention," *Atten Percept Psychophys.,* vol. 72, no. 8, pp. 2031-2046, 2010.

[175] A. Mouraux and G. Iannetti, "Across-trial averaging of event-related EEG responses and beyond," *Magnetic Resonance Imaging,* vol. 26, pp. 1041-1054, 2008.

[176] S. Usui and N. Toda, "An overview of biological signal processing: non-linear and non-stationary aspects.," *Front Med Biol Eng.,* vol. 3, no. 2, pp. 125-129, 1991.

[177] D. Husmeier, "DBmcmc Inferring Dynamic Bayesian Networks with MCMC," 2003. [Online]. Available: https://www.bioss.ac.uk/people/dirk/software/DBmcmc/. [Accessed 2016].

[178] K. Murphy, "Bayes Net Toolbox for Matlab," [Online]. Available: https://www.cs.utah.edu/~tch/notes/matlab/bnt/docs/bnt_pre_sf.html. [Accessed 2016].

[179] R. M. and S. O., "Complex network measures of brain connectivity: Uses and interpretations," *NeuroImage,* vol. 52, pp. 1059-69, 2010.

[180] G. M. Ljung and G. E. P. Box, "On a Measure of a Lack of Fit in Time Series Models," *Biometrika,* vol. 65, no. 2, p. 297–303, 1978.

[181] L. Xu, T. Fan, X. Wu, K. Chen, X. Guo, J. Zhang and L. Yao, "A pooling-LiNGAM algorithm for effective connectivity analysis of fMRI data," *Front. Comput. Neurosci,* vol. 8, p. 125, 2014.

[182] C. Porcaro, F. Zappasodi, P. M. Rossini and F. Tecchio, "Choice of multivariate autoregressive model order affecting real network functional connectivity estimate," *Clinical Neurophysiology,* vol. 120, no. 2, p. 436–448, 2009.

[183] R. Palaniappan, P. Raveendran, S. Nishida and N. Saiwaki, "Autoregressive Spectral Analysis and Model Order Selection Criteria for EEG Signals," in

TENCON Proceedings. Intelligent Systems and Technologies for the New Millennium (Cat. No.00CH37119), Kuala Lumpur, Malaysia, 2000.

[184] D. M. Simpson, A. F. C. Infantosi, J. F. C. Junior, A. J. Peixoto and L. M. d. S. Abrantes, "On The Selection of Autoregressive Order For Electroencephalographic (EEG) Signals," *Circuits and Systems, 1995., Proceedings., Proceedings of the 38th Midwest Symposium,* vol. 2, pp. 1353-1356, 1995.

[185] J. Malmivuo and R. Plansey, Bioelectromagnetism, Durham, North Carolina; Tampere, Finland, 1993.

APPENDIX A

DISCRETIZATION OF CONNECTIVITY MATRICES

The discretization procedure for connectivity matrices: Let the mean value of all non-diagonal units be μ and let x_{ij} denote the units in connectivity adjacency matrix where i indicates row and j indicates column and $i \neq j$. Then, if $x_{ij} > \mu$; value of x_{ij} is changed with 1. Similarly, if $x_{ij} < \mu$; value of x_{ij} is changed with 0. Here, 1 indicates "connection" and 0 indicates "no connection".

The diagonal units (i=j) of the matrix represent the self-connectivity. Therefore, they are expected to have the highest values of the whole connectivity matrix. Diagonal units in a real weighted connectivity matrix in Table 5 are 10^2 to 10^5 times larger than other values. So, applying the discretization procedure would yield a diagonal matrix consist of 0's for non-diagonal elements. To avoid this, first, the values of all the diagonal units were set as 0. Then the discretization procedure is applied. Finally, the diagonal elements were set as 1. The following figure is an example of discretization of the connectivity adjacency matrix in Table 5.

Table 24 - An example of discretization of the weighted adjacency table in Table 5.

Node #	1	2	3	4	5	6
1	1	0	0	0	0	1
2	0	1	0	1	0	1
3	0	0	1	0	0	0
4	0	0	0	1	1	0
5	0	0	1	0	1	0
6	0	0	1	0	1	1

APPENDIX B

CHANNELS WITH SIMILAR BEHAVIOURS

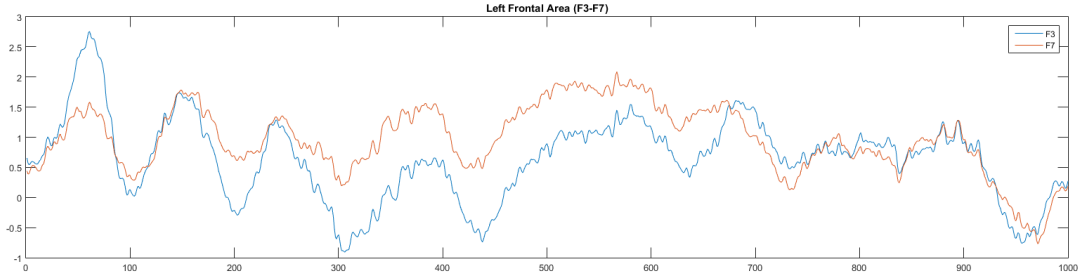

Figure 20 – Representation of grand average values of after stimulus condition of control subjects for left frontal area electrodes: F3 and F7.

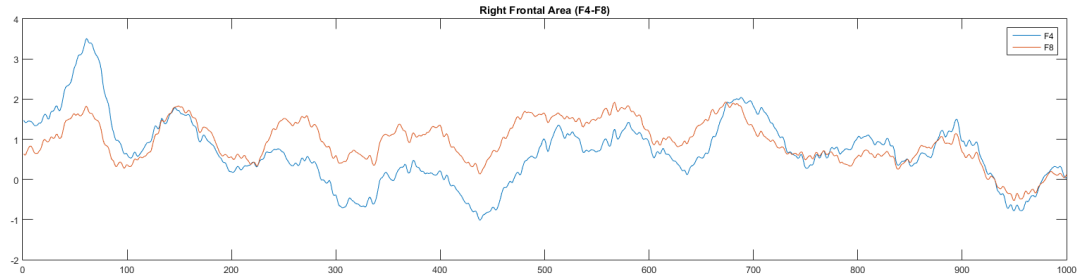

Figure 21 – Representation of grand average values of after stimulus condition of control subjects for right frontal area electrodes: F4 and F8.

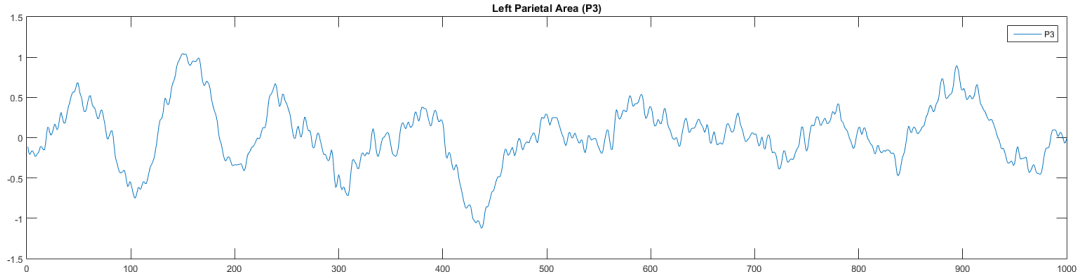

Figure 22 – Representation of grand average values of after stimulus condition of control subjects for left parietal area electrode: P3.

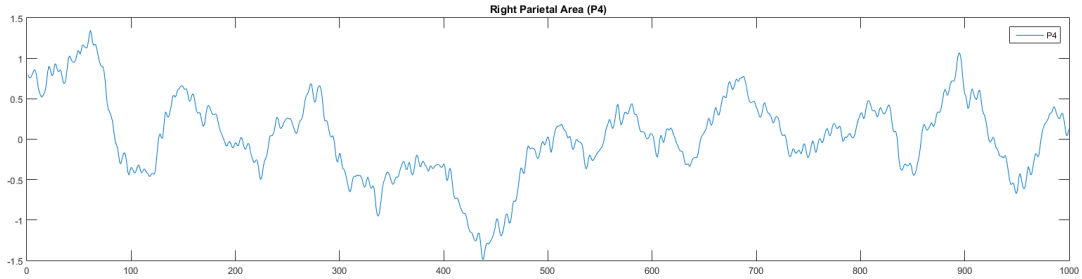

Figure 23 – Representation of grand average values of after stimulus condition of control subjects for right parietal area electrode: P4.

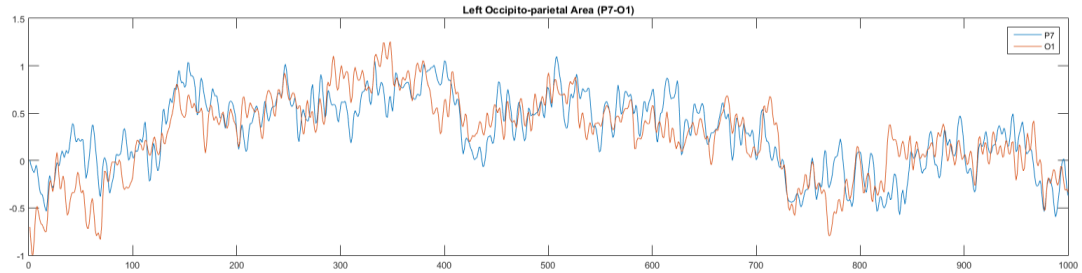

Figure 24 – Representation of grand average values of after stimulus condition of control subjects for left occipito-parietal area electrodes: P7 and O1.

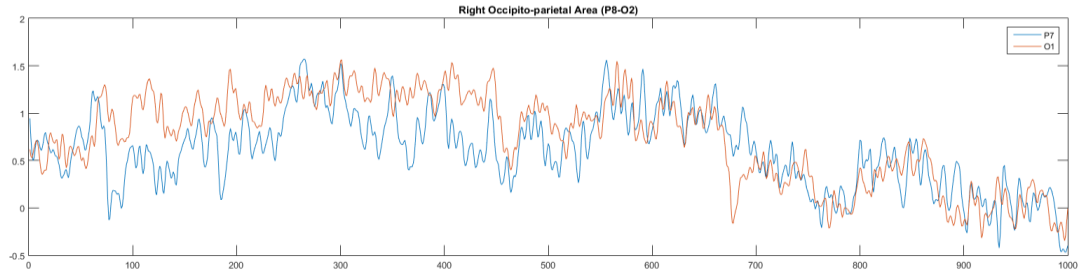

Figure 25 - Representation of grand average values of after stimulus condition of control subjects for right occipito-parietal area electrodes: P8 and O2.